ความเสถียรภาพของฟิล์มบางพอลิสไตรีนที่มีโคพอลิเมอร์และอนุภาคระดับนาโนของ Fe_3O_4 เป็นสารเติมแต่ง

นางสุนทรี แสงจันทร์

วิทยานิพนธ์นี้เป็นส่วนหนึ่งของการศึกษาตามหลักสูตรปริญญาวิทยาศาสตรดุษฎีบัณฑิต
สาขาวิชาวัสดุศาสตร์ ภาควิชาวัสดุศาสตร์
คณะวิทยาศาสตร์ จุฬาลงกรณ์มหาวิทยาลัย
ปีการศึกษา 2554
ลิขสิทธิ์ของจุฬาลงกรณ์มหาวิทยาลัย

STABILITY OF POLYSTYRENE THIN FILMS CONTAINING COPOLYMERS AND Fe$_3$O$_4$

NANOPARTICLES AS ADDITIVES

Mrs. SUNTREE SANGJAN

A Dissertation Submitted in Partial Fulfillment of the Requirements

for the Degree of Doctor of Philosophy Program in Materials Science

Department of Materials Science

Faculty of Science

Chulalongkorn University

Academic Year 2011

Thesis Title   STABILITY OF POLYSTYRENE THIN FILMS CONTAINING

COPOLYMERS AND Fe$_3$O$_4$ NANOPARTICLES AS ADDITIVES

By   Mrs. Suntree Sangjan

Field of Study   Materials Science

Thesis Advisor   Assistant Professor Nisanart Traiphol, Ph.D.

Thesis Co-advisor   Assistant Professor Rakchart Traiphol, Ph.D.

Accepted by the Faculty of Science, Chulalongkorn University in Partial Fulfillment of the Requirements for the Doctoral Degree

…………………………………………….. Dean of the Faculty of Science

(Professor Supot Hannongbua, Ph.D.)

THESIS COMMITTEE

…………………………………………….. Chairman

(Associate Professor Supatra Jinawath,Ph.D.)

………………………………………….…… Thesis Advisor

(Assistant Professor Nisanart Traiphol, Ph.D.)

…………………………………………….. Thesis Co-Advisor

(Assistant Professor Rakchart Traiphol, Ph.D.)

…………………………………………….. Examiner

(Kanoktip Boonkerd, Ph.D.)

…………………………………………….. Examiner

(Assistant Professor Rojana Pornprasertsuk, Ph.D.)

…………………………………………….. External Examiner

(Assistant Professor Toemsak Srikhirin, Ph.D.)

สุนทรี แสงจันทร์ : เสถียรภาพของฟิล์มบางพอลิสไตรีนที่มีโคพอลิเมอร์และอนุภาค ระดับนาโนของ Fe_3O_4 เป็นสารเติมแต่ง. (STABILITY OF POLYSTYRENE THIN FILMS CONTAINING COPOLYMERS AND Fe_3O_4 NANOPARTICLES AS ADDITIVES) อ. ที่ปรึกษาวิทยานิพนธ์หลัก : ผศ. ดร. นิสานาถ ไตรผล, อ. ที่ปรึกษา วิทยานิพนธ์ร่วม : ผศ. ดร. รักชาติ ไตรผล 131 หน้า.

งานวิจัยนี้ศึกษาประสิทธิภาพของสารเติมแต่ง โคพอลิเมอร์พอลิสไตรีนคลอโรเมททิลสไตรีน และอนุภาคระดับนาโนของ Fe_3O_4 ในการทำหน้าที่เป็นตัวยับยั้งการแตกฟิล์มบางพอลิสไตรีน ซึ่งมีความหนาน้อยกว่า 50 nm อัตราส่วนหมู่คลอโรเมททิลสไตรีนในโคพอลิเมอร์ที่ใช้คือ 5, 20 และ 45 mol% และกำหนดความเข้มข้นของโคพอลิเมอร์เพื่อให้มีปริมาณหมู่คลอโร เมททิลสไตรีน (CIMS group) เท่ากับ 0.5, 1.0, 1.5 และ 2.0 mol% ในฟิล์มบาง สำหรับ อนุภาคระดับนาโนของ Fe_3O_4 ใช้ในปริมาณ 0.005, 0.01, 0.02 และ 0.03 wt% กล้อง จุลทรรศน์แรงอะตอมและกล้องจุลทรรศน์แบบใช้แสง นำมาใช้ติดตามการเปลี่ยนแปลงสัณฐาน วิทยาของฟิล์มบาง ภายหลังการอบที่อุณหภูมิสูงกว่าอุณหภูมิการเปลี่ยนจากสถานคล้ายแก้ว ของพอลิสไตรีน จากการทดลอง พบว่า ความเสถียรทางความร้อนของฟิล์มพอลิสไตรีน เพิ่มขึ้นอย่างมากเมื่อเติมสารเติมแต่งโคพอลิเมอร์ปริมาณเล็กน้อยประมาณ 1 mol% ของหมู่ CLMS ลงในระบบ ซึ่งคาดว่าหมู่คลอโรเมททิลสไตรีนซึ่งมีความเป็นขั้วจะยึดเกาะกับ ฐานรองรับซิลิคอน ซึ่งมีความเป็นขั้วเช่นกันในขณะที่ส่วนของสไตรีนจะเกิดอันตรกิริยากับ ฟิล์มพอลิสไตรีนที่เป็นเมตริกซ์ โดยประสิทธิภาพของโคพอลิเมอร์ในการทำหน้าที่เป็นตัว ยับยั้งการแตกของฟิล์มบาง ขึ้นกับอัตราส่วนของหมู่คลอโรเมททิลสไตรีนและความหนาของ ฟิล์มบาง สำหรับฟิล์มบางพอลิสไตรีนที่เติมอนุภาคระดับนาโนของ Fe_3O_4 ผลบ่งชี้ว่าการเติม อนุภาคระดับนาโนของ Fe_3O_4 สามารถยับยั้งกลศาสตร์การการแตกโดยความร้อนบน ฐานรองรับซิลิกอนได้โดยประสิทธิภาพของอนุภาคระดับนาโน Fe_3O_4 ขึ้นอยู่กับความหนา ของฟิล์มและความเข้มข้นของ Fe_3O_4 โดยคาดว่าอนุภาคระดับนาโน Fe_3O_4 จะตรึงฟิล์มบาง และตามด้วยกระบวนการลดการไหลของของเหลวแบบอุทกพลศาสตร์ระหว่างการแตกของ ฟิล์มซึ่งนำไปสู่การเพิ่มความเสถียรของฟิล์ม

ภาควิชา ....วัสดุศาสตร์............ ลายมือชื่อนิสิต..
สาขาวิชา.........วัสดุศาสตร์............ ลายมือชื่อ อ.ที่ปรึกษาวิทยานิพนธ์หลัก.................
ปีการศึกษา ....2554............ ลายมือชื่อ อ.ที่ปรึกษาวิทยานิพนธ์ร่วม ....

5073889023 : MAJOR   Materials Science

KEYWORDS :   Dewetting inhibitor / Polystyrene / Thin film / Surface energy / Additives

SUNTREE SANGJAN : STABILITY OF POLYSTYRENE THIN FILMS CONTAINING COPOLYMERS AND Fe_3O_4 NANOPARTICLES AS ADDITIVES. ADVISOR : ASST. PROF. NISANART TRAIPHOL, Ph.D., CO-ADVISOR : ASST. PROF. RAKCHART TRAIPHOL, Ph.D., 131 pp.

This research investigates efficiency of poly(styrene-stat-chloromethylstyrene (ClMS)) (P(S-ClX)) copolymers and Fe_3O_4 nanoparticles as dewetting inhibitors for polystyrene (PS) thin films of thickness less than 50 nm. Chloromethylstyrene (ClMS) ratios in the P(S-ClX) copolymers are 5, 20 and 45 mol% and the copolymer concentrations are controlled to provide 0.5, 1.0, 1.5 and 2.0% of ClMS group in thin films. Concentration of Fe_3O_4 nanoparticles are 0.05, 0.01, 0.02 and 0.03 wt%. The atomic force microscopy and optical microscopy are utilized to follow the morphological change of the blended and filled films upon annealing above their glass transition temperature. We have found that thermal stability of the PS films is greatly improved when small amount of the copolymers is added into the system, estimates 1 mol% of ClMS group. The polar ClMS groups provide anchoring sites with polar SiO_x/Si substrate while the styrene segments favorably interact with PS matrix. The effectiveness of the copolymers as dewetting inhibitors is also found to vary with molar ratio of ClMS group in the copolymers and film thickness. For polystyrene (PS) thin film filled with magnetic Fe_3O_4 nanoparticles, the results indicate that the addition of Fe_3O_4 nanoparticles suppresses dewetting dynamics of the thin film coated on Si/SiO_x solid substrate. The efficiency of Fe_3O_4 nanoparticles depend on film thickness and Fe_3O_4 concentration. We expect that Fe_3O_4 nanoparticles provide a pinning effect followed by a decrease in hydrodynamic fluid flow process during film rupture, which in turn leads to the increase of film stability.

Department : Materials Science   Student's Signature

Field of Study : Materials Science   Advisor's Signature

Academic Year : 2011   Co-advisor's Signature

Acknowledgements

I would like to express sincere thanks to Assist. Prof. Dr. Nisanart Traiphol and Assist. Prof. Dr. Rakchart Traiphol for support and guidance throughout my Ph.D. studying at Chulalongkorn University.

I would like to thank my family; mother, husband, daughter and friends for their encouragement that give me strength all these years.

Contents

LIST OF TABLES

LIST OF FIGURES

CHAPTER I

INTRODUCTION

Polymeric thin films have played important roles in materials science and engineering. The utilizations of polymeric films ranges from simple applications such as coatings, paints and adhesives to more advanced technologies including insulating layer in microelectronic devices and resisting layer for lithography.

One of the major problems in thin film technology involves the issue concerning its instability on supported solid substrates. It has been known that the polymeric thin film tends to dewet on unfavorable surface when its thickness decreases. Increasing in temperature during operation also accelerates dynamics of dewetting process by increasing amplitude of interfacial fluctuation [1-9] The dewetting of polymeric thin films, in turn, deteriorates their properties. For example, the dewetting of insulating polymeric layer used in electronic circuit board results in the breakdown of voltage (Figure 1.1).
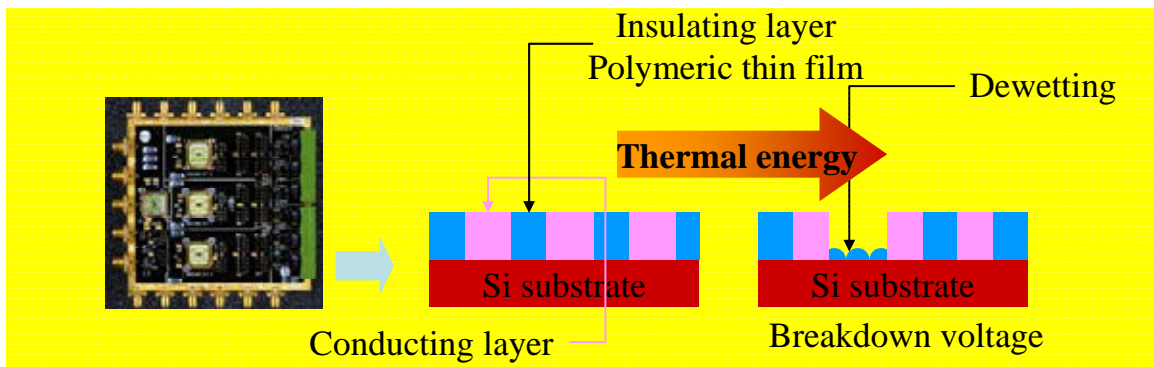
Figure 1.1 Dewetting of insulating layer on electronic devices

The dewetting phenomenon of polymeric thin films can take place via spinodal[1,4,5] and/or heterogeneous nucleation mechanisms [7-9] Increasing of interfacial thermal fluctuation mainly contributes to the spinodal one while the heterogeneity of surface energy on solid substrate leads to another process. The dewetting behavior is influenced by various parameters including interfacial energy and film thickness. Unfavorable interfacial interactions and the decrease in film thickness are known to accelerate the dynamics of dewetting process.

In recent years, researchers have been seeking for methods to suppress the dewetting of polymeric thin films[10-40] In general, it can be categorized into two approaches. The first one involves chemical modification of polymeric chains and/or solid substrate, which leads to an increase in interfacial interaction. The modification of polymeric chains can be achieved by attaching moieties along a main chain, side chains and end groups. For example, it has been demonstrated that the incorporation of sulfonated group into main chain or end group of polystyrene (PS) can result in a drastic increase in thin film stability. However, this method inevitably alters physical properties of the modified polymer due to an existence of ionic pendent in the system [12,14,15] The second approach utilizes foreign molecules/nanoparticles as additives. The dewetting of the film can be retarded by the addition of foreign materials such as nanoparticles[10,19,20,22,27,32,35], homopolymers[21,36], copolymers[37,38] and metal/metal oxide nanoparticles[10,27,32,35]. The additives are expected to suppress the dewetting process by increasing the interfacial interaction between the film and the substrate, and providing a pinning effect followed by a decrease in hydrodynamic fluid flow process during film rupture. Example of additive are diblock copolymer [37,38], bisphenol-A polycarbornate [21], random copolymers [41], dendrimers [39], hyperbranched polymers [40] and several nanoparticles such as silica [27], gold [44], and polyhedral oligomeric silsesquioxane (POSS) [19,20]

In this research, PS is selected to use as matrix in the system because dielectric constant of PS is relatively high which is desired for insulating materials. The statistical copolymer poly(styrene-stat-chloromethylstyrene) (P(S-stat-ClMS)) and Fe_3O_4 nanoparticles are used as additives in PS film of thickness less than 50 nm. The PS films are fabricated with various additive concentrations and under different heat treatment conditions. The dewetting behavior and film stability are investigated by means of atomic force microscopy (AFM), optical microscopy (OM) and contact angle meter. The Cl atom in random copolymer (P(S-Clx)) expected to enhance the interfacial interaction between PS film and solid substrate by altering bond polarity to increase the dipolar interaction. We expected that the chloromethylstyrene groups (ClMS) in copolymer should anchor on SiO_x/Si substrate via dipolar interaction while styrene segments interact with the matrix polymer as illustrated in Figure 1.2. For nanoparticle addition, Fe_3O_4 nanoparticles are expected to increase the film stability by pinning effect, which controls fluid spreading on rough surface. The retardation of dewetting by pining implied that the filler particles are on the solid substrate, reducing flow dynamics and increasing film stability as illustrated in Figure 1.3.
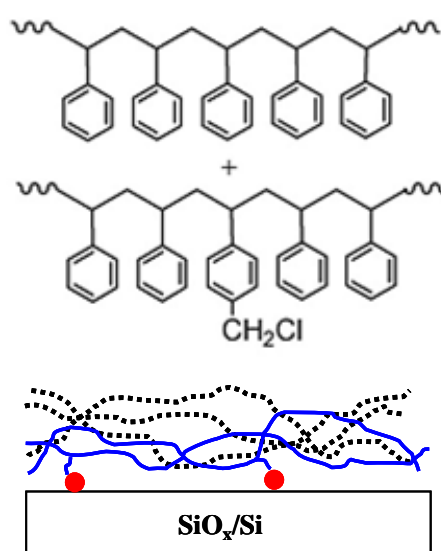
Figure 1.2 (top) Chemical structures of PS and P(S-Clx) copolymer additive and (bottom) illustration of interfacial interaction between copolymer and substrate. The ClMS groups are expected to anchor on SiO_x/Si substrate.

Fe$_3$O$_4$ nanoparticles
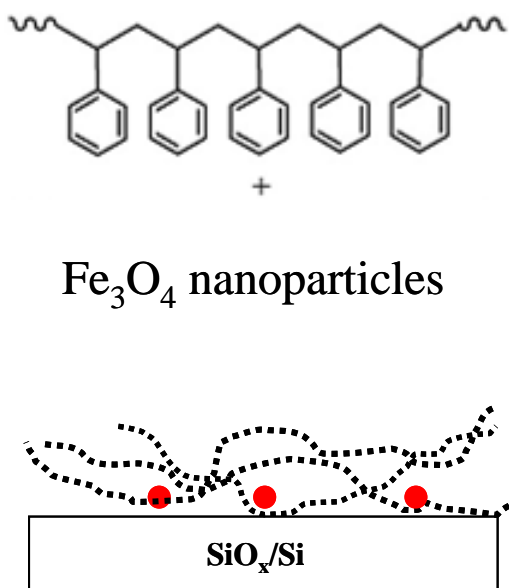
Figure 1.3 Schematic of pinning effect by Fe$_3$O$_4$ nanoparticles on SiO$_x$/Si substrate to increase PS film stability.

Objectives of this research

1. To study interfacial interaction between pure, blended and filled polystyrene thin films and inorganic substrate.
2. To investigate methods for suppressing the instability of the polymeric thin films on Si-wafer substrate.

Expected benefit of this research

1. Thin films with high stability can be obtained by addition of copolymers and Fe$_3$O$_4$ nanoparticles.
2. The fundamental knowledge from this study is also important for designing or selecting structure of additives used to improve the stability of polymeric thin films.

CHAPTER II

THEORETICAL BACKGROUND
AND LITERATURE REVIEWS

2.1   Mechanism of dewetting in polymer-based thin film

Ultrathin (less than 100 nm) polymeric films play important roles in many applications such as coatings, paints, adhesives, insulating layer in microelectronics and resisting layer for lithography. To retain their intended properties, these films are required to remain stable when exposed to various conditions, such as heat and humidity. Depending on thin film geometry and/or capillary fluctuation, phase separation can occur, which lead to film rupture and droplet formation [1-9,70-78] The film instability (film rupture and droplet formation) called dewetting process is an important factor in technological applications of thin films. The dewetting process has been studied in the areas of experiment, simulation, and theory.

The mechanism of the rupture process of the liquid films is described by two theoretical approaches. The first is growing fluctuation wave mechanism or spinodal mechanism or spinodal decomposition, which appears on fluid interface under the influence of attractive force; i.e. electrostatic, van-der-Waals, and maybe long-rage hydrophobic force (LRHF). The spinodal decomposition is initiated when thermal fluctuations modulate the interfacial interaction amplitude of film topography which is called annealing process [1,4,5,64] as shown in Figure 2.1. In this mechanism, the same spinodal wavelengths are observed, which cause the appearance of the correlate holes. They are same dimensions and exhibit random distribution. The characteristic of spinodal mechanism is continuous breakup of holes. In this mechanism, the spinodal

wavelength (λ_s) is amplitude of spinodal dewetting of film, which relate with surface energy of film as shown in equation 2.1. [1]

$$\lambda_s = \left[\frac{-8\pi\gamma}{\varphi''(h)}\right]^{1/2}$$ (2.1)

Where $\varphi''(h)$ is second derivative of effective interface potential, which is function of film thickness (h). When film thickness is decrease to lass than λ_s, dewetting area can occurs. In polymer, annealing process is done by heating to above the glass transition temperature [71], maintaining for a period of time, and then cooling. The second is heterogeneous nucleation inside the film suggested by Derjaguin and Gutop. [5,68] No attractive forces are necessary. Density fluctuations inside the film in the vicinity of hydrophobic spots or tiny gas bubbles can cause the rupture. For heterogeneous nucleation, decreasing surface energy of thin film leads to appear uncorrelated holes that are different in dimensions and exhibit non-random distribution as shown in Figure 2.2. In addition, heterogeneous nucleation appears if the film thickness decreases below critical thickness (h_0) ($\varphi''(h_0) \rangle 0$). A currently described example is rupture of polystyrene layers on silicon wafers. The breakup of films by spinodal dewetting is controlled by interfacial fluctuation. On the other hand, the rupture of films by nucleation strongly depends on the initial conditions such as air bubbles, defects, and the occurrence of strain in the films.
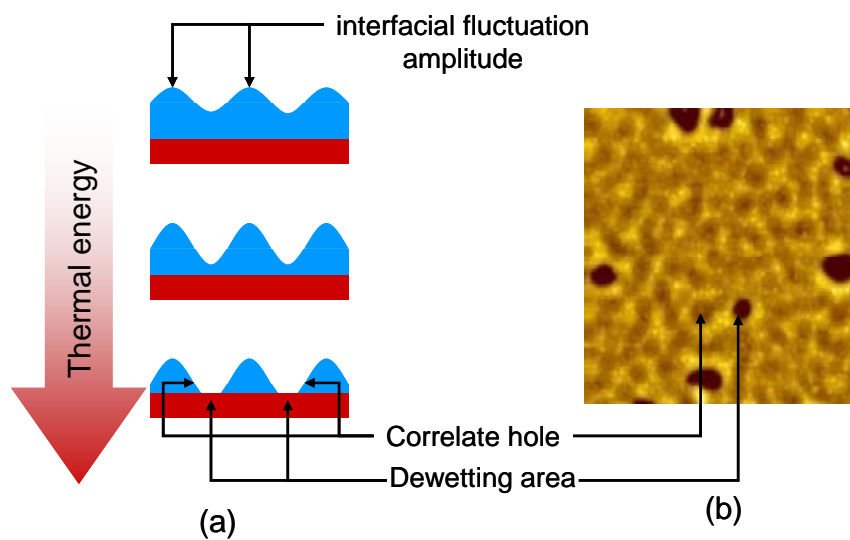
Figure 2.1 spinodal decomposition (a) illustration (b) AFM topography
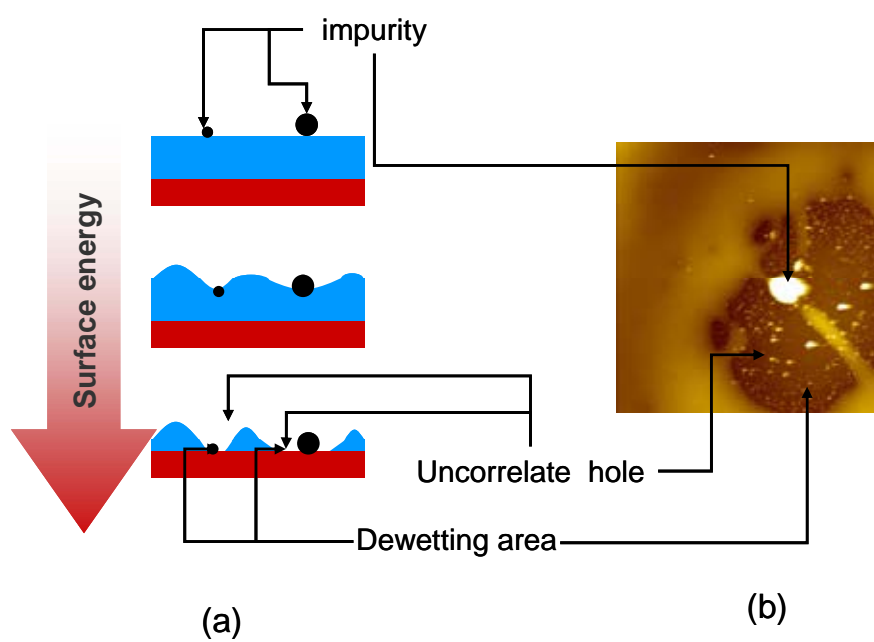
Figure 2.2 heterogeneous nucleation (a) illustration (b) AFM topography

Under normal circumstances, polymeric thin films on non-wettable surfaces become unstable and undergo a self-destructive process once annealed at a temperature higher than the glass transition temperature (T_g) of the polymer. At $T>T_g$, the molecules of polymers start to rotate and vibrate, initiating the dewetting process. At the first stage of dewetting process, the film breaks up into holes. Then, the holes grow and coalesce to form a morphology consisting of a polygon pattern of unstable ribbons, which is the intermediate stage. The final stage is the broken of the ribbons into droplets. Stages of dewetting process are shown in Figure 2.3.

(a)   (b)   (c)
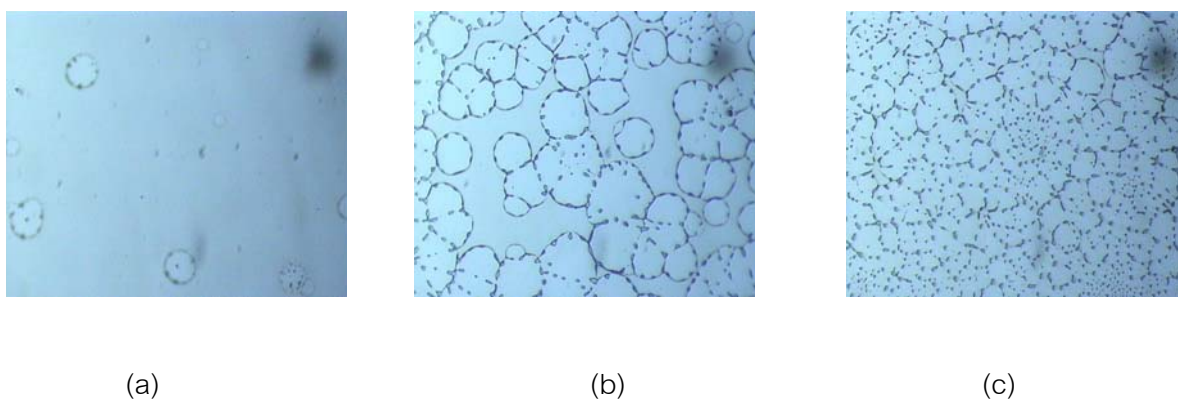
Figure 2.3 Three stages of dewetting process (a) holes,(b) polygon pattern of ribbons and (c) droplets

2.2   Young's equation

Dewetting or instability of polymeric thin films is driven by the effective molecular interactions acting between all the interfaces that separate the three media: substrate, film and surrounding gas. Favorable interfacial energy between film and solid substrate leads to adhesion between an organic phase and a solid substrate. The film stability or equilibrium between the three interfacial energy (substrate/film/air) can be expressed by Young's equation [45] associated with the contact angle (θ):

$$\gamma_S = \gamma_{SF} + \gamma_F \cos\theta \tag{2.2}$$

Equation (2.2) is developed for the case of an ideal surface, which is defined morphology of surface such as smooth, rough or homogeneous. Surface free energies of the solid substrate and polymer thin film are expressed as γ_S and γ_F respectively, and γ_{SF} is the interfacial free energy between polymer thin film and substrate. Young's equation is based on the balance of surface force acting on the triple line where the solid, liquid, and vapor phases meet. The surface force (per unit of length of triple line) of the solid-vapor surface is equal to the total of the solid substrate-film surface force and the component of the surface force of the film-vapor surface along the surface of the substrate. Young's equation can be demonstrated as mechanical equilibrium condition, as shown in Figure 2.4. When $\cos\theta$ is positive (when $\theta \in \left(0, \dfrac{\pi}{2}\right)$), the liquid wets the solid. Therefore, when $\gamma_S - \gamma_{SF} \rangle \gamma_F$,no contact angle can be defined by Young's equation and the liquid spreads over the solid, forming a homogeneous film. Sometimes, $\gamma_S - \gamma_{SF}$ is called the adhesion tension and $\cos\theta$ is called the relative adhesion coefficient. When the films are not ultrathin or thick, the film is considered homogeneous or wet when $S \rangle 0$ and heterogeneous or dewet when $S \langle 0$. For $S \langle 0$, the dynamics of dewetting on the film is heterogeneous nucleation and/or growth of hole (spinodal decomposition), and the film eventually breaks up into a patterned arrangement of droplets [45].
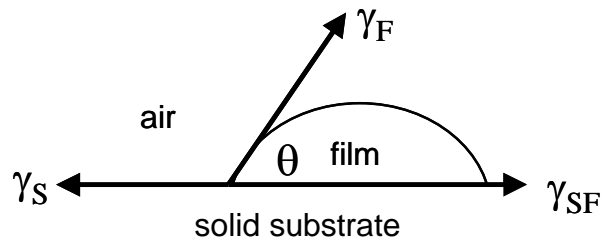
Figure 2.4. Definition of contact angle

The dewetting behavior of thin film is characterized by a spreading coefficient, S.

$$S = \gamma_S - \gamma_{SF} - \gamma_F \qquad (2.3)$$

2.3   Solid surface tension calculations

Measurements of surface tension data, directly reflects thermodynamic characteristics of the thin film. Measurement of contact angles yield data, which reflect the thermodynamics of a liquid/solid interaction and can significantly indicate film stability. If you wish to characterize the wetting behavior of a particular liquid/solid pair you only need to report the contact angle. It is possible to characterize the wettability of your solid in a more general way. To characterize the thermodynamics of the solid surface itself more analysis is required. Various methods are used but the same basic principle applies for each. The solid is tested against a series of liquids and contact angles are measured. On the other hand, the surface tension of polymer with a low surface energy can not be directly because of the elastic and viscous restraints of bulk phase, which necessitates the use of indirect methods.

Calculations based on these measurements produce a parameter (critical surface tension or surface free energy), which quantifies the characteristics of the solid and mediates the properties of the solid substrate. The critical surface tension or the surface free energy obtained in this way can be regarded as the "surface tension" of the solid substrate, which is a characteristic property of the solid in the same way as the surface tension is for a liquid. Five different approaches are mainly used for determining the energy of solid substrates [45]: 1. Fowkes' and later Owens and Wendt's method), 2. Critical Surface Tension (Zismann), 3. Equation of state approach (Neumann's method) and 4. Acid-Base (van Oss-Good method).

2.3.1 Fowkes' and later Owens and Wendt's method

In this research, using the Geometric Mean (Fowkes' and later Owens and Wendt's method) calculates the surface tension of solid substrate and thin film. This approach divides the surface energy which consists of two components, dispersive and polar which can explains the result of interaction between solid substrate and additives. The contact angle between solid substrate and thin film uses to calculate the surface tension. Owens and Wendt assumed that the surface free energy of contact area between polymers with liquid can be represented by the equation by the equation

$$W_a = 2\left(\sqrt{\gamma_s^d \gamma_l^d} + \sqrt{\gamma_s^h \gamma_l^h}\right)$$

(2.4)

The resulting equation when combined with Young's equation:

$$\gamma_l\left(1+\cos\theta\right) = 2\left(\sqrt{\gamma_s^d \gamma_l^d} + \sqrt{\gamma_s^h \gamma_l^h}\right)$$

(2.5)

Where θ is the contact angle, γ_l is liquid surface tension and γ_s is the solid surface tension, or free energy. The total free surface energy is the sum of its two components i.e. dispersive surface energy $\left(\gamma^d\right)$ and polar surface energy $\left(\gamma^h\right)$.

$$\gamma = \gamma^d + \gamma^h$$

(2.6)

In addition to that method, Owens and Wendt selected only two liquid which are polar and non-polar liquid to form droplet on surface that lead to measure the contact angle and determine the surface tension of solid. The Fowkes theory generally requires the use of only two probe liquids, as described above, and the recommended ones are diiodomethane or methylene iodine, which should have no polar component due to its molecular symmetry, and water, which is commonly known to be a very polar liquid.

This method determines surface energy of solid substrate ($\gamma_s = \gamma_s^d + \gamma_s^h$) by the measurements of the θ of two liquids with known γ_l, γ_l^d, γ_l^h values i.e. water and diiodomethane. Surface energy of water (γ_{water} =72.7 mJ/m^2, γ_{water}^d = 21.8 mJ/m^2, γ_{water}^h = 50.9 mJ/m^2) and diiodomethane ($\gamma_{diiodomethane} = \gamma_{diiodomethane}^d$ = 50.0 mJ/m^2, $\gamma_{diiodomethane}^h$ = 0 mJ/m^2) are used in this study [45]

2.3.2 Zisman's method

This approach is used for the calculation of critical surface tension of solid substrates which are low surface energy, and is represented by Zisman and coworker. They measure the contact angle with various non-polar liquids test and plot graph between $\cos\theta$ and surface tension of liquid test. This graph is probably straight line as shown in Figure 2.5. When $\cos\theta = 1$, they can indicate the surface tension value (γ_l) which is called the critical surface tension (γ_c). The relation between contact angle and surface tension can describe by equation 2.7

$$\cos\theta = 1 - \beta(\gamma_l - \gamma_c) \qquad (2.7)$$
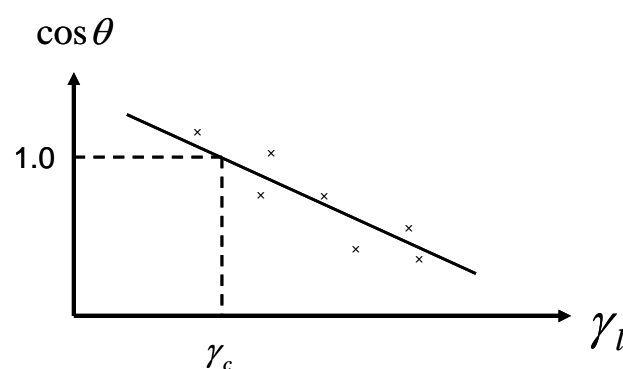
Figure 2.5. Determining the critical surface tension according to Zisman's method

2.3.3 Neumann's method

Neumann and coworker introduce the solid substrate – film interfacial tension which is a function of film and surface energy of solid substrate as shown in equation (2.8)

$$\gamma_{sl} = (\gamma_S + \gamma_l) - \left[2\left(\sqrt{\gamma_s\gamma_l}\right)\exp{-\beta(\gamma_l - \gamma_s)^2}\right]$$ (2.8)

Where β = 0.000115 $(m^2mJ^{-1})^2$. From Young equation, it can now be written as equation (2.9)

$$\cos\theta = -1 + 2\sqrt{\frac{\gamma_s}{\gamma_l}}\exp{-\beta(\gamma_l - \gamma_s)^2}$$ (2.9)

This approach assume that the surface of solid substrates are imaginary surface which are smooth, continuous, rigid, homogenuous and non-deformable. Also, these method is not favorable in many research.

2.3.4 van Oss-Good method

Van Oss, Good and Chaudhury introduce to determine free surface energy by adhesion. This approach suggests that surface tension consist of two components i.e. Lifshitz –van der Waals interaction $\left(\gamma^{LW}\right)$ and the acid-base interaction at interface $\left(\gamma^+, \gamma^-\right)$.

$$\gamma_{sl} = \left(\sqrt{\gamma_s^{LW}} - \sqrt{\gamma_l^{LW}}\right)^2 + 2\left(\sqrt{\gamma_s^+} - \sqrt{\gamma_l^+}\right)\left(\sqrt{\gamma_s^-} - \sqrt{\gamma_l^-}\right)$$ (2.10)

This equation is combined with Young's equation as shown in below equation

$$\gamma_l(1 + \cos\theta) = 2\left(\gamma_l^{LW}\gamma_s^{LW}\right)^{1/2} + 2\left(\gamma_l^+\gamma_s^-\right)^{1/2} + 2\left(\gamma_l^-\gamma_s^+\right)^{1/2}$$ (2.11)

2.4   **The dewetting parameter**

A thermodynamically unstable polymer film can be mechanically deposited onto a substrate by spin-coating. The polymer chains become frozen in a vitrified state that stabilizes the film because the chains lose their mobility by quenching to room temperature below its glass transition temperature (T_g) or exposure to solvent vapor [64] The annealing temperature above T_g of polymeric thin film causes the film to dewet from the substrate. The dewetting dynamics is controlled by many parameters; surface energy, film thickness [47,50,51,57,58,66,67] , molecular weight [36,69] and substrate [80]

2.4.1   Surface energy

Surface energy is quantity of energy for the disruption of intermolecular bonds when a surface is created on material such as crack or rupture. The surface energy may therefore be defined as the excess energy at the surface of a material compared to the bulk. For a liquid, the surface tension (ratio of force per unit length) and the surface energy density are same definition. For example, water has a surface energy density of 0.072 J/m^2 and a surface tension of 0.072 N/m.

In recent years, one of the major interests is to understand the dynamics of dewetting process of the films; so that, the dewetting can be suppressed and the film stability can be promoted. Film stability and dewetting mechanisms involve an effective interface potential energy or the surface free energy of the film, which result from the presence of the two interfaces as shown in Figure 2.6. When surface energy between polymeric thin films and Si substrate are very different, the dewetting behavior occurs. The decreasing of surface energy difference between solid substrate and thin film enhance film stability. In addition, dewetting rate of liquid polymers is influenced by annealing temperature, annealing time and flow velocity at the solid/liquid interface.

```
┌─────────────────────────────────────┐
│         Polymeric thin film          │ ←──── SiO₂/Si
├─────────────────────────────────────┤
│                                      │
│            Si substrate              │
│                                      │
└─────────────────────────────────────┘
```
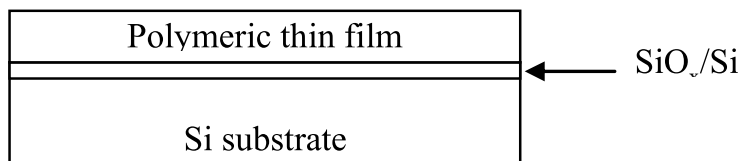
Figure 2.6. A polymeric thin film is confined between 2 interfaces; substrate and air.

2.4.2   Effect of film thickness on dewetting behavior

In addition to the surface and interfacial energy, thin film dewetting greatly depends on the film thickness [47,50,51,57,58,66,67] The quality of the films appears to rapidly degrade as the thickness of the film decreases. Bertrand, et.al [3] shown that the initial thickness of the thin films have an effect on the dewetting rate. The dewetting dynamics was inversely proportional film thickness. This can also be explained by an increasing mobility of the film. The increase in the overall mobility within the film is due to the increasing proportion of molecules that are adjacent free liquid surface, and that the mobility near this surface is greater than in the bulk. These results imply not only that the mobility of the liquid increase with decreasing solid-liquid interaction, but also that the mobility adjacent to the free surface of the film is higher than in the bulk, so that the average viscosity of the film decreases with thickness.

2.4.3   Effect of molecular weight on dewetting behavior

Dewetting dynamics depend on molecular weight of polymer matrixs and polymer additives. When molecular weight of polymer matrix is less than entanglement molecular weight of polymer, dewetting dynamics rapidly appear. Chain entanglement is the difficulty in untangling their chains, which makes polymers strong and elastic. For example, chain entanglement molecular weight of PS is around 18,000 g/mol. Henn, et al., [69] reported that increasing molecular weight of monofunctional chain could cause

chain entanglements in polymer and inhibited dewetting dynamic in thin film. This research suggested that high molecular weight of monofunction chain as polymer additive suppressed dewetting on thin film. In addition, the dewetting rate was slower for high molecular weight of polymer due to enhance viscosity with reduce dewetting dynamics. On the other hand, high molecular weight of polymer additives in thin film led to film instability. X. Li et al., [36] reported that dewetting dynamics depended on molecular weight of PMMA as additive in PS thin film. The low molecular weight of PMMA can effectively retarded dewetting in thin film more than with high molecular weight. They suggested that increasing of polymer additive aggregation increased with molecular weight and caused nucleation site, dewetting dynamics could easily appear.

2.4.4   Effect of substrate on dewetting behavior

The controlling surface morphology and stabilization on thin film depend on properties of hydrophilic and hydrophobic substrates [80,81] X. Han, et al.,[80] studied surface morphology of polymer blend film via polymer-substrate interaction with various substrate. They found that the stabilization of polymeric thin film depended on interaction between solid substrate and thin film. For hydrophilic solid substrate, the dewetting dynamics were accelerated on thin film as shown in Figure 2.7(a-b) because thin films were made of hydrophobic polymer. On the other hand, for hydrophobic silanized glass, dewetting area was less than hydrophilic solid substrate (Figure 2.7(c)). This result suggested that the different of solid substrate and thin film could enhance film instability.
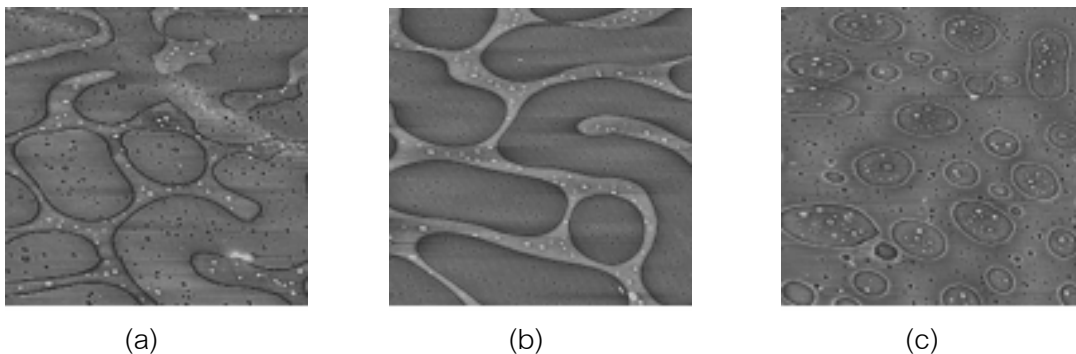
Figure 2.7. AFM image of thin films spin-coated on (a) hydrophilic (b) gold surface and (c) hydrophobic silanized glass [80]

2.5 Measurement techniques for dewetting behavior

2.5.1 Optical microscope (OM)

Optical microscope use visible light (wavelength ranging from 400-700 nm) and system of lenses, which consists of objective lenses and eyepiece lenses, to observe image surface of small samples. The processes of optical microscope let start following, visible light from source is aimed toward a lens beneath the stage, through sample, through objective lens and finally, to eye through a eyepiece lens. In this research, the magnifications of optical microscope are ranging from 5x, 10x, 20x and 50x. The application of optical microscopy is used worldwide in microelectronic, nanomaterial, biotechnology and microbiology.

2.5.2 Atomic force microscope (AFM)

Atomic force microscope (AFM) is the main microscopic method for generation of the surface topography which was invented by Gerd Binning in 1980 s. The AFM is sometime called colloidal probe technique because it can be measured substrate surface in ambient condition and colloidal particle in liquid condition. The AFM is scanning probe technique based on detection near-field force between the sharp

cantilever tip and sample. The near-field force is detected by AFM, which is divided to four types including short-rang forces, Van der Waals force, electrostatic force and capillary force. These forces are described as follow. First, short-range Forces are interactive force in pair electrons between atoms. The valence bond theory can describe short-rang forces as chemical bonds forming of shared electron between two or more atoms. These forces depend on distance between atoms and appear close to atomic spacing. The efficiency of AFM able to detect short-rang forces which are approximately 0.5-1 nN. Second, Van der Waals forces are a weak dipolar intermolecular interaction and described by the inverse square law in physics shown in equation 2.12. For AFM technique, the effect of Van der Waals forces on the objects varies by the inverse square of the distance between the sharp tip cantilever and sample.

$$F_{vdW} = \frac{HR}{6d^2}$$
(2.12)

Where H is the Hamaker constant ($\sim 10^{-19}$J), R is radius of spherical tip and d is distance between cantilever tip and sample. Next, electrostatic force is often called Coulomb force that interacts between electric charges on cantilever and specimen. The physical of electric force is long-rang force and distance of interactive force is more than shot-rang force. The last one is capillary force, which refers to surface tension force of water vapor between cantilever tip in AFM and sample. In ambient condition, capillary forces have played important in AFM technique. The decreasing of this force in system can enhance efficiency in measurement.

General force sensors in AFM consist of a cantilever and a sharp tip at the end of the cantilever. The interaction forces (e.g. Van der Waals Forces, electrostatic forces) can be determined the deflection of the sharp cantilever tip, which has a known spring constant. The elastic bending of sharp cantilever tip is detected from the reflection of

laser beam as shown in Figure 2.8. There are three types of operational modes in AFM i.e. static contact mode, dynamic non-contact mode and phase mode.
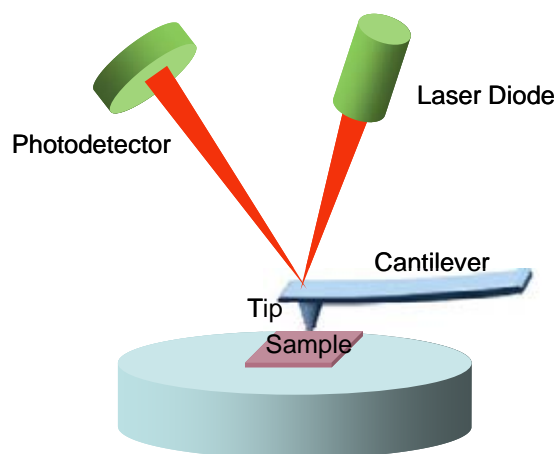
Figure 2.8. Schematic illustration of AFM

2.5.2.1 Static contact mode

In recent years, static contact mode is widely used in research. Because this mode is advantage for a small scan area and high speed scan. However, the cantilever tip in static contact mode must touch the surface sample, which can cause destruction of surface. In this mode, the tip-cantilever closes to the surface of the sample, attractive forces can be strong. Also, the stiffness of tip-cantilever or spring constant must be less than 1 N/m

2.5.2.2 Dynamic non-contact mode

Dynamic non-contact mode is similar alternating-current system (AC), which use of oscillating-tip cantilever. When tip-cantilever is vibrated at high frequency under attractive forces with surface and moves very close to the surface sample, but not touching with surface. The force between the tip-cantilever and sample surface is very low, estimated in order of pN or 10^{-12} N. The cantilever tip and sample surface are

separated in non-contact mode. Therefore, the non-contact mode is suitable for soft surface such as polymers and biological materials.

2.5.2.3 Phase mode

In phase mode, the cantilever is excited into resonance vibration with a piezoelectric driver in controller system. This phase mode imaging can be correlated with specific material properties that effect between the tip-cantilever with surface sample interaction. Also, this mode can detects differentiate areas on a surface sample with variation in composition, adhesion, viscoelasticity and other properties. The most application in phase mode is could be identification of contaminants on surface sample.

2.5.3   Contact angle measurements

The determine of interfacial surface energies are important to solve problem in materials science and pure science. However, they don't directly measure but can be determined by using contact angle. Because contact angle measurements are easy, which are separated in two types i.e. direct measurement of static and dynamics contact angle.

2.5.3.1 Direct measurement of static contact angle

The goniometer-microscope equipment, which was developed by Dr. William Zismann of United States Naval Research Laboratory in Washington .DC. is widely used to measure the contact angle of a liquid drop resting on solid surface. The equipment consists of an eyepiece, a camera and image-analysis solfware to calculate the tangent value of the capture image of droplet.

2.5.3.2 Direct measurement of dynamic contact angle

Wilhelmy plate method or the tensiometric contact angle method uses for measurement dynamic contact angle. The measurement in these method consist of thin rectangular plate or Wilhelmy plate, which is made of platinum, computer for including data and control system. For this method, dynamic equilibrium is used for expansion process as shown equation 2.13

$$F = P\gamma_{LV} \cos\theta + mg - \rho_L g \varpi H d \qquad (2.13)$$

F is force acts on the electrobalance or Wilhelmy plate. It determines from surface tension force or wetting force, gravity force and buoyancy force. Where m is mass of Wilhelmy plate, g is acceleration of gravity, ρ_L is density of liquid, ϖ is Wilhelmy plate thickness, H is plate width, d is depth of the immersion, P is perimeter of plate, γ_{LV} is surface tension of liquid and θ is contact angle. The process in this method is immersion of Wilhelmy plate in liquid, which measures surface tension with depth of immersion. The computer software concludes and analysis data, which consist of the wetting force and depth of immersion. The graph of wetting force versus depth of immersion relates to measure receding and advancing contact angle. In this technique, there are two types of contact angle i.e. advancing contact angle (θ_a) and the receding contact angle (θ_r)[45] The advancing contact angle (θ_a) is close to maximum value and the receding contact angle (θ_r) is close to minimum value of contact angle. These contact angles depend on properties of surface such as roughness, shapes and chemical structure on surface. The advancing contact angle and receding contact angle can be calculated at the sample is immersed in liquid test (Figure 2.9(c)) and withdrawn out liquid test (Figure 2.9(d)), respectively. The good point in this method, the accuracy is more than static contact angle measurement and this measurement is without human uncertainty.
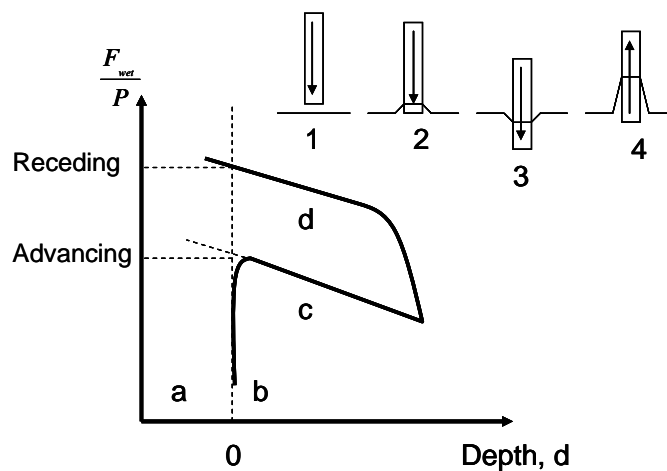
Figure 2.9. Wilhelmy plate method: a. the sample is above liquid; b. the sample touches the liquid surface; c. the sample is immersed into liquid test; d. the sample is withdrawn of liquid test [45]

2.6   Literature review on retardation of dewetting

2.6.1   Retardation of dewetting by chemical modification

In recent years, researchers have been seeking for methods to prevent the dewetting of polymeric thin films. One method involves chemical modification of polymeric chains, which leads to the increase in interfacial interaction with solid substrate.

Akhrass, et al., [25] presented that addition of photoactive additives to cross-linking PS-PDMS films could retarded dewetting of the thin films. The principle of the cross-linking process was irradiating PS-N_3 thin film under ambient conditions by an ultraviolet (UV) light with a wavelength of 365 nm. This energy was able to break up the photosensitive azide functionality (-N_3) and to create highly reactive nitrene radicals as shown in Figure 2.10. The series of the optical images indicated decrease of density and dimension of holes as UV radiation time increase are in Figure 2.11. This result

indicated that cross-linking led to macromolecule network and increased elastic force which could suppress the dewetting velocity on PS-PDMS films. However, this method inevitably altered the physical properties of the modified polymer due to the existence of ionic pendent in this system.
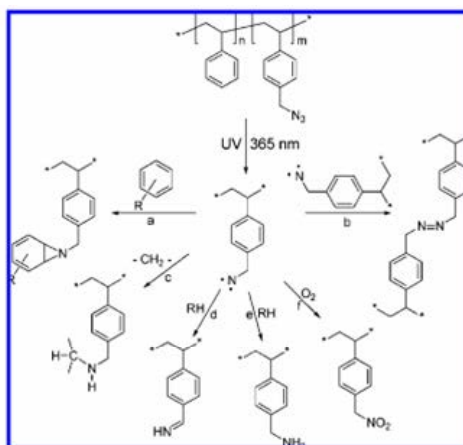
Figure 2.10. Principle of the cross-linking reaction of PS-PDMS [23]

(a)

(b)
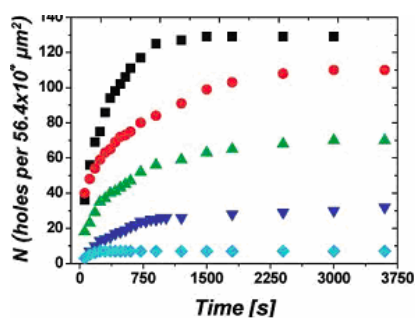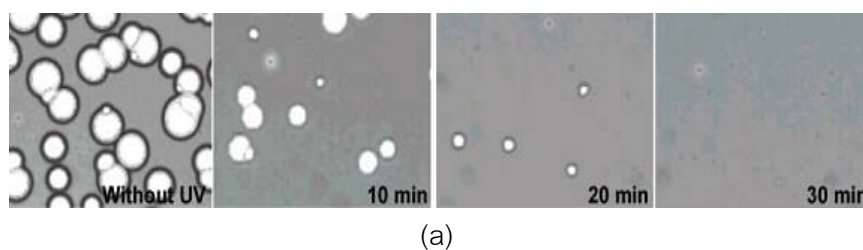
Figure 2.11. Influences of the cross-linking on film stability (a) optical images showing the decrease in dimension of holes as UV radiation time increases and (b) density of hole per area as a function of UV radiation time [25]

Gregorg, et al., [46] used a bi-functional photoactive molecule as an additive in polystyrene thin film. There were two steps for cross-linking PS by bi-functional photoactive molecule (Figure 2.12). The first step, recombination between PS and a benzophenone ketyl radical resulted in a covalent bond. This happened on both benzophenone chromophores. The second step, radicals created on PS chain by hydrogen abstraction and could recombine to form cross-links. Researchers reported that the film containing bi-functional photoactive molecule shown a less amount of holes (Figure 2.13). The mechanism for dewetting suppression was assumed to involve a photochemical cross-linking reaction that limited the mobility of the polymer chains needed to form holes. This result suggested that the dewetting was inhibited by to result in a quasi-two-dimention network.
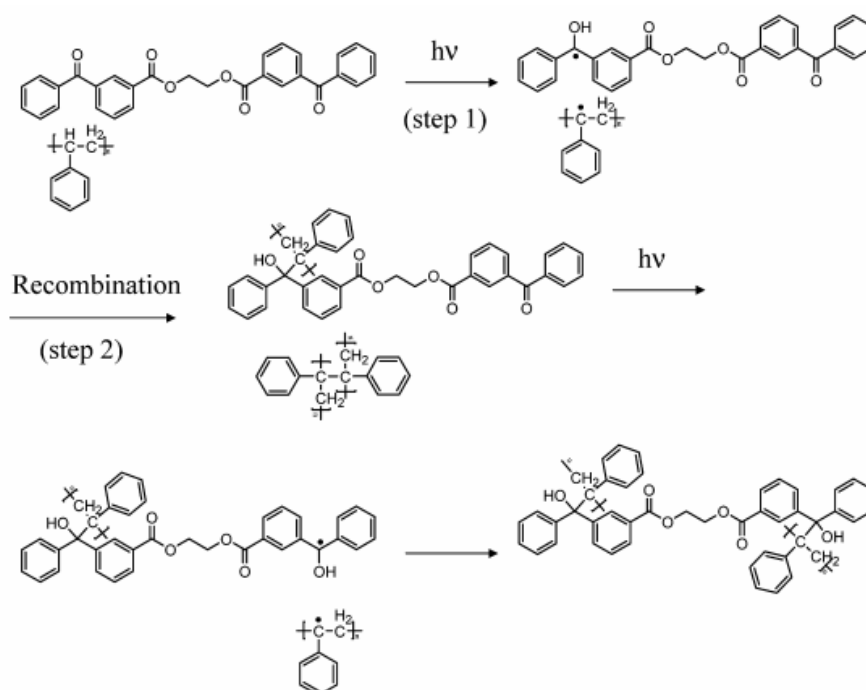
Figure 2.12. Principle of the cross-linking reaction of PS by bi-functional photoactive molecule [46]
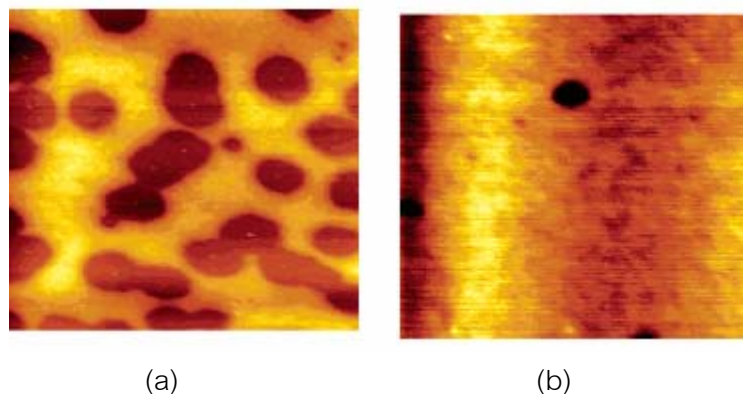
Figure 2.13. AFM topography of PS films after annealed at 170 $^{\circ}$C (a) pure PS (b) Irradiated PS film containing bi-functional photoactive molecule to PS [46]

S.H. Choi, et al., [33] studied suppression of the dewetting process of PS thin films by modifying silicon substrate surface. Si substrates were prepared by immersing into aminopropyltriethoxysilane(APTES) solution in HPLC hexane. It was found that the dewetting process of PS thin film on the APTES surface was suppressed. Hole density and hole diameters decreased compared to the control surface.

This research observed that dewetting suppression occured for the PS/APTES thin film annealed at 80 and 120 $^{\circ}$C. In addition, strong suppression was observed for PS having a molecular weight higher than entanglement molecular weight as shown in Figure 2.14. They expected that the APTES molecule could generate hydrogen bonding with hydroxyl group on silicon substrate and the hydroxylated head group in itself (Figure 2.15). In addition, PS chain can increase enough mobility due to high annealing temperature to crosslink the APTES molecule, and penetrated into APTES network while extended aminopropyl groups.
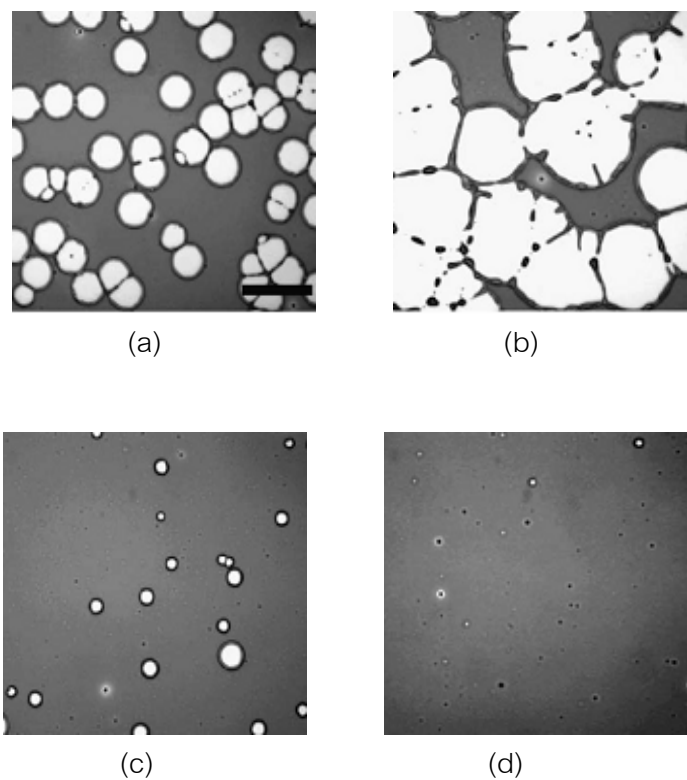
Figure 2.14. Optical image showing hole density and dimension of hole in PS films

(a) PS-9.3k on control surface (b) PS-63k on control surface, (c) PS-9.3k on APTES surface and (d) PS-63k on APTES surface [33]
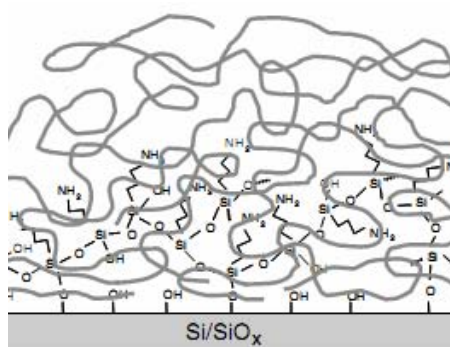
Figure 2.15. The strategy of PS/APTES interface structure for films annealed at 80 $^{\circ}$C [33]

2.6.2   Retardation of dewetting by foreign molecules or nanoparticles

The second approach for suppression the dewetting is by utilizing foreign molecules or nanoparticles as additives. The addition of molecules or nanoparticles in polymer matrix can retards dewetting behavior of polymeric thin films by enhancing the favor interactions between polymer matrix and solid substrate and a result of pining effect. The dewetting of the film can be retarded by the addition of foreign materials such as nanoparticles [10,19,20,22,27,32,35,48,49,55,60,63], homopolymers [21,36], copolymers [37,38,56,62,79] and metal/metal oxide nanoparticles[10,27,32,35]. These organic and inorganic additives are already in used for tailoring mechanical, electrical and optical properties of the polymer matrix. Additionally, the added amount is small and the additive is inert. Thus, chemical properties of the polymer matrix remain unchanged. The additives are expected to suppress the dewetting process by increasing the interfacial interaction between the film and the substrate, and providing a pinning effect followed by a decrease in hydrodynamic fluid flow process during film rupture, which result in film stabilization over a long period of time. Additives that are reported to use in PS include tetramethylbisphenol polycarbonate (TMPC) [21], polyhedral oligomeric silsesquioxanee (POSS) [19,20], carbon black and silicon dioxide nanoparticles [1,27]

Traiphol [14] reported that the incorporation of chloromethyl group into phenyl rings of polystyrene resulted in the increase of thin film stability. The existence of only 5 mol% of the chloromethyl group in the system could significantly inhibit the dewetting dynamics of ultra thin films with thickness of about 5 nm. Since the polymeric chain was slightly modified in this system, the physical property of polystyrene is hardly affected. In addition, the film stability depended on mole ratio of chloromethyl group. Increasing the chloromethyl mole ratio ranging from 20-100 mol% was found to systematically increase film stability. This result suggested that increasing of mole ratio of chloromethyl group

implied the shorter distance between chloromethyl group that led to interfacial interaction enhancement between –CH$_2$Cl group and SiO$_x$/Si substrate (Figure 2.16).
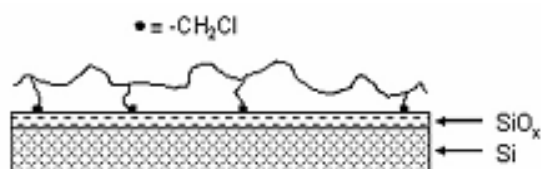
Figure 2.16. Illustration of interfacial interaction between choromethylstyrene group (–CH$_2$Cl) group and SiO$_x$/Si substrate. The choromethylstyrene group is expected to anchor on substrate while the styrene moiety favorably interacts with polystyrene matrix.[14]

Newby, et al., [47] investigated thin film behavior of poly(methyl methacrylate)/poly(styrene-ran-acrylonitrile) hybrid films with thickness ranging from 10 nm to 600 nm. They reported that the addition of random copolymer in thin films led to an inhibition of dewetting. AFM topography in Figure 2.17 showed that dewetting area of the thin films containing 75 wt% of coplymer is much smaller compared to the one with 25 wt% of copolymer on film thickness around 30-600 nm. At 50 wt% copolymer in thin films (50/50 films), dewetting dynamics were retarded for film thickness between 20-100 nm. Stable and unstable films can be indicated by the graph of roughness of the surface and interface as a function of film thickness as shown in Figure 2.18 for film contained 50 wt% of copolymer. It was clear that the stability of poly(methyl methacrylate)/poly(styrene-ran-acrylonitrile) hybrid films depended on film thickness and copolymer concentration.

(a)   (b)
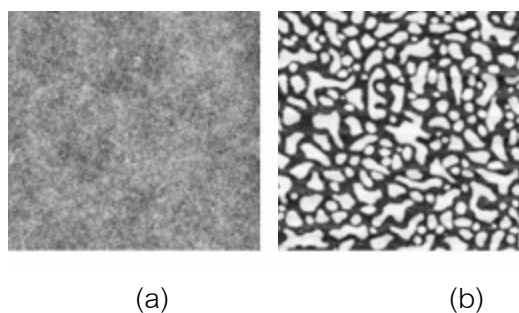
Figure 2.17. AFM topography of thin films (~60 nm thick) containing (a) 75 wt% and (b) 25 wt% random copolymer[47]
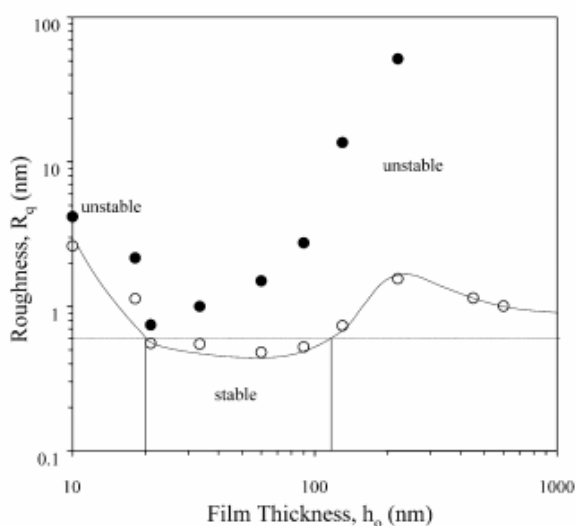
Figure 2.18. The surface and interface roughness analyzed from the AFM scan as a function of the original film thickness. Stable films can be observed for thickness values ranging from 20 to 110 nm [47]

Li, et al., [36] reports that addition of a small amount of poly(methyl methacrylate) (PMMA) into polystyrene (PS) inhibits the dewetting process of thin PS film through phase separation of the off-critical polymer mixture (PS/PMMA). The growth of hole diameter in polystyrene and PS/PMMA10 (4 wt% of PMMA) were displayed in Figure 2.19. It was clearly shown that adding 4 wt% of PMMA greatly reduced the rate of hole growth. Film dewetting was inhibited by separation of PMMA to the substrate due to higher surface energy of PMMA compared to PS. Thus, PMMA was expected to

interface between polystyrene and SiO_x/Si substrate, which changed the film structure and decreased the interfacial tension between polystyrene and substrate.
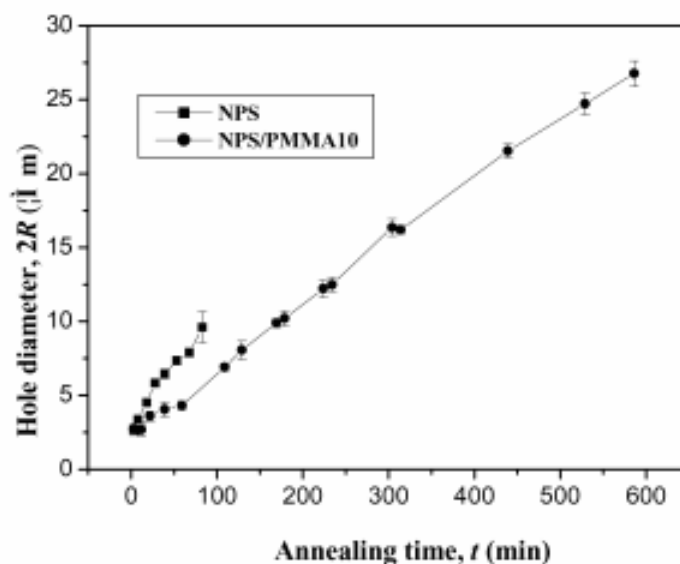
Figure 2.19. Hole diameter versus annealing time at 150°C for PS and polystyrene/PMMA 4 wt% (NPS/PMMA10) [36]

Recently, inorganic nanoparticles are very important as fillers because the desired properties such as mechanical, optical, electrical and thermal properties can be rendered to the final products. Addition of the inorganic fillers in the polymer matrix can also suppress the dewetting process. The inhibition of deweting in blended polymer films can occur because of the enrichment of the filler particles at air-polymer or polymer-substrate interfaces. The nanoparticles such as silica, gold, C_{60} fullerene, carbon nanotubes and polyhedral oligomeric silsesquioxane (POSS) were investigated in polystyrene and leaded to a drastic increase in thin film stability.

Barnes, et al., [35] used C_{60} fullerene to suppress the dewetting process in homopolymer and reported that adding a small amount of nanofiller particle in a spun-cast polystyrene thin film could reduced dewetting dynamics. Comparing at the same

annealing condition and film thickness, fullerene-filled polymer films exhibit different morphology at various additive concentration. In thin films with low fullerene concentration (0.005 wt%), the holes stopped growing and the usual hole coalescence process was greatly inhibited (Figure 2.20). This result indicated that the inhomogeneously distributed nanofillers bound to the surface and arrested the growth of dewetting regions by a result of pining effect as shown in Figure 2.21. fullerene fillers affect fluid spreading on surface. Oles were inhibited to grow and dewetting process cannot be progressed. The retardation of dewetting by a result of pining implied that the filler particles were fixed to the solid substrate resulted in a strong interaction between the nanoparticle and the substrate.

(a)　　　　　　　　　　　　　　　(b)
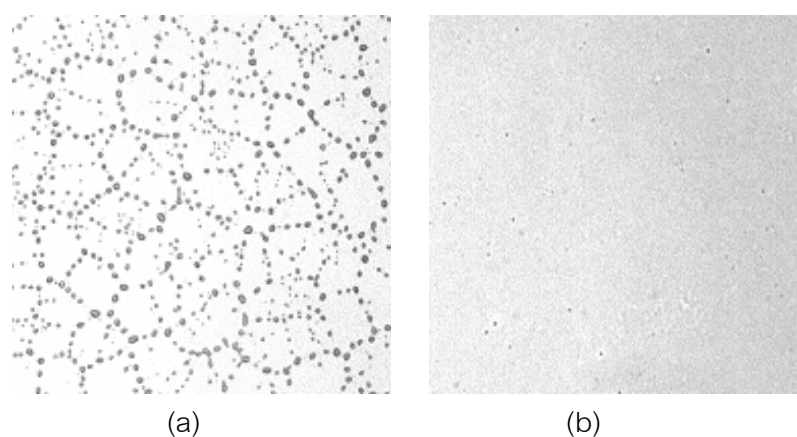
Figure 2.20. Optical images of thin films annealed at 100 $^{\circ}$C for 30 min (a) pure PS and (b) PS with C_{60} fullerene at 0.005 wt% [35]
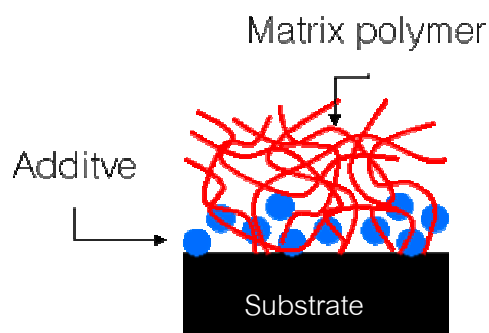
Figure 2.21. Inhibition of dewetting by pining effect.
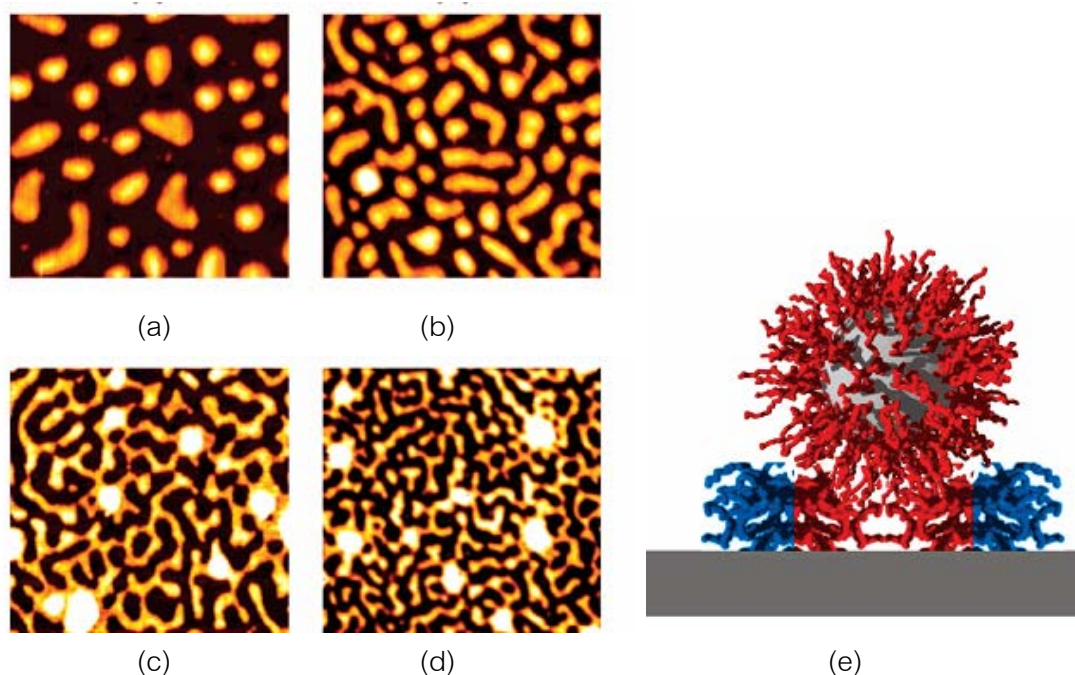
Figure 2.22. AFM topography images of polystyrene-*block*-polyisoprene diblock copolymer/ Fe_2O_3. Ratio of Fe_3O_4 are (a) 0%, (b) 1%, (c) 20%, (d) 30% and (e) Schematic side view picturing the PS masked nanoparticle sitting on top of the diblock copolymer nanostructure on solid substrate.[28]

Kashem, et al., [28] used maghemite nanoparticles (Fe_2O_3) to suppress the dewetting process in polystyrene-*block*-polyisoprene diblock copolymer and reported that dewetting process was retarded by preceding microphase separation (Figure 2.22(a-d)). These results showed that addition of nanoparticles in thin film. The nanoparticles located on top of PS-b-polyisoprene diblock copolymers, connecting the interface between the superstructure was formed and dewetting was retarded. Thin film stability was found to increase with increasing amount of nanoparticles.

H. Zhang, et al., [48] reported the use of Fe_3O_4 nanoparticles to increase stability of 2-nitro-N-methyl-4-diazonium-formaldehyde resin (NDR) thin film. Poly(methacrylic acid) (PMAA)-capped Fe_3O_4 nanoparticles were prepared by coprecipitation with PMAA in aqueous solution and introduced into the polymer matrix. Once UV irradiated, covalent bonds between the nanoparticles and polymer were fromed, which significantly

improved stability of the thin film. Reaction of the covalent bond forming was suggested in fig. 2.23.
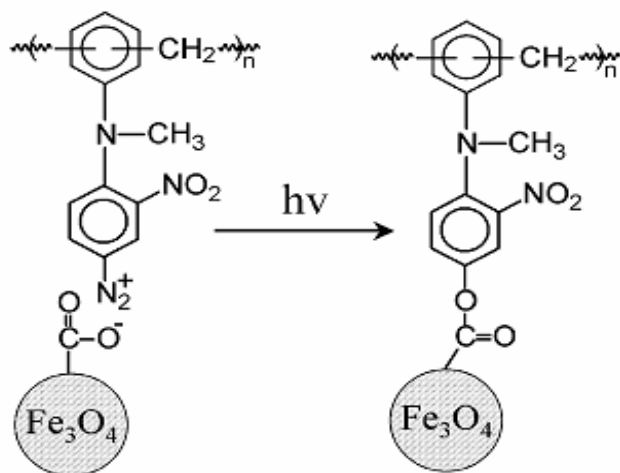
Figure 2.23. The schematic scheme of the photoreaction of NDR and PMAA-capped Fe_3O_4 nanoparticle in a self-assembled film [48]

Sharma, et al., [27] studied Si and carbon black nanoparticles as fillers in polystyrene thin film. It was found that the rim appears slightly irregular and seems to be composed of particle clusters (Figure 2.24(a)). The particles were clearly seen in the the lateral force image where they appeared darker than the surrounding polymer. After annealing for 24 h., particle at the rim of the some hole were clearly shown and the individual clusters appeared. The contrast of the particle was no longer visible in the lateral force image, indicating that they were now covered with a PS layer. This result indicated that Si nanoparticles strongly interacted with PS and inhibited dewetting by pinning effects. On the other hand, an unfavorable interaction existed between carbon black and the polymer, causing phase separation and increasing in the rate and magnitude of dewetting of the films.

(a)

(b)
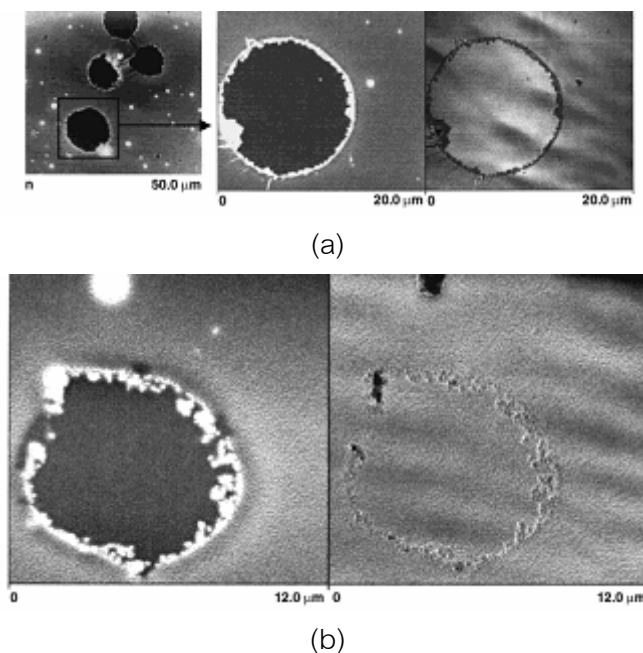
Figure 2.24. (a) AFM image of several holes on PS surface with Si particle. (b) AFM image scaned of the same hole after annealing for 24 h. The particle clusters in the rim were now clear [27].

N. Hosaka, et al., [19,20] studied the improvement of thermal stability of PS species by addition of the polyhedral oligomeric silsesquioxane (POSS), which POSS is a nanosize particle and a well-defined cluster with an inorganic silica-like core (Si_8O_{12}) surrounded by eight organic corner groups. This nanoparticle itself was an inner inorganic-organic hybrid system at the molecular level. So, with respect to other inorganic nanoparticles, it can be uniformly dispersed into a polymer as an inorganic particle without further surface modification. Hybrid nanocomposites of PS-POSS containing various POSS contents were prepared by a solution blending method. The researchers reported that, at a relatively low POSS content, a new stronger dipole-dipole interaction between POSS and the carbonyl of PMMA species and a hindrance effect of nanosize on the motion of PS molecular chain resulted in an increase Tg of the hybrid nanocomposites. At a relatively high POSS content (>0.84 mol%), the dipole-dipole interactions between the POSS and the carbonyl of the PS species decreased because

of a strong aggregation effect of POSS. This led to a decrease in Tg of the hybrid nanocomposite.

CHAPTER III

EXPERIMENTAL METHODS

3.1   Materials

3.1.1   Polymer matrix and copolymer additives

The objective of this study is to investigate effects of additives on stability of polymeric thin films under annealing condition. Our system consisted of polystyrene (PS)(M_w=34,300 g/mol, M_w/M_n=1.04) as polymer matrix, statistical copolymer poly(styrene-*stat*-chloromethylstyrene)) (P(S-ClX)) with various ratios of chloromethylstyrene group (ClMS) as additive. Ratios of ClMS group in copolymers are 5 mol% (P(S-Cl5))(M_w=33,000 g/mol, M_w/M_n=1.12), 20 mol% (P(S-Cl20))(M_w=32,900 g/mol, M_w/M_n=1.18)   and 45 mol% (P(S-Cl45))(M_w=46,000 g/mol, M_w/M_n=1.48). All polymers were purchased from Polymer source Inc. (Canada). Properties of PS matrix and copolymer additives were listed in table 3.1 and chemical structures of polymers were illustrated in figure 3.1.

Table 3.1. Properties of PS matrix and P(S-ClX) statistical copolymer additives (Appendix A)

Properties	Polystyrene (PS)	poly(styrene-*stat*-chloromethylstyrene) (P(S-ClX))		
		P(S-Cl5)	P(S-Cl20)	P(S-Cl45)
Weight-average molecular weight (g/mol)	34,300	33,000	32,900	46,000
Molecular weight distribution (M_w/M_n)	1.04	1.12	1.18	1.48
Glass transition temperature($^\circ$C) [14]	100	103	95	104
Ratios of ClMS group (mol%)	0	5	20	45
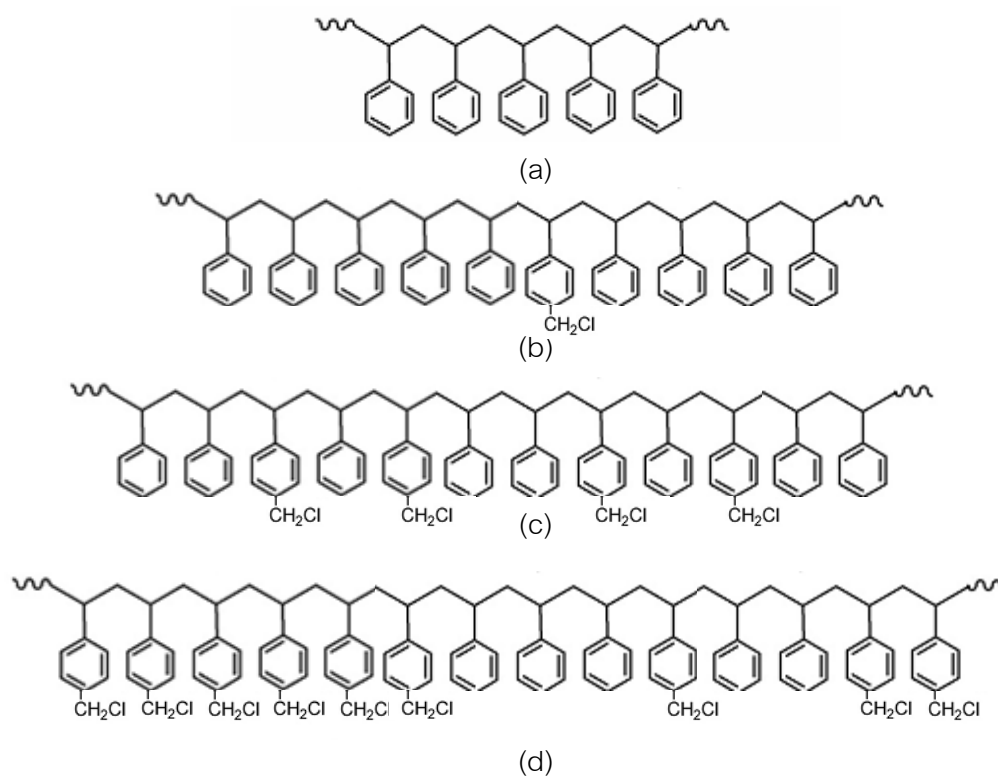
Figure 3.1 Chemical structures of (a) PS, (b) P(S-Cl5) copolymer (c) P(S-Cl20) copolymer and (d) P(S-Cl45) copolymer. The amount of PS groups within 20 repeating units of each copolymer

3.1.2 Fe_3O_4 nanoparticles

Ferric chloride anhydrous ($FeCl_3$) (M_w=162.20 g/mol) and iron (II) chloride tetrahydrate ($FeCl_2.4H_2O$) (M_w=198.83 g/mol) were purchased from Merch Schuchardt OHG (Germany) and used as reactants to synthesize Fe_3O_4 nanoparticles. Co-precipitation was employed for synthesis of Fe_3O_4 nanoparticles [59] First, $FeCl_3$ (4.98 g) and $FeCl_2.4H_2O$ (3 g) were dissolved in 120 ml of water. The mixed solution was added into a solution of ammonium hydroxide (25 wt% in water), which was used as precipitating agent. The chemical reaction is expressed in equation 3.1.

$$Fe^{2+} + 2Fe^{3+} + 8OH^- \longrightarrow Fe(OH)_2 + 2Fe(OH)_3 \longrightarrow Fe_3O_4 + H_2O \qquad (3.1)$$
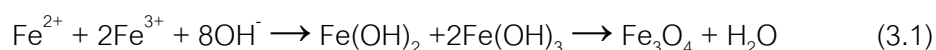
Then, the solution was stirred under an atmospheric pressure and centrifuged at 3,000 rpm. The precipitate was collected and sequentially washed with deionized water. Fe_3O_4 nanoparticles powder was obtained upon drying at 120°C for 2 h. The morphology, size and phase of Fe_3O_4 nanoparticles were examined by using transmission electron microscope (TEM)(JEM-2100, JEOL Ltd., Japan) and X-ray diffractometer (XRD) (Bruker AS, Diffraktometer D8, Germany). The Fe_3O_4 nanoparticles were sphere with ~ 9.0 nm in diameter as shown in Figure 3.2. XRD pattern of the Fe_3O_4 nanoparticles in figure 3.3 showed the phase of pure magnetite.
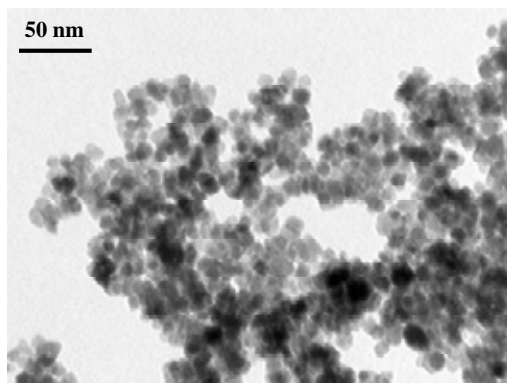
Figure 3.2 TEM micrograph of Fe_3O_4 nanoparticles
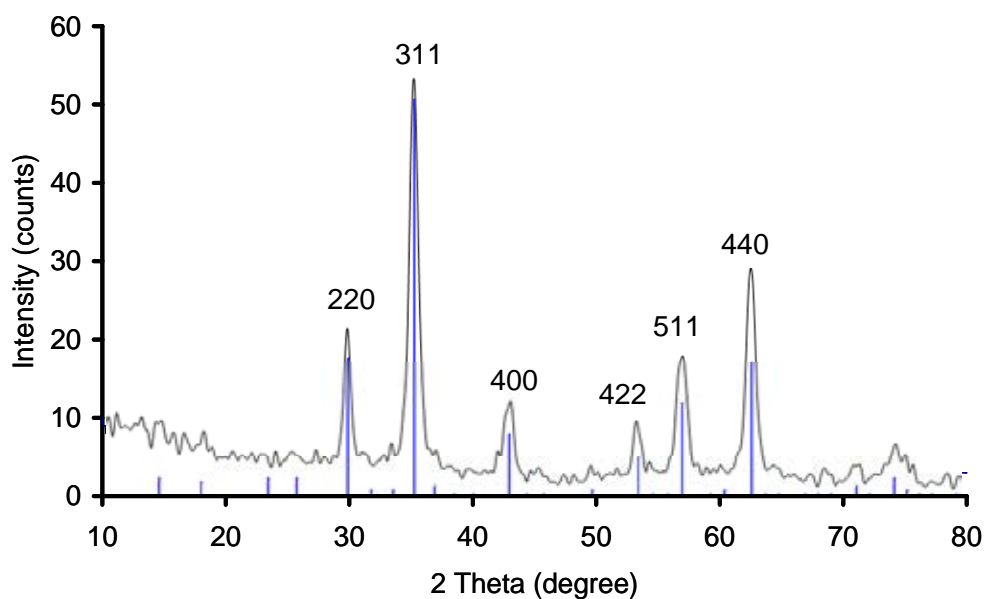
Figure 3.3 XRD pattern of Fe_3O_4 nanoparticles

3.1.3 Chemicals for cleaning silicon wafer substrates

Organic compounds, dust and lipid cover naturally on the bare silicon (Si) surface after a short period of time. The organic compounds were removed before using Si wafer as a substrate. Chemical mixture used for cleaning oxidized Si wafer substrate consists of sulfuric acid (H_2SO_4) (Acidimetric 95-97%, M 98.08 g/mol, Merck in Germany) and hydrogen peroxide (H_2O_2) (35% v/v, Vidhyasom co.,Ltd in Thailand) at 70/30 v/v. The oxidized Si wafer was cleaned in the mixed solution at 80 $^\circ$C for 1 hr. Then the Si wafer was rinsed in deionized water for several times and dried with compressed N_2 gas before using as a substrate for polymeric thin film.

3.2   Preparation of thin films

3.2.1   Preparation of PS thin films

PS solutions were prepared by dissolving the PS in toluene solution (RCI Labscan Limited, Thailand) at concentrations ranging from 0.1, 0.2 and 0.3 wt%. PS solutions were spin-coated at 1000 rpm for 10 s on Si wafer. The obtained film thickness was less than 50 nm. The annealing temperatures were above the glass transition temperatures of the PS for 30 min, 2, 12, 36 and 104 h and then quenched to room temperature by placing on a cold metal surface. The annealing temperatures were varied with film thickness. Since the dewetting rate of polymeric thin film decreased with increasing film thickness, annealing temperature for the thicker films was increased to observe dewetting dynamics in a reasonable time. Therefore, this research used annealing temperatures of 120 and 165 $^\circ$C for 5 and 11-17 nm thick PS films, respectively.

3.2.2   Preparation of P(S-ClX)/PS thin film

P(S-ClX)/PS solutions were prepared by mixing PS with P(S-ClX) copolymers in toluene at solution concentrations ranging from 0.1, 0.2 and 0.3 wt%, which yielded film thickness between 5-17 nm. P(S-ClX) with ratios of ClMS group ranging from 5, 20 and 45 mol% were added at concentrations ranging from 0-40 wt% of copolymer. The P(S-ClX)/PS solutions were spin-coated at 1000 rpm for 10 s on oxidized Si wafer. All films were annealed in vacuum oven at 120 and 165°C for 5 nm and 11 nm thick films, respectively. Increasing annealing temperature could accelerate dewetting rate and allow observation of dewetting behavior on thin films. Annealing temperatures were above the glass transition temperatures of the PS and the statistical copolymer. Annealing times were 30 min, 2, 12, 36 and 104 h. After that, the films were quenched to room temperature by placing on a cold metal surface.

3.2.3 Fe_3O_4 nanoparticles/PS thin films

PS solutions and Fe_3O_4 nanoparticles solutions were separately prepared at concentrations of 0.1, 0.3 and 0.6 wt% in toluene. Fe_3O_4 solutions were sonicated in ultrasonic bath for 30 min and mixed with ultrasonic probe for 5 min. After that the Fe_3O_4 solutions were settled for 5 min to precipitate the large agglomerates, leaving nanosize particles in the clear supernatant. Then, Fe_3O_4/PS solutions were prepared by mixing PS solution with supernatant containing Fe_3O_4 nanoparticles at 5, 10, 20 and 30 wt% supernatant. The mixed solutions were used to prepare thin films by spin coating on SiO_x/Si substrate, which described in details later on.

To prove the presence of Fe_3O_4 nanoparticles and determine the corresponding actual concentration in thin film, TGA and UV-vis were employed.(Perkin Elmer, TGA7HT) For TGA analysis, the Fe_3O_4 /PS solutions were dried at $100^{\circ}C$ for 2 h. The received Fe_3O_4/PS powder was analyzed with TGA in condition of temperature ranging from 200-500 $^{\circ}C$. The result for solution containing 50 wt% supernatant was shown in Figure 3.4. It was found that percentage of mass loss of PS in Fe_3O_4/PS powder was 99.95 %. Therefore, the corresponding actual concentration of Fe_3O_4 in the solution is 0.05 wt%.
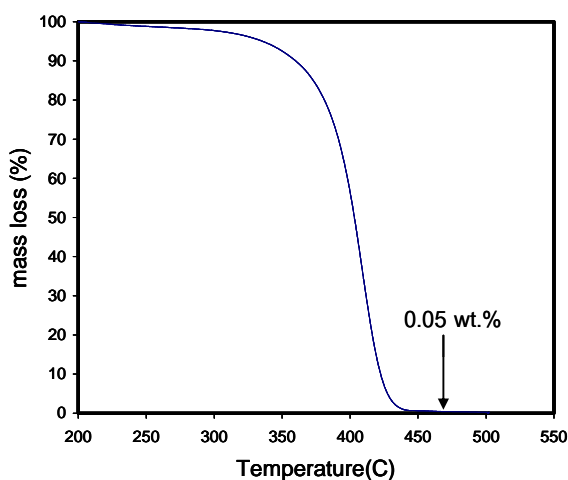
Figure 3.4 TGA result of Fe_3O_4/PS (50/50 w/w) operating in air showing the residual mass.

In this research, UV-VIS spectroscopy was used to determine the presence of Fe_3O_4 nanoparticles in Fe_3O_4/PS solutions, using PS in toluene as a reference. Absorption peak was found at 247 nm, showing the existence of Fe_3O_4 nanoparticles. Since the solutions were clear, peaks at visible ranges (400-700 nm) were not observed as shown in Figure 3.5.

(a)

(b)

(c)

(d)
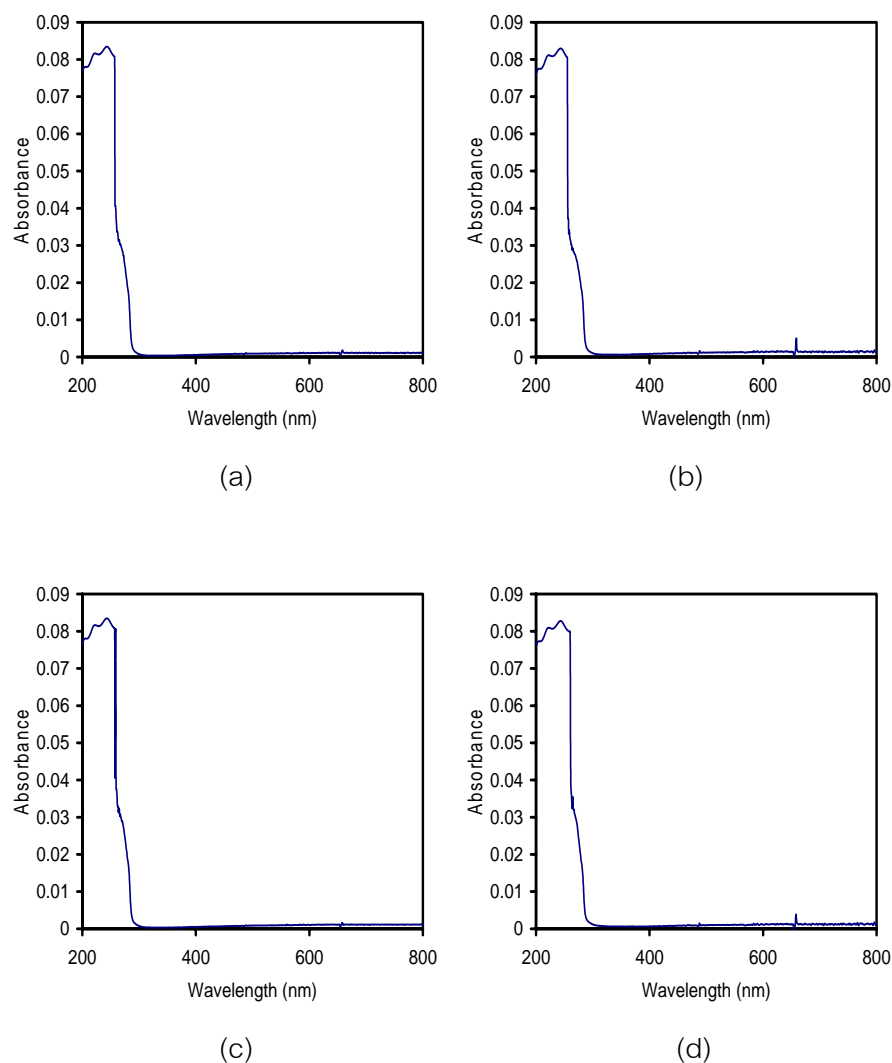
Figure 3.5 UV–visible absorption spectrum of Fe_3O_4/PS solutions prepared with (a) 5 wt.% (b) 10 wt.% (c) 20 wt% and (d) 30 wt% of supernatant containing Fe_3O_4 nanoparticles.

The Fe$_3$O$_4$/PS thin films were fabricated from Fe$_3$O$_4$/PS solutions of concentrations of 0.1, 0.3 and 0.6 wt%, which yielded film thickness between 5-38 nm. The Fe$_3$O$_4$/PS thin films were prepared by spin coating at 1000 rpm for 10 s on Si wafer. All films were annealed in vacuum oven at annealing temperatures above the glass transition temperature of PS which were 120, 165 and 180°C for 5 nm, 17 and 38 nm thick films, respectively. Annealing times were ranging from 20 min to 1 h. The films were periodically quenched to room temperature. The morphology of Fe$_3$O$_4$/PS ~38 nm thick film containing 0.03 wt% Fe$_3$O$_4$ nanoparticles annealed at 180 $^{\circ}$C for 60 min is shown in Figure 3.6. AFM images of the annealed Fe$_3$O$_4$/PS films showed a phase separation in thin films. The diffusion of Fe$_3$O$_4$ nanopartices to form agglomerates was expected to cause film instability.
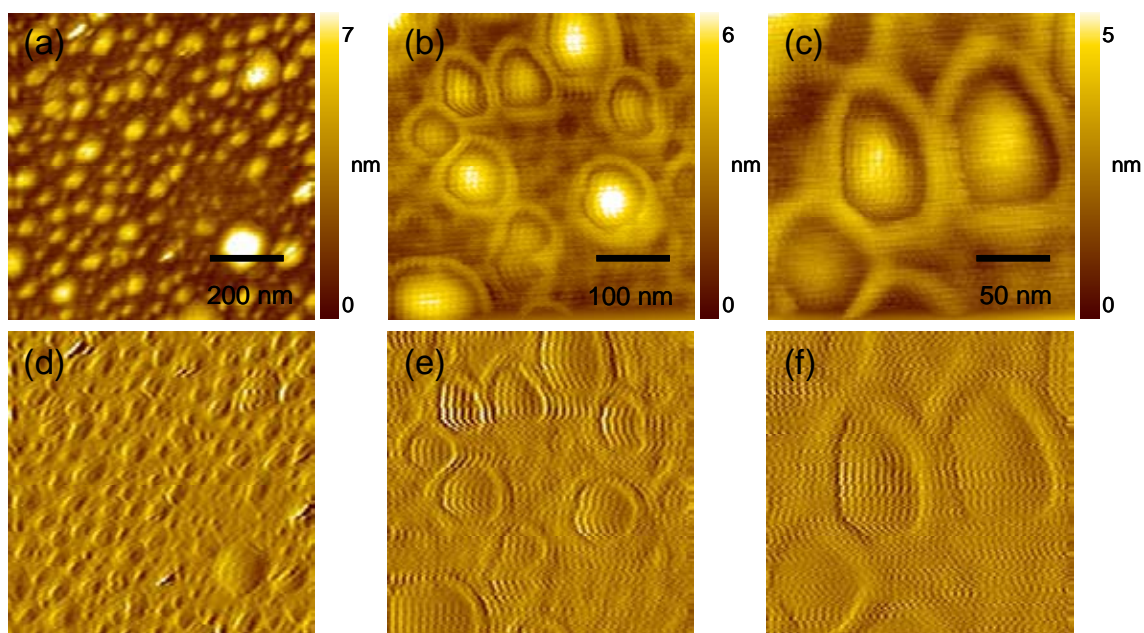
Figure 3.6 (a)-(c) AFM topography image of~38 nm thick Fe$_3$O$_4$/PS films annealed at 180 $^{\circ}$C for 60 min and (d)-(e) corresponding AFM phase images of AFM topography, respectively

3.3   Characterization of thin films

3.3.1   Surface topography and dewetting area

In our research, atomic force microscopy (AFM) and optical microscopy (OM) were used to study surface topography of polymeric thin films of thickness less than 100 nm. AFM is a very high-resolution type of scanning probe microscopy. The resolution is the same as scanning tunneling microscopy and transmission electron microscopy which is on the order of nanometer. The magnification of images in AFM is more than 1000 times better than the optical microscope limit. AFM technique provides three dimensional images of sample and could generate the resulting map of the area which represented the topography of the sample. In addition, AFM could work completely in ambient air or a liquid condition.

Stability of P(S-ClX)/PS and Fe_3O_4/PS thin films at various annealing times were detected by AFM. Morphology of thin films was investigated by intermittent contact AFM (SPI3800N Nanoscope II, Seiko Instrument Inc., Japan) under ambient conditions. In this work, the cantilevers were fabricated from Si_3N_4 with a spring constant of about 20 N/m. All samples were scanned with different scan ranges i.e., 150 µm✕150 µm to 5 µm✕5µm to reveal topography of samples at different length scales. Hole diameter and depth of hole can be detected, then dewetting area and roughness can be analyzed by extended Grain analysis in AFM software as shown in figure 3.7.

In addition, surface topography was examined by OM (WV-F15HSE, Matsushita Communication Industrial Co.,Ltd., Japan). Although, magnification of OM was less than AFM technique, OM could confirmed the results by larger area. Magnifications of 5x, 10x, 20x and 50x were used to observe surface topography in ambient air condition. Steps of dewetting process were investigated and dewetting area can be calculated by using equation 3.2 after process the image with a commercial picture adjusting

program. For example, the dewetting area and total area in OM image in figure 3.8(a) were process by record measurement analysis in Adobe® Photoshop program as shown in figure 3.8(b). After that, percentage of deweting area was calculated by using equation 3.2

$$dewetting\ area\left(\%\right) = \frac{dewetting\ area}{total\ area} \times 100 \qquad (3.2)$$

Furthermore, film thickness (ΔZ) could be detected by using surface analysis in AFM software [82-84] as shown in figure 3.9. The process of measurement of film thickness is on the following steps.

Step 1: Needles (Hypodermic needle regular wall, NIPRO) with diameter of 0.4 mm and length of 25 mm were immersed in toluene.

Step 2: The needles were used to make multiple scratches in various direction on homogeneous polymeric thin film.

Step 3: Surface analysis software in AFM was used to measure film thickness by scanning a scratch in straight line as shown in figure 3.9(a). The software measured the differential in vertical axis (ΔZ) which was determined as film thickness.

(a)   (b)
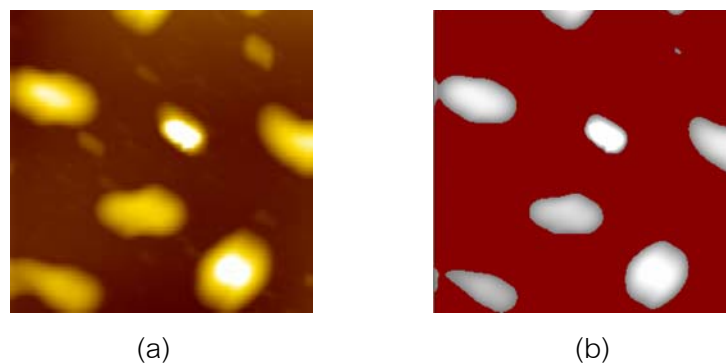
Figure 3.7. AFM topography (a) before and (b) after using extended Grain analysis software

<div align="center">(a)   (b)</div>
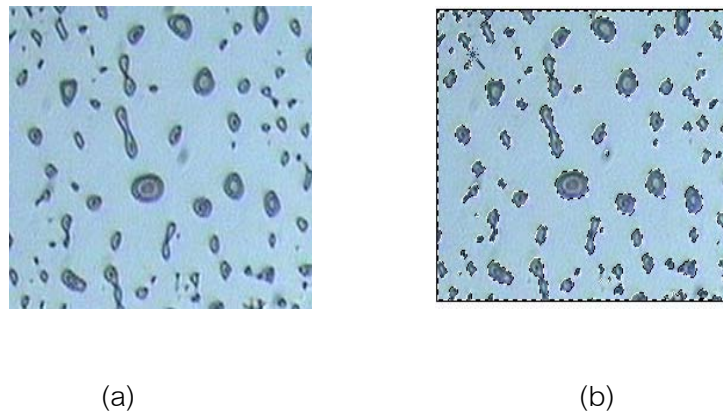
Figure 3.8.OM images (a) before and (b) after using a picture adjusting program.

<div align="center">(a)   (b)</div>
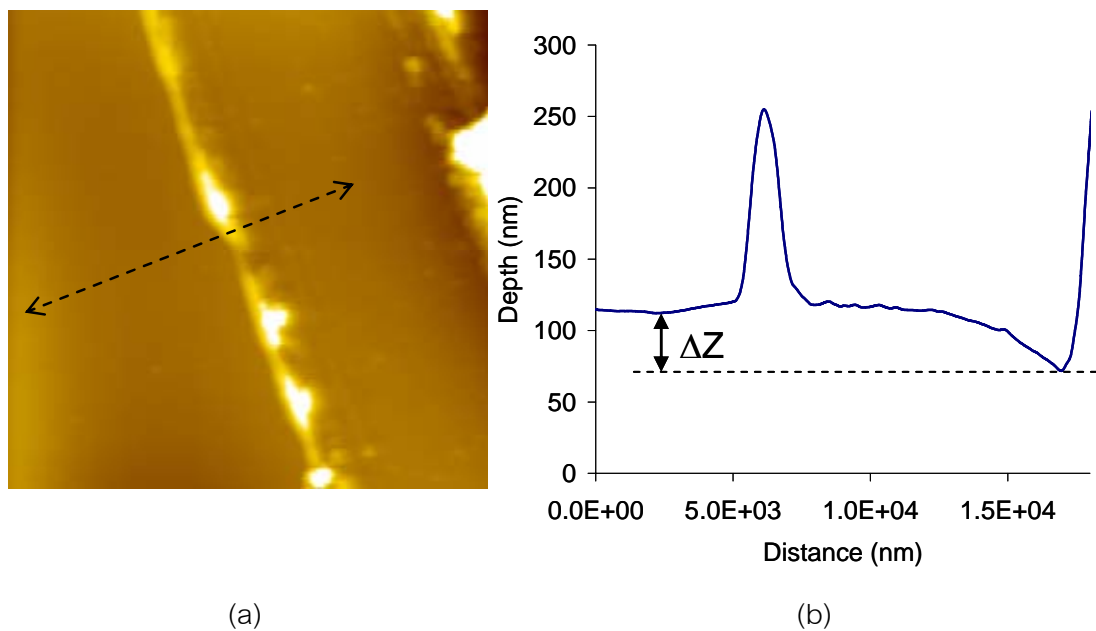
Figure 3.9. Film thickness measurement (a) AFM topography and (b) depth profile (ΔZ) from software analysis.

3.3.2   Contact angle and surface energy

Contact angle measurement detects the angle between liquid drop and substrate, which sometime was called drop shape analysis. The contact angle was the angle at which a liquid/vapor interface contacted a solid surface. The contact angle measurement can be used to determine surface energy or surface tension on substrate.

In this research, contact angle meter (CAM-PLUS Tantec, U.S. Pantent, USA) was used to measure contact angle(θ) of solid i.e. polystyrene thin film, poly(vinyl benzyl chloride) thin film and Si wafer substrate. Then surface energy, which is an important factor to describe the film stability could be determined using Owens-Wendt-Kaelble approach as shown in equation 3.3

$$\gamma_l(1+\cos\theta) = 2\sqrt{\gamma_s^d \gamma_l^d} + 2\sqrt{\gamma_s^h \gamma_l^h}$$

(3.3)

Where γ_l is surface tension of films, θ is contact angle, γ_s^d is dispersive surface tension component of solid substrate, γ_l^d is dispersive surface tension component of film, γ_s^h is surface tension component due to hydrogen bonding and dipole-dipole interaction of solid substrate and γ_l^h is surface tension component due to hydrogen bonding and dipole-dipole interaction of film.

Table. 3.2 liquid surface tension components of water and diiodomethane [42]

Liquid	γ_l (mJ/m^2)	γ_l^d (mJ/m^2)	γ_l^h (mJ/m^2)
Deionized water	72.7	21.8	50.9
Diiodomethan	50	50	0

Table. 3.3 Contact angles of water and diiodomethane

Type of Surface	Contact angle (degree)	
	Deionized water	Diiodomethane
SiO$_x$/Si	43±2	37±3
PS	86±1	22±2
P(CIMS)	72±2	31±3

The data in table 3.2-3.3 were used to calculate the surface energy of solid substrate. For example, surface energy of silicon substrate was calculated by using equation 3.3. Substitution of surface tension of diiodomethane and water in equation 3.3 as represented in equation 3.4 and 3.5, respectively could solve γ_S^d and γ_S^h which were 40.4 and 21.7, respectively.

$$50(1 + \cos 37) = 2\sqrt{50 \times \gamma_S^d} + 2\sqrt{0 \times \gamma_S^h} \qquad (3.4)$$

And

$$72.7(1 + \cos 43) = 2\sqrt{21.8 \times \gamma_S^d} + 2\sqrt{50.9 \times \gamma_S^h} \qquad (3.5)$$

Experimental diagram

| PS solutions PS concentrations 0.1-0.3 wt.% | P(S-ClX)/PS solution X=5, 20 and 45 mol% Copolymer concentrations 10-40 wt.% | Fe_3O_4 nanoparticles/PS solution Fe_3O_4 concentrations 0.005- 0.03 wt.% |

Spin casting
1000 rpm 10 s

Spin casting
1000 rpm 10 s

Spin casting
1000 rpm 10 s

| PS films Thickness 5, 11, 17 nm | P(S-ClX)/PS films Thickness 5, 11, 17 nm | Fe_3O_4 nanoparticles/PS films Thickness 5, 17, 38 nm |

Annealing at 120 and 165 °C
For 0.5, 2, 12, 36, 104 h

Annealing at 120 and 165 °C
For 0.5, 2, 12, 36, 104 h

Annealing at 120, 165 and 180 °C
For 20, 40 and 60 min

•Study of dewetting process and film stability
-AFM (scan ranges 25 µm × 25 µm to 1 µm × 1 µm)

⟶ Topography
⟶ Hole diameter
⟶ Hole depth
⟶ Roughness
⟶ Dewetting area

-OM (magnification 5, 10, 20, and 50)
⟶ Dewetting area

•contact angle measurement
-contact angle meter (air ambient condition)

⟶ contact angle
⟶ surface energy

CHAPTER IV

RESULTS AND DISCUSSIONS

4.1. Surface energies

In this research, Owens-Wendt Kaelble approach detailed in 2.3 is used for surface energy calculation. This approach explains total energy (γ_s) which consists of dispersion energy (γ^d) and polar interaction (γ^h) on surface. According to this approach, the surface energies of PS, PCIMS and SiO$_x$/Si substrate are evaluated and summarized in Table 4.1. In this research, the surface energy of PS is close to Neumann's method which is approximately 42 mJ/m^2[45] The SiO$_x$/Si substrate exhibits higher surface energy compared to that of PS. In general, if the surface energies of thin film and solid substrate are very different, thin film will break up into holes. The total surface energies of PCIMS and PS are comparable. It is indicated that both polymers can mix well and polymeric thin films are homogeneous. The existence of CIMS group causes the increase of the polar component (γ_s^h). Therefore, it is expected that the addition of copolymers containing CIMS group into PS film enhances the interfacial dipolar interaction with SiOx/Si substrate.

Table. 4.1 Solid surface tension components of SiOx/Si, polystyrene and poly(chloromethylstyrene) calculated from contact angles of water and diiodomethane using the Owens-Wendt-Kaelble approach

Type of Surface	γ_s (mJ/m^2)	γ_s^d (mJ/m^2)	γ_s^h (mJ/m^2)
SiO$_x$/Si	62.1	40.4	21.7
Polystyrene (PS)	47.4	46.4	1.0
Poly(chloromethylstyrene) (PCIMS)	48.7	43.1	5.6

4.2. Effects of P(S-Clx) copolymers on film stability

4.2.1 Dewetting behavior of PS thin film

In general, the dewetting of PS thin film proceeds through several stages upon annealing above the glass transition temperature [1,4-6]. The dewetting begins with the breaking of continuous film into small holes induced by capillary fluctuation and interfacial heterogeneity. The holes expand with the increase of annealing time and eventually merge into each other, forming interconnected structures. In final stage, the structures disintegrate into hemispherical droplets, where the interfacial interactions between polymer and solid substrate are determined by their contact angle [42].

The dewetting behavior of pure PS film is presented in the first section as a control set of the experiment. Figure 4.1 shows AFM topography images of ~5 nm thick pure PS films before (Figure 4.1(a)) and after annealed at 120 ^{o}C for various times (Figure 4.1(a-e)). Annealing of pure PS film for 30 min (Figure 4.1(b)) causes the formation of large holes with the diameter of > 0.5 μm and the depth ranges from 5 to 6 nm. A number of randomly-distributed small holes, corresponding to an early stage of dewetting, can also be observed on the sample. Their width and depth are ~0.1-0.6 μm and ~1.4-3.2 nm, respectively. Numbers and dimensions of the holes increase with increasing annealing time to 2 h (Figure 4.1(c)) and 12 h (Figure 4.1(d)). The PS droplets are detected when the annealing time reaches 36 h (Figure 4.1(e)). The droplet height is in the range of 36-50 nm.
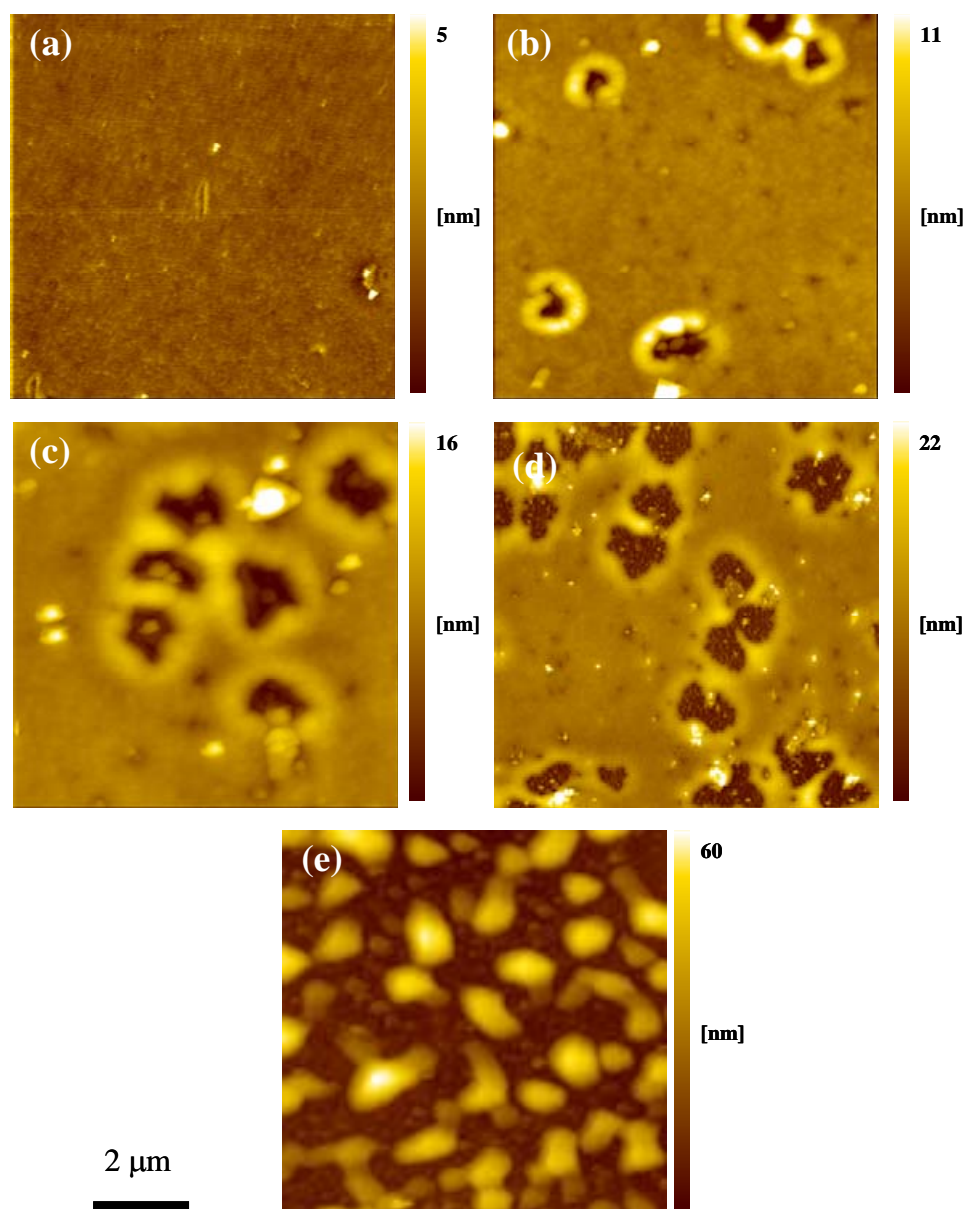
Figure 4.1. AFM topography images of ~5 nm thick pure PS films (a) before annealed and (b)-(e) after annealed at 120 °C for 30 min, 2 h, 12 h and 36 h, respectively.

4.2.2   Effect of P(S-Cl5) copolymer

In this research, blend films are prepared using P(S-Cl5) copolymer at concentrations of 10, 20, 30 and 40 wt% which are corresponding to ClMS group concentration of 0.5, 1.0, 1.5 and 2.0 mol%, respectively. Figure 4.2 illustrates the surface morphology of thin films containing different ratios of the P(S-Cl5) copolymer before annealing process. Surface morphology of all films is homogeneous and smooth. In annealing process, all films are annealed at 120 °C above Tg of PS thin film. It is found that surface morphology of films annealed for 30 min start to dewet as shown in Figure 4.3. A number of randomly-distributed small holes, corresponding to an early stage of dewetting, can be observed on the samples. The dewetting area of thin films containing of P(S-Cl5) copolymer at concentration of 0, 10, 20, 30 and 40 wt.% are around 3.0±0.8, 2.8±1.0, 3.3±1.0, 3.1±1.0 and 1.4±0.4%, respectively. At 30 min annealing time, the dewetting areas of all films are similar and retardation of dewetting dynamics by the addition of P(S-Cl5) copolymer is not obvious. When increasing annealing time to 2 h, the dewetting area on thin films containing various ratios of P(S-Cl5) copolymer are clearly different as shown in Figure 4.4. The dewetting areas are approximately 9.0±1.0, 7.0±1.5, 4.0±0.3, 4.4±0.3 and 2.0±0.4% on thin films containing P(S-Cl5) copolymer ratios ranging from 0-40 wt.%, respectively. This result obviously shows that adding P(S-Cl5) copolymer into PS thin films enhance film stability.

To accelerate flow dynamic of polymeric thin film, annealing time is increased to 12 h. It is clear that the dewetting dynamics slow down significantly when the P(S-Cl5) copolymer is added into the PS film. Figure 4.5 illustrates the surface morphology of thin films containing different ratios of the copolymer. In the pure PS film (Figure 4.5(a)), irregular-shaped holes with diameter of ~1 μm are observed with nanodroplets inside the holes. The width and height of the nanodroplets are 42±8 nm and 2.5±0.7 nm, respectively. The nanodroplets reflect the existence of the so called "mesolayer" (intermediate layer) near solid interface. Nature of the mesolayer and its dewetting

behavior were discussed in details in the literatures [13,32] The mesolayer also play a significant area in the interfacial interaction between layers. Increasing of the interaction between substrate and film layers in the mesolayer arises film stability. The addition of 10 wt% copolymer into PS film hardly improves the suppression of dewetting process although the dewetting area slightly decreases. Irregular-shaped holes and nanodroplet can still be observed (Figure 4.5(b)). The diameter of hole is similar to that of pure PS film. Increasing of the copolymer ratio to 20 wt% causes a drastic suppression of the dewetting dynamics. As shown in Figure 4.5(c), the holes detected in the film are 0.5±0.1 μm in diameter and 3.6±0.7 nm in depth. It is clear that the diameters of holes are much smaller compared to those of pure PS film subjected to the same annealing condition. In fact, the pure PS film annealed for 30 min already exhibits the formation of much lager holes (Figure 4.3(a)). The result demonstrates that the addition of 20 wt% of the copolymer leads to a significant increase in polystyrene film stability. It is important to note that only ~1 mol% of ClMS group exists in this film. Therefore, one can expect the minimal perturbation of other physical properties of system i.e. glass transition temperature. Further increasing the copolymer ratios to 30 and 40 wt% the consistent results of dewetting suppression can be obtained. As shown in Figure 4.5(d), the width and depth of hole detected in the film containing 30 wt% of the copolymer are 0.4±0.05 μm. and 2.1±0.9 nm, respectively. Further decrease in numbers and dimension of holes is observed when the copolymer ratio is increasing to 40 wt% (Figure 4.5(e)). From the analyses of hole dimensions, it is clear that the stability of PS thin film systematically increases with ratio of the copolymer.

To gain more information about the stability of these films, the annealing time is increased to 36 and 104 h. Figure 4.6 illustrates AFM topography images of the polymeric films annealed for 36 h. the pure PS film already breaks up into droplets while the film containing 10 wt% of the copolymer partially dewets the substrate as shown in Figure 4.5(a) and (b), respectively. Although the holes slightly expand in the films containing 20 to 40 wt.% of the copolymer, the films are still intact at this annealing

condition (Figure 4.5(c-e)). Further increasing the annealing time to 104 h as shown in Figure 4.7 still does not cause the total dewetting of the film containing 10 wt.% of the copolymer (Figure 4.7(b)). Other films containing higher ratios of the copolymer are hardly affected. These results show that the addition of P(S-Cl5) copolymer into the PS film can delay the dewetting dynamics significantly.
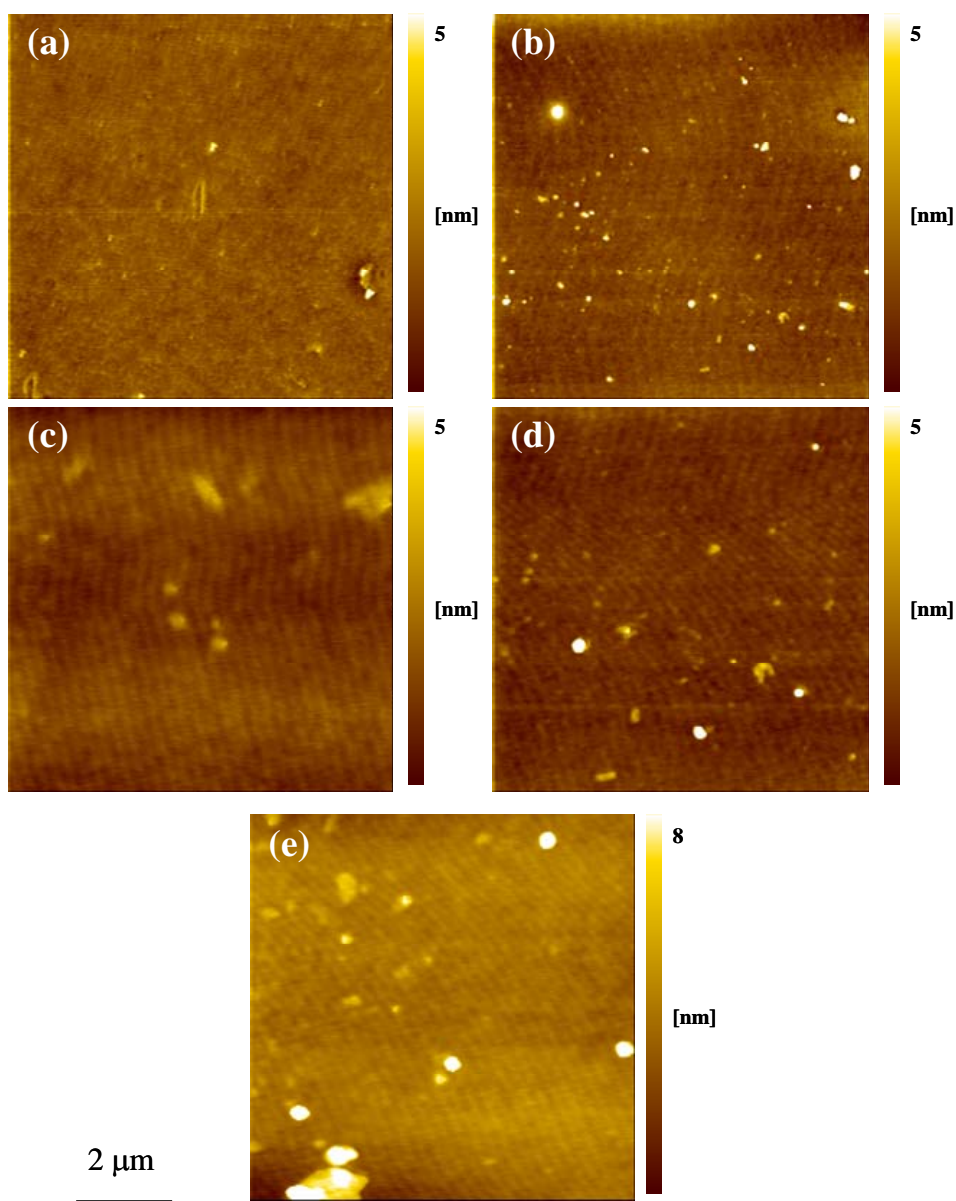
Figure 4.2 AFM topography images of ~5 nm thick P(S-Cl5)/PS films before annealed. Ratios of P(S-Cl5) copolymer are (a) 0 wt%, (b) 10 wt%, (c) 20 wt%, (d) 30 wt%, and (e) 40 wt%.
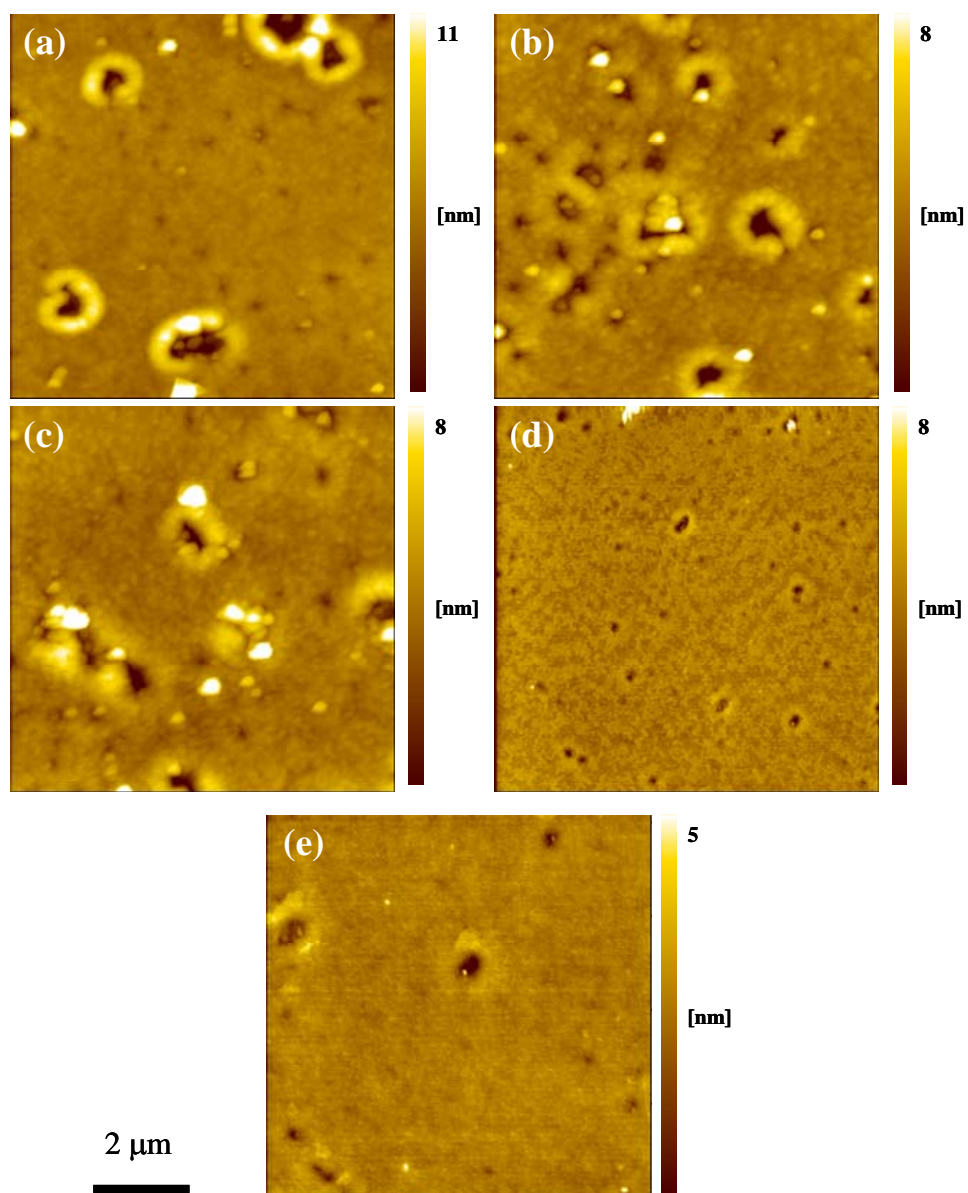
Figure 4.3 AFM topography images of ~5 nm thick P(S-Cl5)/PS films annealed at 120 $^{\circ}$C for 30 min. Ratios of P(S-Cl5) copolymer are (a) 0 wt%, (b) 10 wt%, (c) 20 wt%, (d) 30 wt%, and (e) 40 wt%.
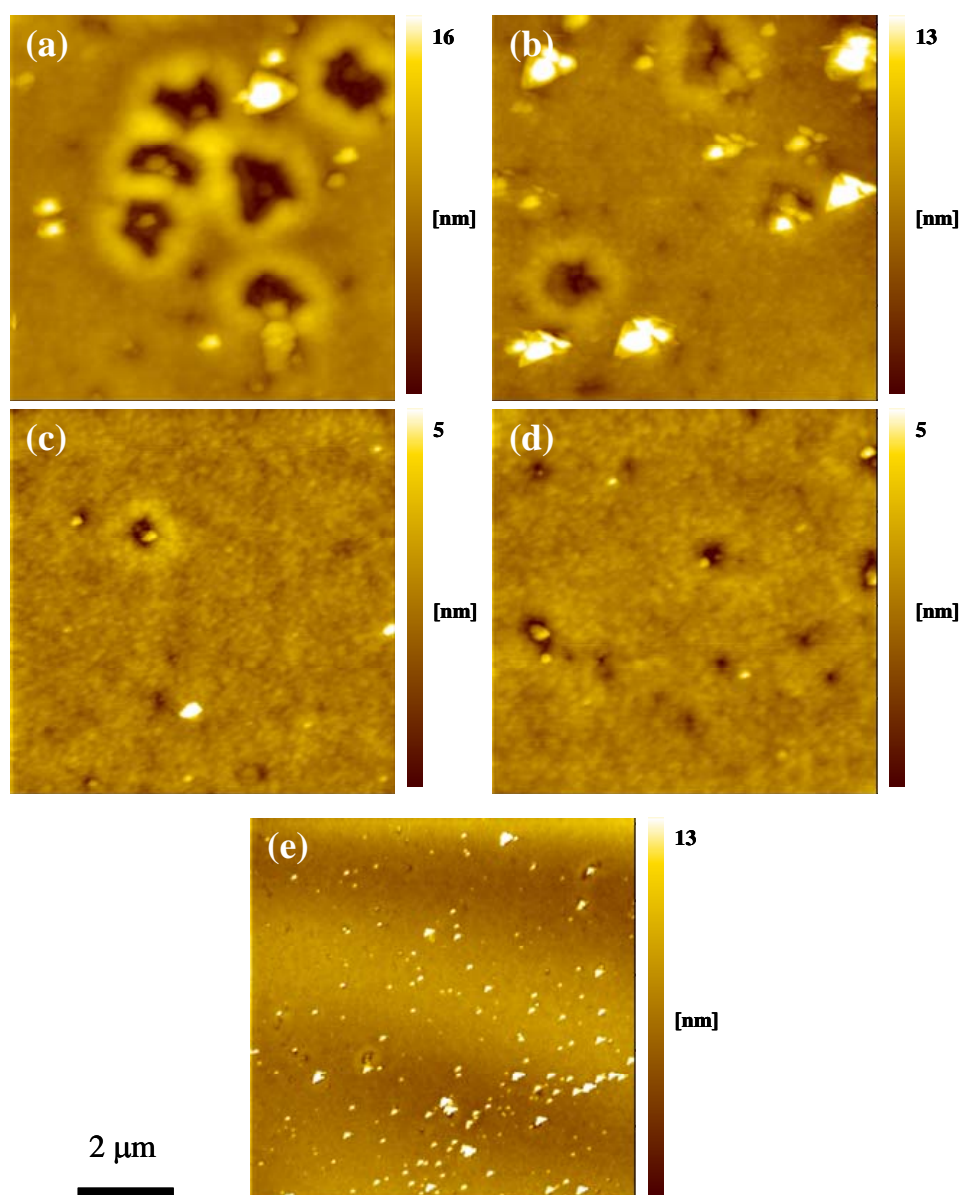
Figure 4.4 AFM topography images of ~5 nm thick P(S-Cl5)/PS films annealed at 120 °C for 2 h. Ratios of P(S-Cl5) copolymer are (a) 0 wt%, (b) 10 wt%, (c) 20 wt%, (d) 30 wt%, and (e) 40 wt%.
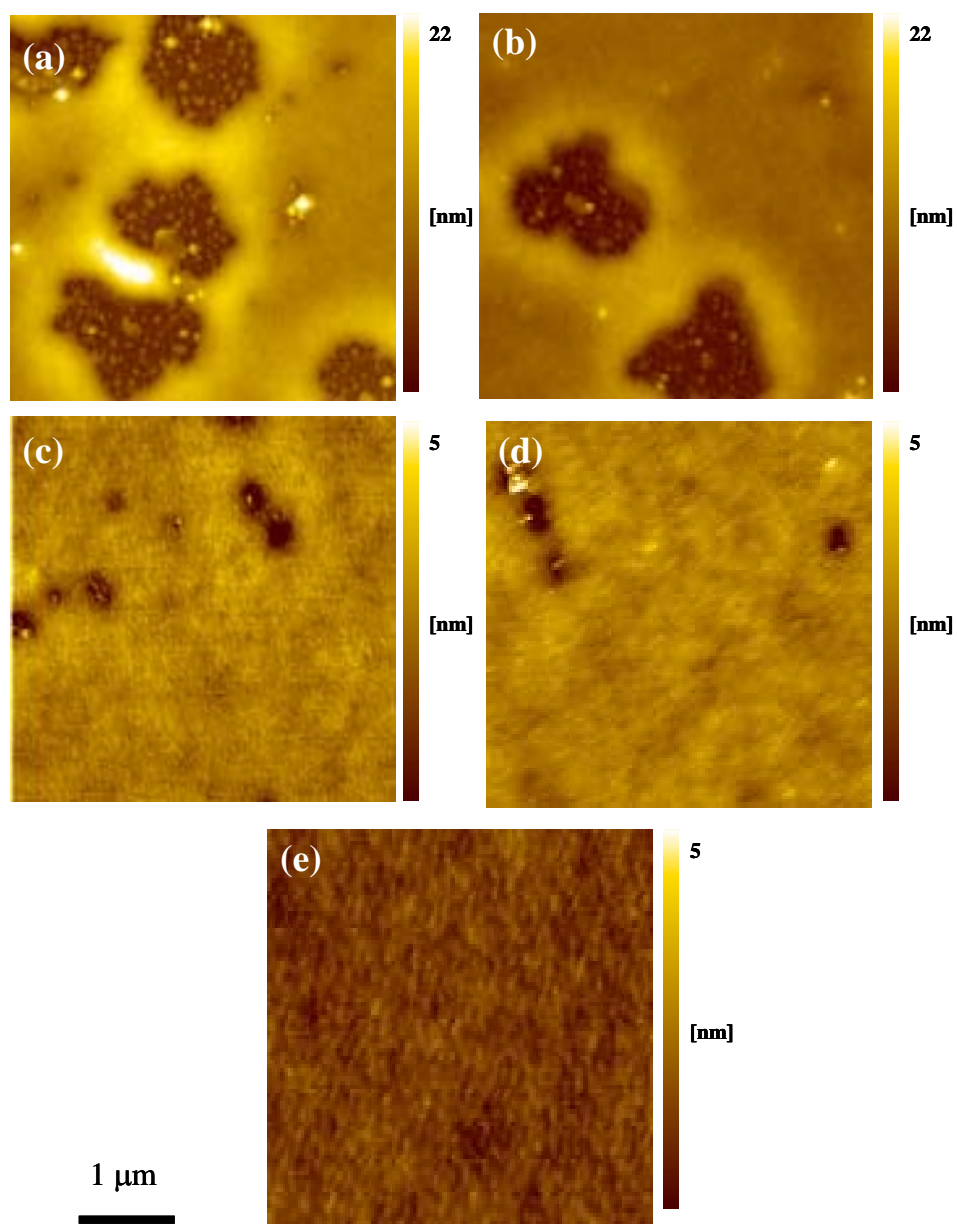
Figure 4.5 AFM topography images of ~5 nm thick P(S-Cl5)/PS films annealed at 120 $^\circ$C for 12 h. Ratios of P(S-Cl5) copolymer are (a) 0 wt%, (b) 10 wt%, (c) 20 wt%, (d) 30 wt%, and (e) 40 wt%.
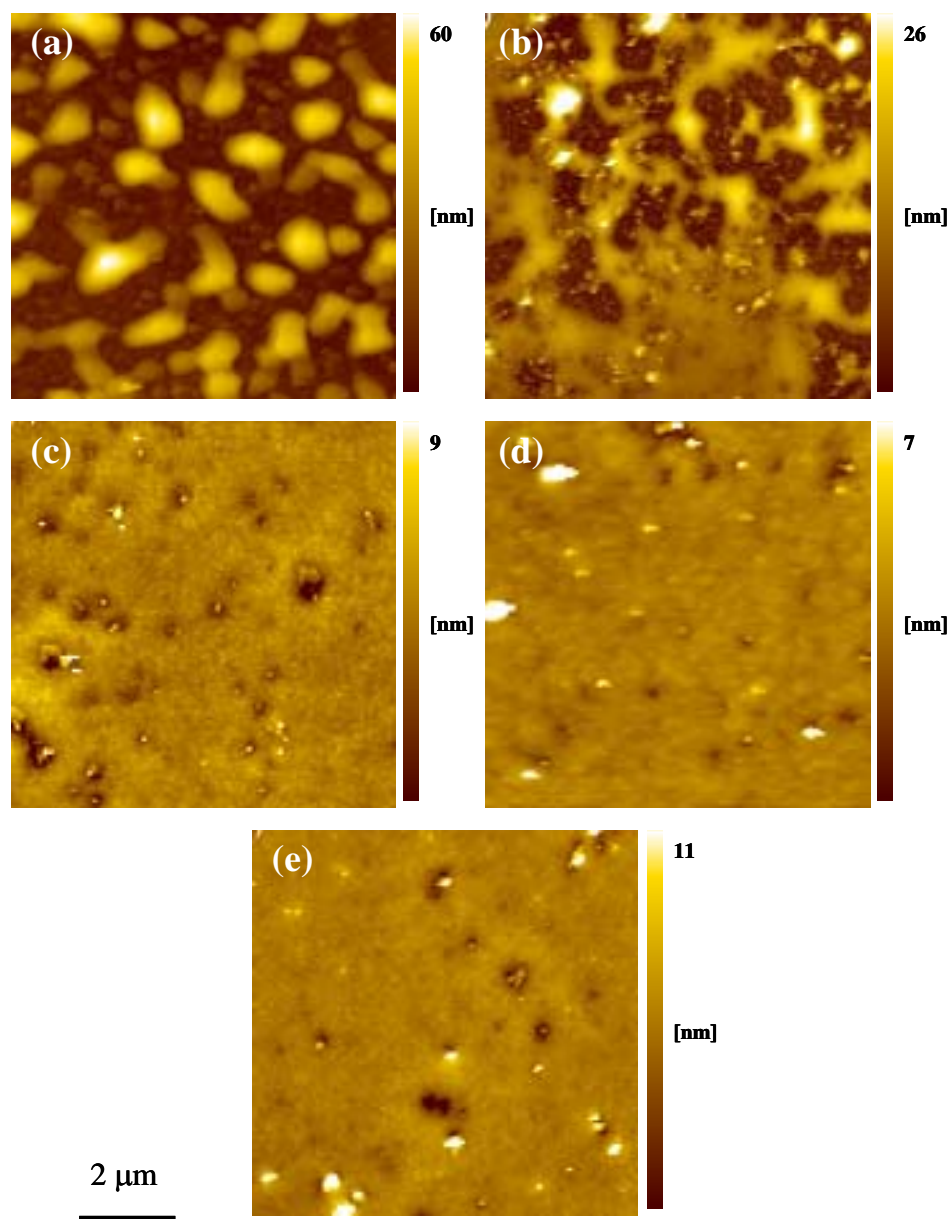
Figure 4.6 AFM topography image of~5 nm thick P(S-Cl5)/PS films annealed at 120 °C for 36 h. Ratios of P(S-Cl5) copolymer are (a) 0 wt%, (b) 10 wt%, (c) 20 wt%, (d) 30 wt%, and (e) 40 wt%.
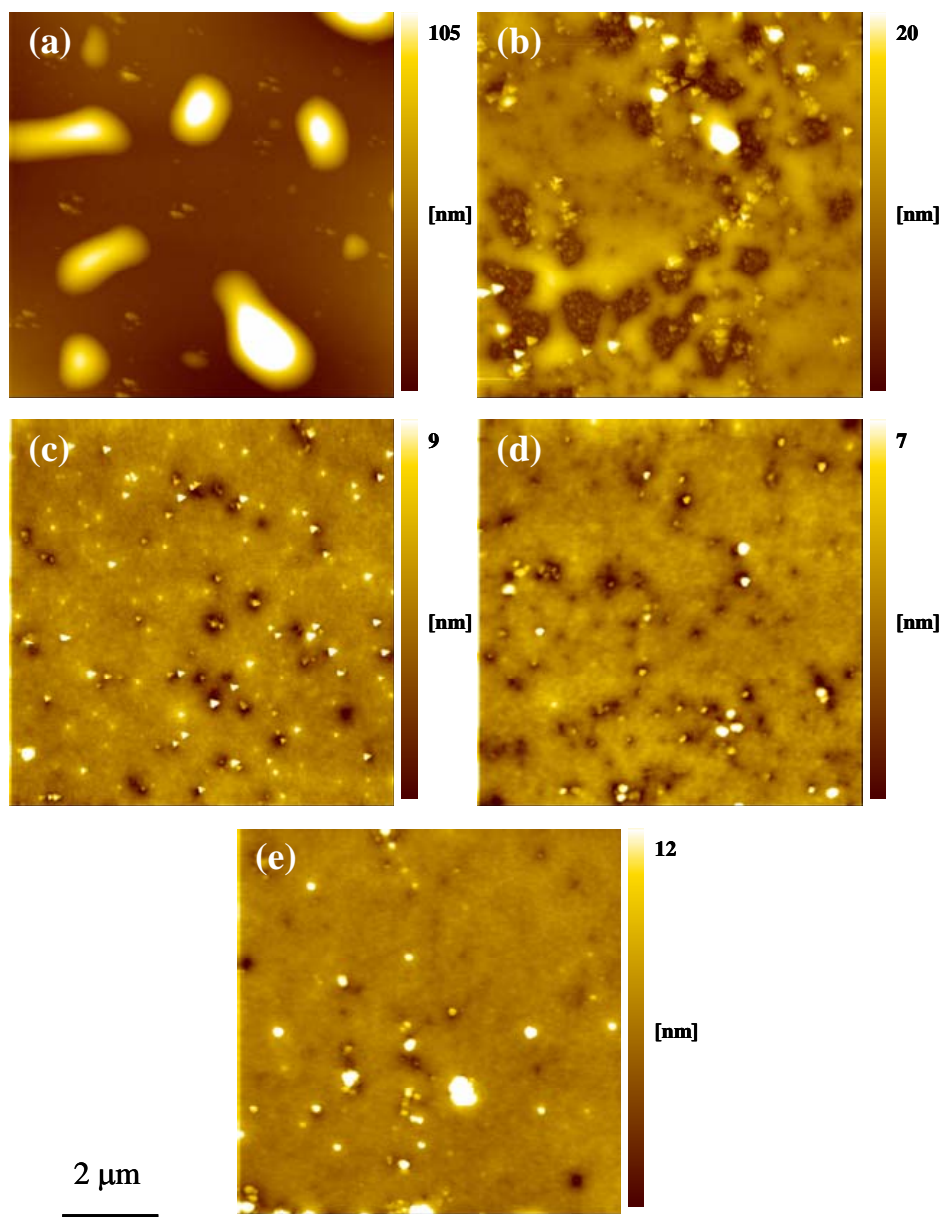
Figure 4.7 AFM topography image of~5 nm thick P(S-Cl5)/PS films annealed at 120 $^{\circ}$C for 104 h. Ratios of P(S-Cl5) copolymer are (a) 0 wt%, (b) 10 wt%, (c) 20 wt%, (d) 30 wt%, and (e) 40 wt%.

The graph between dewetting area versus annealing time of P(S-Cl5)/PS films containing ratios of P(S-Cl5) copolymer ranging from 0-40 wt.% annealed at 120 $^{\circ}$C are shown in Figure 4.8.The dewetting rate of polymeric films relates to the slope of the plot. The dewetting rate of thin films with P(S-Cl5) copolymer concentration ranging from 0-40 wt.% are 1.9, 1.4, 0.17, 0.07 and 0.05 h^{-1}, respectively. It is obvious that the dewetting rate systematically decreases upon the addition of P(S-Cl5) copolymer into PS film. The dewetting rates of the film containing 30 and 40 wt.% copolymer are almost zero. Figure 4.9 shows root mean square roughness (rms roughness) versus annealing time of P(S-Cl5)/PS films containing ratios of P(S-Cl5) copolymer ranging from 0-40 wt.% and annealed at 120 $^{\circ}$C. The Rms roughness result is in agreement with result of dewetting area on polymeric thin films.

Figure 4.10 illustrates the dewetting area as a function of the P(S-Cl5) copolymer concentrations ranging from 0-40 wt.%. To clearly show the result, only plots for annealing time of 30 min and 12 h are illustrated. For short annealing time (30 min), the dewetting area is less than 4% in all films. Upon increasing the annealing time to 12 h, the dewetting area of the pure PS film increase to 16%. The dewetting areas reduce to about 14%, 10% and 5% in the blend films containing 10, 20 and 30 wt.% of the P(S-Cl5) copolymer, respectively. For the film containing 40 wt.% of the copolymer, the dewetting area remains at ~1% despite the increase in the annealing time. The measurements of Rms roughness as a function of copolymer ratio is in agreement with the dewetting area results as shown in Figure 4.11. It can be concluded from the results that addition of statistical copolymer containing 5 mol% of ClMS group into the 5 nm thick PS films results in significant improvement of film stability. The existence of polar ClMS groups provides anchoring sites with polar SiOx/Si substrate while styrene segments in the copolymer favorably interact with PS matrix.
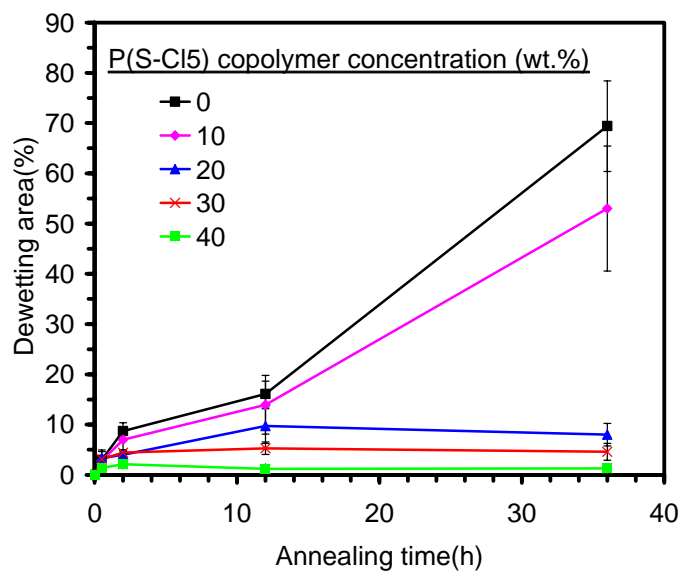
Figure 4.8 Dewetting area versus annealing time of P(S-Cl5)/PS films annealed at 120 °C. P(S-Cl5) copolymer concentrations are 0 wt.%, 10 wt.%, 20 wt.%, 30 wt.% and 40 wt.%.
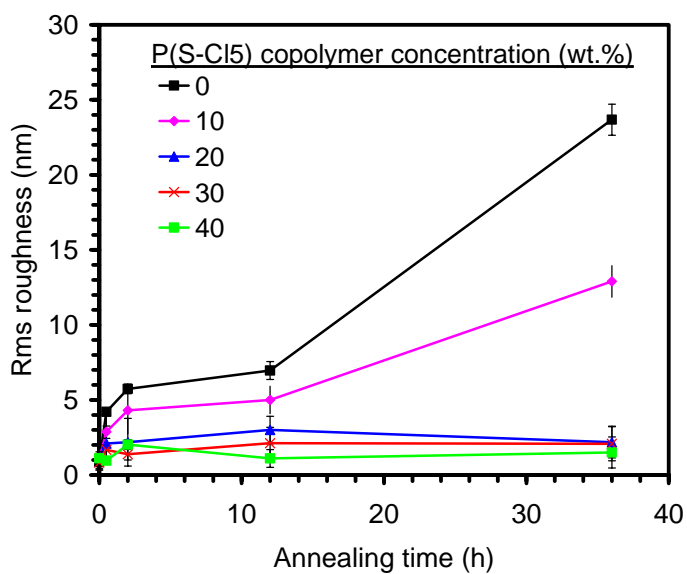
Figure 4.9 Rms roughness versus annealing time of P(S-Cl5)/PS films annealed at 120 °C. P(S-Cl5) copolymer concentrations are 0 wt.%, 10 wt.%, 20 wt.%, 30 wt.% and 40 wt.%.
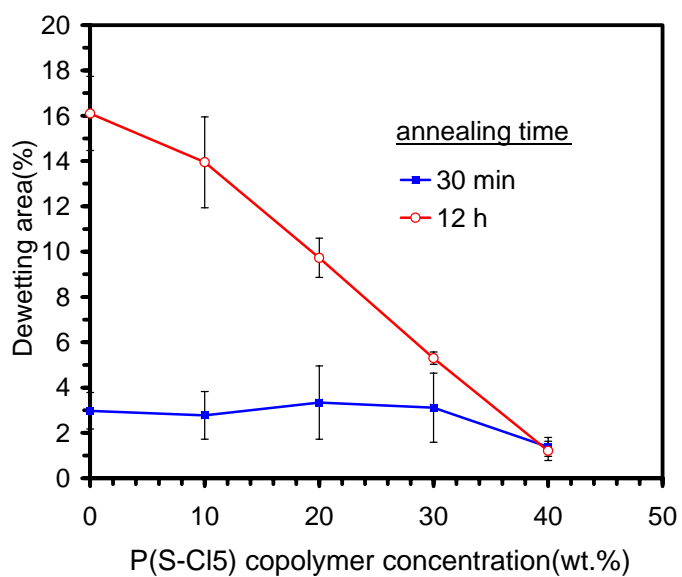
Figure 4.10 Dewetting areas of PS films containing various P(S-Cl5) concentrations.

Films are subjected to 120 $^\circ$C annealing for 30 min and 12 h.
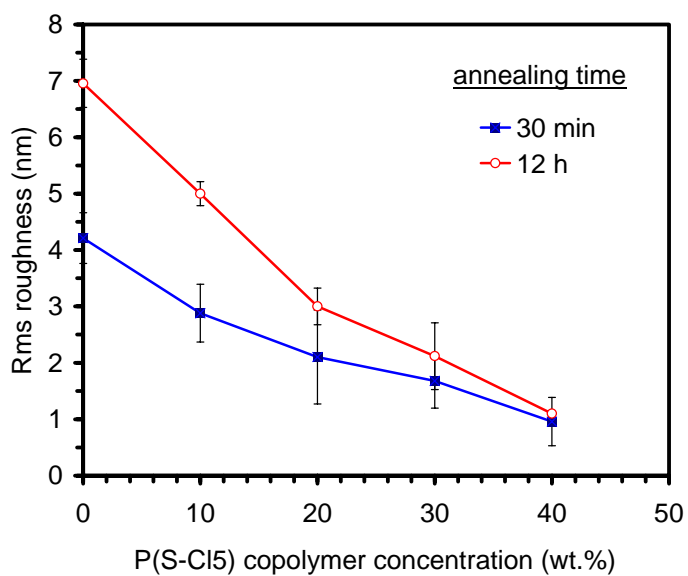
Figure 4.11 Rms roughness of PS films containing various P(S-Cl5) concentrations. Films

are subjected to 120 $^\circ$C annealing for 30 min and 12 h.

4.2.3　Effects of P(S-Cl20) copolymer

To investigate effects of numbers of ClMS group on dewetting behavior of PS thin films, mole ratio of ClMS groups are increased to 20 and 45 mol%. Results for P(S-Cl20) copolymer addition are shown in this section. Films are prepared using P(S-Cl20) copolymer at concentration of 2.5, 5.0, 7.5 and 10 wt.%, which are corresponding to 0.5, 1.0, 1.5 and 2.0 mol% of ClMS group in the films, respectively. Figure 4.12 - 4.15 illustrates AFM topography images of ~5 nm thick PS/P(S-Cl20) films annealed at 120 °C for 30 min, 2 h, 12 h, and 36 h, respectively. For short annealing time (30 min) dewetting areas can be observed on pure PS and thin film containing P(S-Cl20) copolymer 2.5 wt% (0.5 mol% ClMS group) as shown in Figure 4.12(a) and (b). Thin films with higher P(S-Cl20) concentration are continuous and homogeneous. Dewetting area of thin films prepared with P(S-Cl20) copolymer concentrations ranging from 0, 2.5, 5.0, 7.5 and 10 wt.% are around 2.1±0.7, 2.0±0.7, 2.2±0.8, 1.1±0.3 and 1.1±0.2%, respectively. The retardation of dewetting dynamic by the addition of P(S-Cl20) copolymer is not clear in this condition. Flow dynamics are accelerated by increasing annealing time to investigate dewetting process of thin films. When increasing annealing time to 2 h, the dewetting area on thin films containing different ratios of P(S-Cl20) copolymer can clearly observe in Figure 4.13. Dewetting areas are approximately 9.8±1.0, 6.8±1.0, 6.5±1.0, 1.8±0.9 and 1.2±0.5% on thin films which contain P(S-Cl20) copolymer ratios ranging from 0-10 wt.%, respectively. It is clear that the dewetting dynamics slow down significantly when the P(S-Cl20) copolymer is added into the polystyrene film. For annealing time of 12 h, dewetting areas are approximately 9.8±1.0, 6.8±1.0, 6.5±1.0, 1.8±0.9 and 1.2±0.5% on thin films which contain P(S-Cl20) copolymer ratios ranging from 0-10 wt.%, respectively. It is obvious that increasing of P(S-Cl20) copolymer concentration enhance film stability as shown in Figure 4.14. Figure 4.15 illustrates the surface morphology of thin films containing different ratios of the copolymer. All of the thin films are annealed for 36 h. In the pure PS film, irregular-shaped holes are observed with nanodroplets inside the holes. The addition of 10 wt%

copolymer into PS film hardly affects the dewetting process. It is obvious that the addition of P(S-Cl20) copolymer into PS thin films enhance film stability. This result shows that dewetting dynamics is retarded by to add a small amount of P(S-Cl20) copolymer. We expected that ClMS moiety should anchor on SiO_x/Si surface via dipolar interactions while styrene segments interact favorably with the polymeric matrix

The effects of P(S-Cl20) copolymers on the stability of PS films are summarized in Figure 4.16. The degree of dewetting inhibition in each system can be extracted from the plots between dewetting area versus concentration of the copolymers as shown in Figure. 4.16(a). In all annealing conditions, the dewetting area is found to systematically decrease with increasing concentration of the copolymers. The trend is most obvious when the annealing time is increased to 36 h. The dewetting area of pure PS film reaches about 60 % at this annealing condition while dewetting area of the film containing 10 wt.% of P(S-Cl20) (2 mol% of ClMS group) is about 15 %. The dewetting rate of each film relates to slope of the plot between dewetting areas versus annealing time as shown in Figure. 4.16(b). The plots clearly show that the dewetting rate systematically decreases with increasing concentrations of P(S-Cl20) copolymer in PS films. These results indicate that the addition of P(S-Cl20) copolymers into 5 nm thick PS film leads to a significant increase of its thermal stability. These copolymers are expected to anchor on SiO_x/Si substrate via dipolar interaction of ClMS groups while styrene segment provides favorable interactions with PS matrix. The effect of these copolymers on stability of PS film is similar to that of the P(S-Cl5). However, the efficiency of each copolymer as a dewetting inhibitor depends significantly on mole ratio of ClMS group within the copolymers as will be discussed in the following section.

Figure 4.12 AFM topography image of~5 nm thick P(S-Cl20)/PS films annealed at 120 °C for 30 min. P(S-Cl20) copolymer concentrations are (a) 0 wt%, (b) 2.5 wt%, (c) 5.0 wt%, (d) 7.5 wt%, and 10.0 wt%.

Figure 4.13 AFM topography image of~5 nm thick P(S-Cl20)/PS films annealed at 120 °C for 2 h. P(S-Cl20) copolymer concentrations are (a) 0 wt%, (b) 2.5 wt%, (c) 5.0 wt%, (d) 7.5 wt%, and 10.0 wt%.

Figure 4.14 AFM topography image of~5 nm thick P(S-Cl20)/PS films annealed at 120 °C for 12 h. P(S-Cl20) copolymer concentrations are (a) 0 wt%, (b) 2.5 wt%, (c) 5.0 wt%, (d) 7.5 wt%, and 10.0 wt%.

Figure 4.15 AFM topography image of~5 nm thick P(S-Cl20)/PS films annealed at 120 °C for 36 h. P(S-Cl20) copolymer concentrations are (a) 0 wt%, (b) 2.5 wt%, (c) 5.0 wt%, (d) 7.5 wt%, and 10.0 wt%.

Figure 4.16 (a) dewetting area versus copolymer concentrations of ~5 nm thick PS and P(S-Cl20)/PS films. The films are annealed at 120 $^\circ$C for 30 min, 2 h, 12 h and 36 h. and (b) dewetting area versus annealing times of the films containing different concentrations of P(S-Cl20)

4.2.4   Effects of P(S-Cl45) copolymer

Figure 4.17- 4.20 illustrate AFM topography images of ~5 nm thick P(S-Cl45)/PS films annealed at 120 $^\circ$C for 30 min, 2 h, 12 h, and 36 h, respectively. Films are prepared with 0, 1, 2, 3 and 4 wt% P(S-Cl45) copolymer, corresponding to 0, 0.5, 1.0, 1.5 and 2.0 mol% of ClMS group. For short annealing time (30 min and 2 h), dewetting areas can only observe on thin film containing of P(S-Cl45) copolymer 1 wt% and pure PS thin film. For film annealed at 30 min, the dewetting area of thin films containing P(S-Cl45) copolymer ranging from 0, 1, 2, 3 and 4 wt.% are around 3.9±1.0, 0.7±0.2, 0.7±0.2, 0.4±0.2 and 0.6±0.2%, respectively. We have found that the dewetting areas of all films are similar for short annealing time. This result is in agreement with P(S-Cl5)/PS and P(S-Cl20)/PS thin film. For P(S-Cl45)/PS thin films annealed for 2 h (Figure 4.18), the dewetting area increase to 4.1±1.0, 1.3±0.2, 1.4±0.4, 0.9±0.3 and 0.9±0.2% on thin film containing P(S-Cl45) copolymer ranging from 0-4 wt.%, respectively. When increasing annealing time to 12 h, the dewetting area on thin films containing different ratios of P(S-Cl45) copolymer can be clearly observed in Figure 4.19. Dewetting areas are approximately 9.8±1.0, 1.6±0.7, 1.6±0.6, 1.0±0.2 and 0.8±0.2% on thin films which contain P(S-Cl45) copolymer ratios ranging from 0-4 wt.%, respectively. Figure 4.20 illustrates the surface morphology of the thin films annealed for 36 h. The addition of 3 and 4 wt% P(S-Cl45) copolymer into PS film suppresses dewetting process, resulting in highly stable films. It is obvious that adding P(S-Cl45) copolymer into PS thin films enhance film stability. This result shows that dewetting dynamics is retarded by adding a small amount of P(S-Cl45) copolymer. Dewetting dynamics can be significantly delayed with P(S-Cl45) copolymer at concentration in polymeric films higher than 2 wt.%, which corresponds to the existence of higher than 1 mol% of ClMS group in the system.

The effects of P(S-Cl45) copolymers on the stability of PS films are summarized in Figure 4.21. The degree of dewetting inhibition in each system can be extracted from

the plots between dewetting area versus concentration of the copolymers as shown in Figure. 4.21(a). In all annealing conditions, the dewetting area is found to systematically decrease with increasing concentration of the copolymers. The trend is the most obvious when the annealing time is increased to 36 h. For the P(S-Cl45)/PS film of PS with 4 wt.% of copolymer, the dewetting area is only 2 %. The dewetting rate of each film relates to slope of the plot between dewetting area versus annealing time as shown in Figure. 4.21(b). The plot clearly shows that the dewetting rate systematically decreases with increasing concentrations of P(S-Cl45) copolymer in PS films. The dewetting rate of PS film containing 4 wt.% of P(S-Cl45) is close to zero. These results indicate that the addition of and P(S-Cl45) copolymers into 5 nm thick PS film leads to significant increase of its thermal stability. The effect of these copolymers on stability of PS film is similar to P(S-Cl5) and P(S-Cl20) copolymers. However, the efficiency of each copolymer as a dewetting inhibitor depends significantly on mole ratios of ClMS group within the copolymers as will be discussed in the following section.
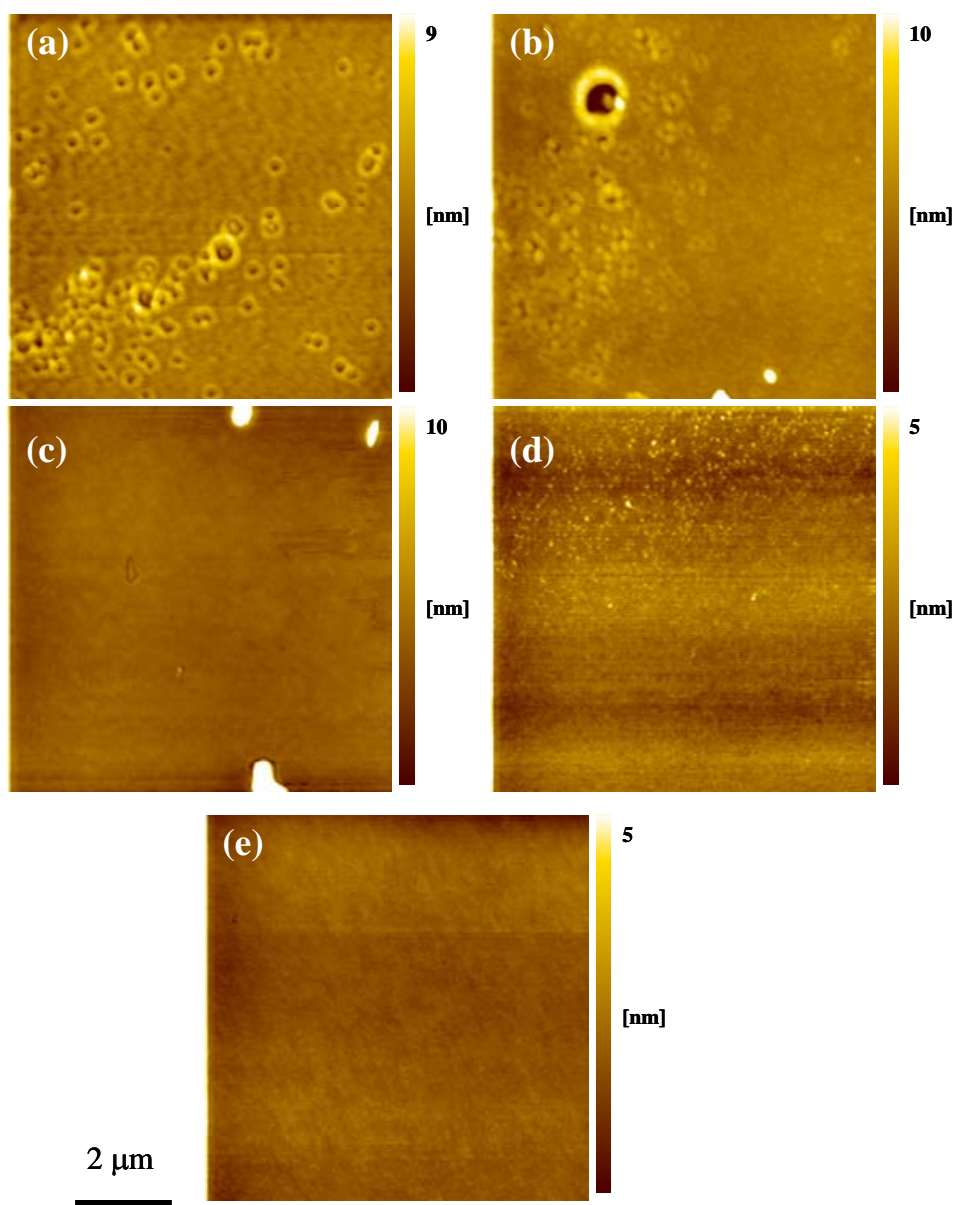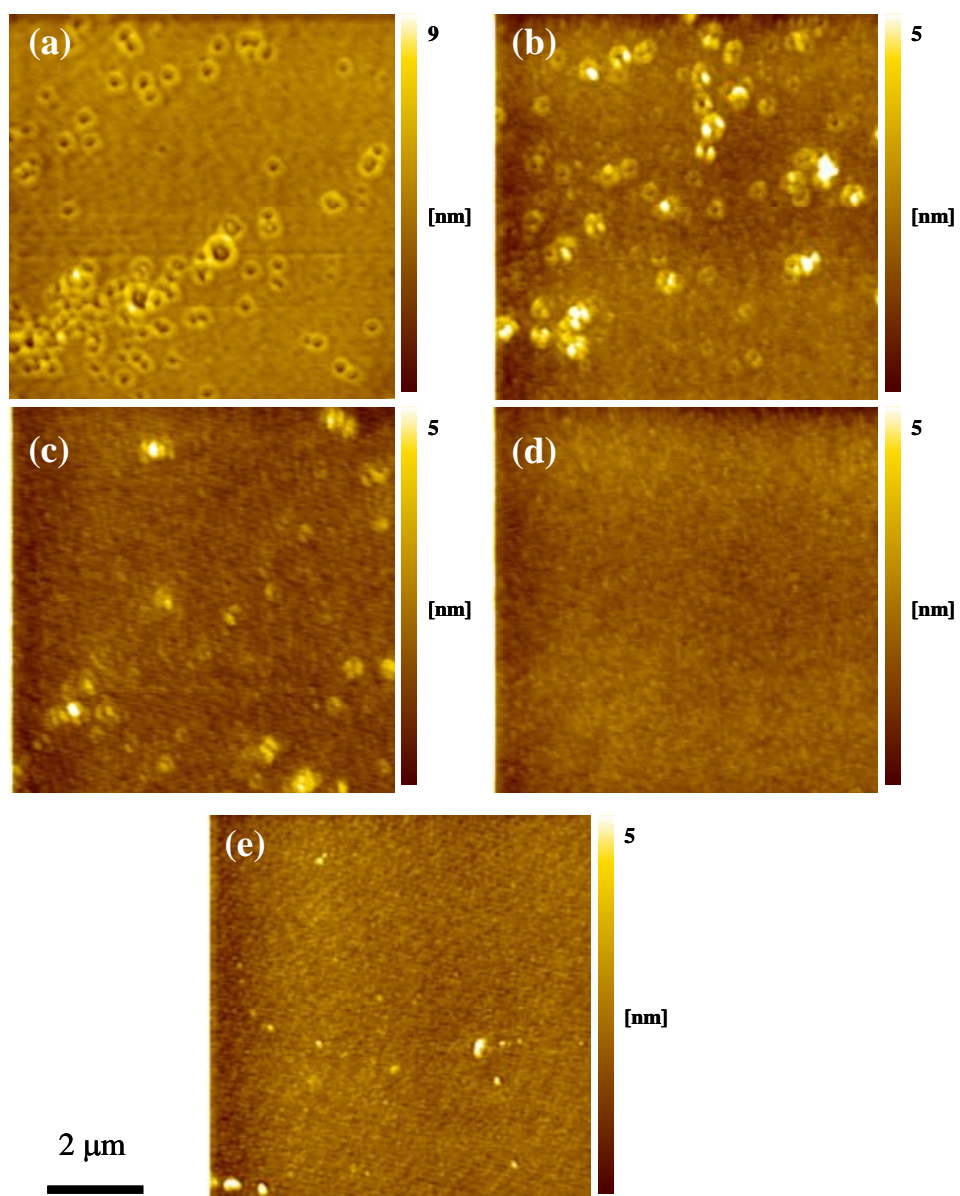
Figure 4.17. AFM topography image of~5 nm thick P(S-Cl45)/PS films annealed at 120 °C for 30 min. P(S-Cl45) copolymer concentrations are (a) 0 wt%, (b) 1 wt%, (c) 2 wt%, (d) 3 wt%, and (e) 4 wt%.
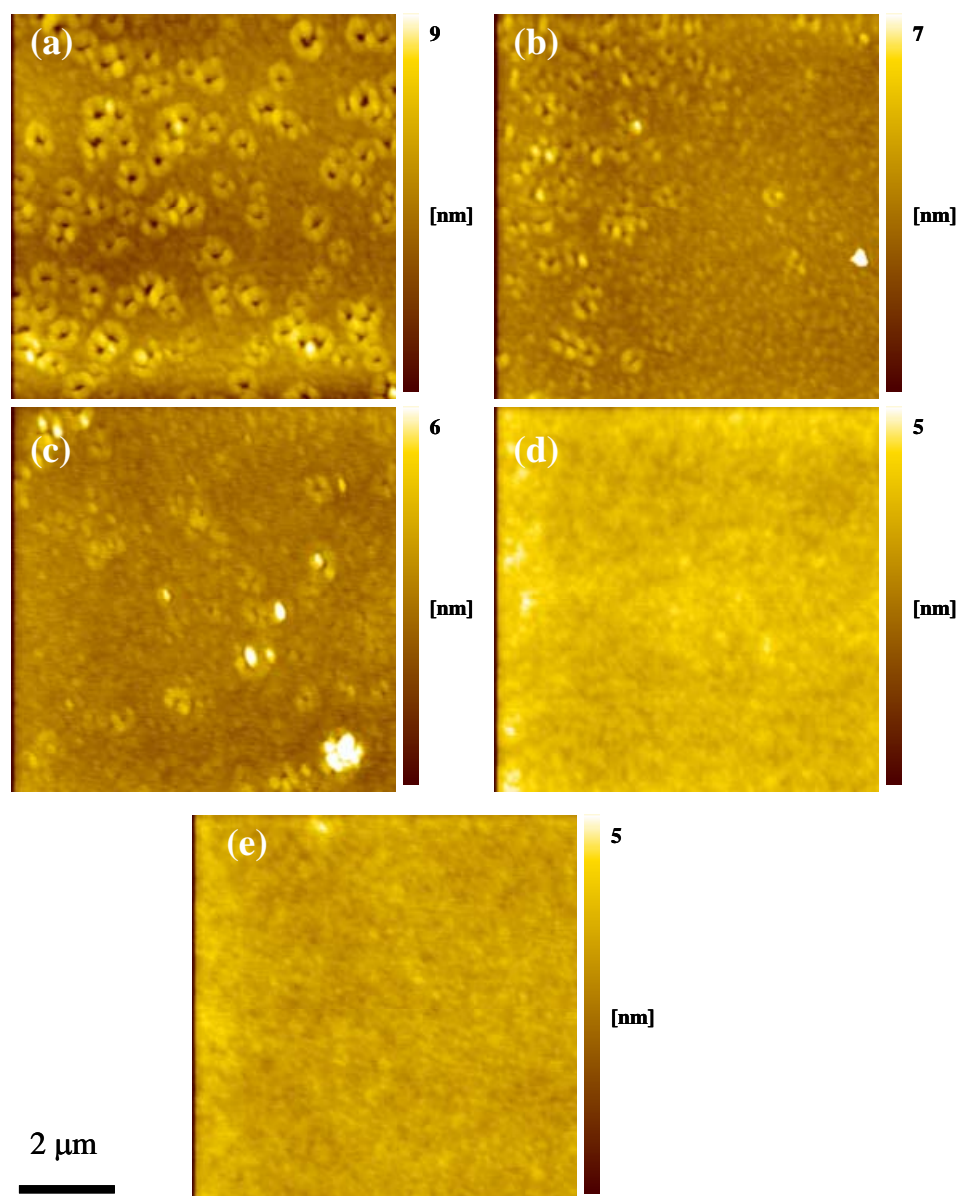
Figure 4.18 AFM topography image of~5 nm thick P(S-Cl45)/PS films annealed at 120 °C for 2 h. P(S-Cl45) copolymer concentrations are (a) 0 wt%, (b) 1 wt%, (c) 2 wt%, (d) 3 wt%, and (e) 4 wt%.
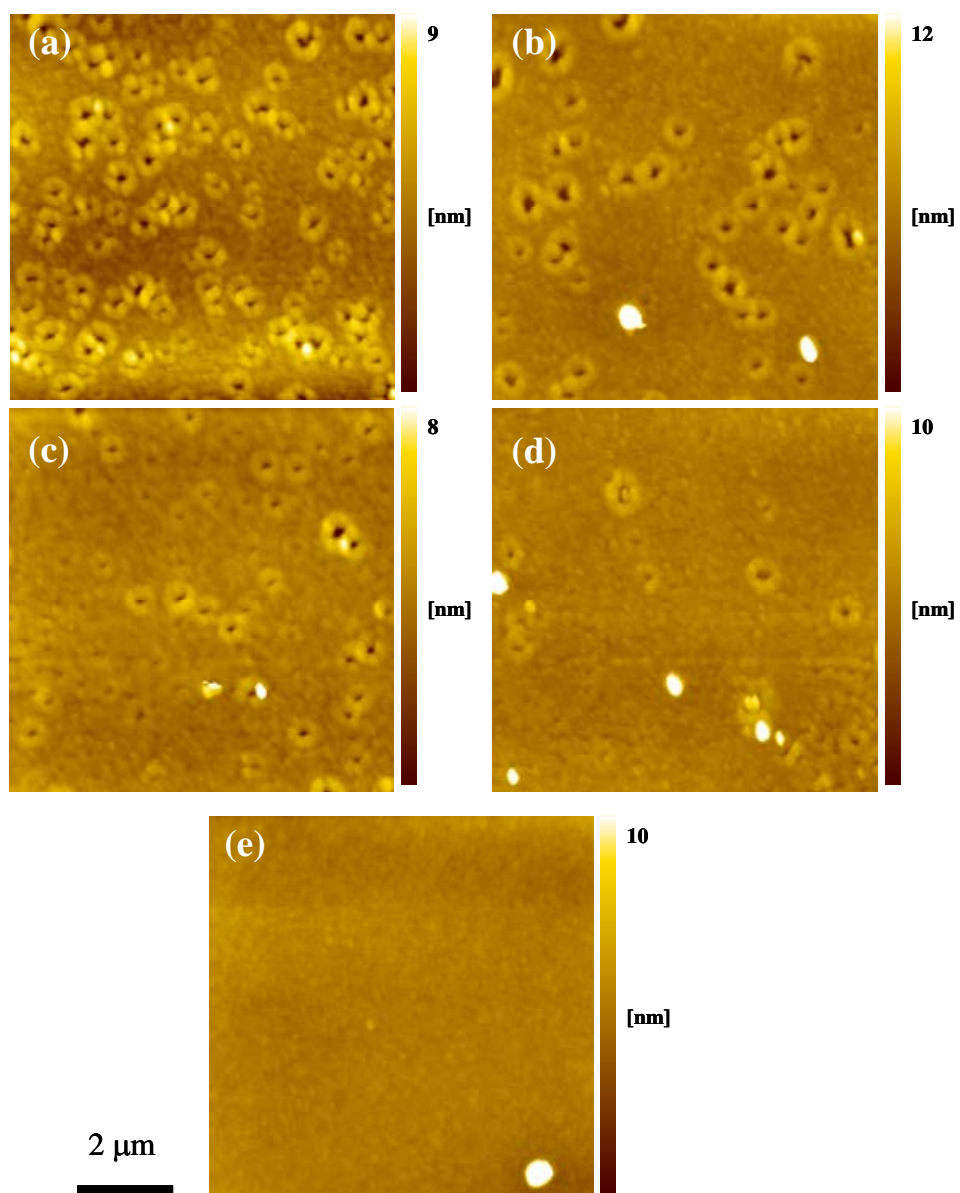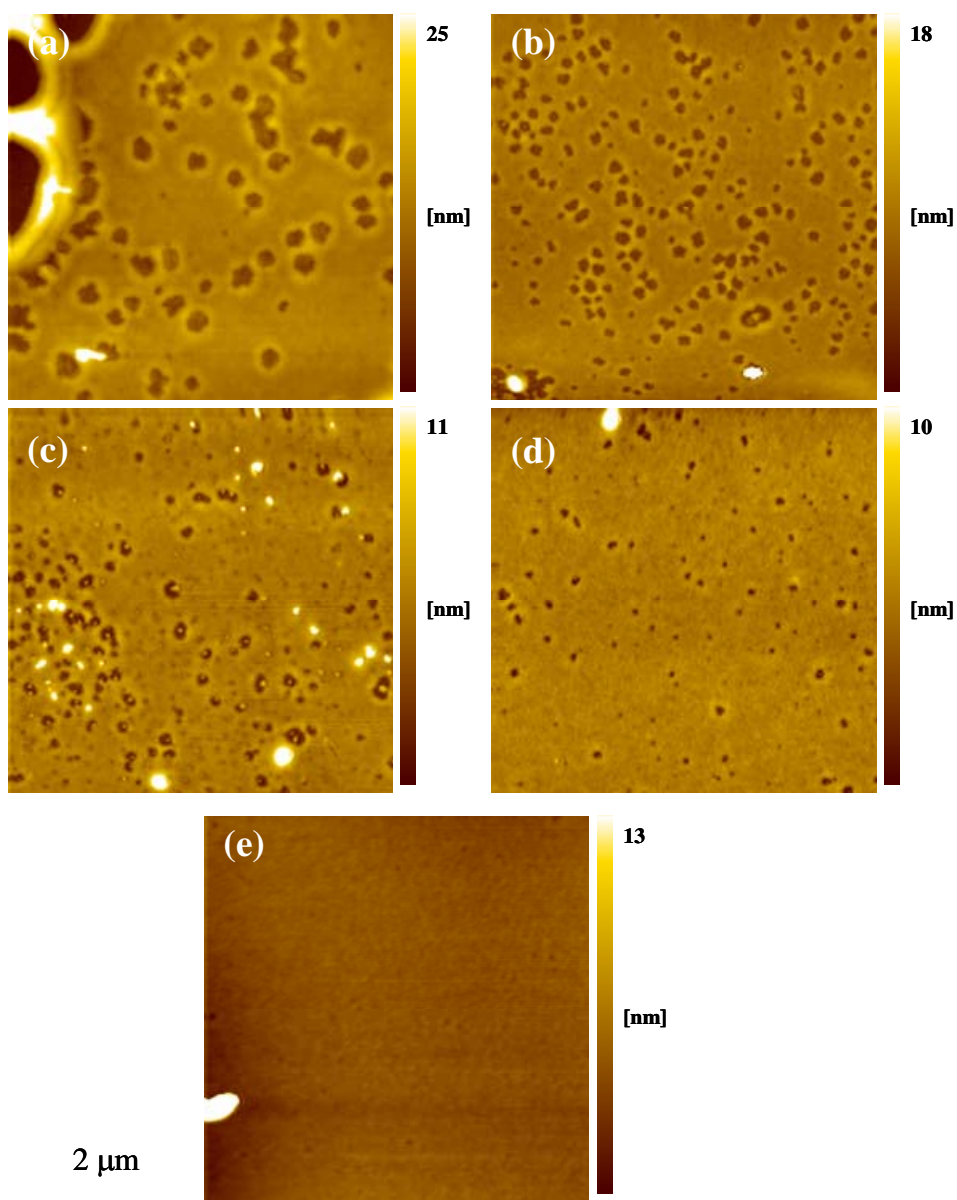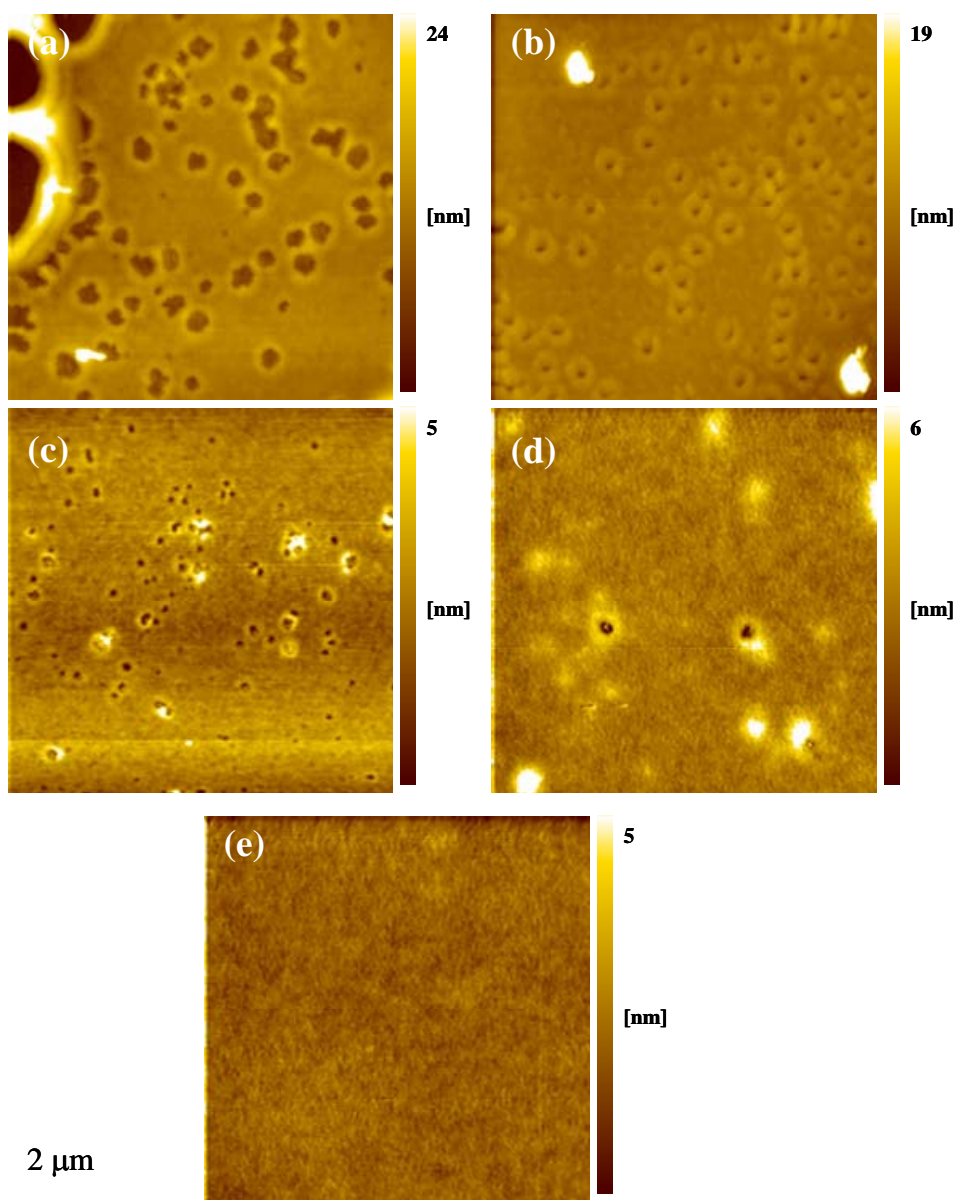
Figure 4.19 AFM topography image of~5 nm thick P(S-Cl45)/PS films annealed at 120 °C for 12 h. P(S-Cl45) copolymer concentration are (a) 0 wt%, (b) 1 wt%, (c) 2 wt%, (d) 3 wt%, and (e) 4 wt%.
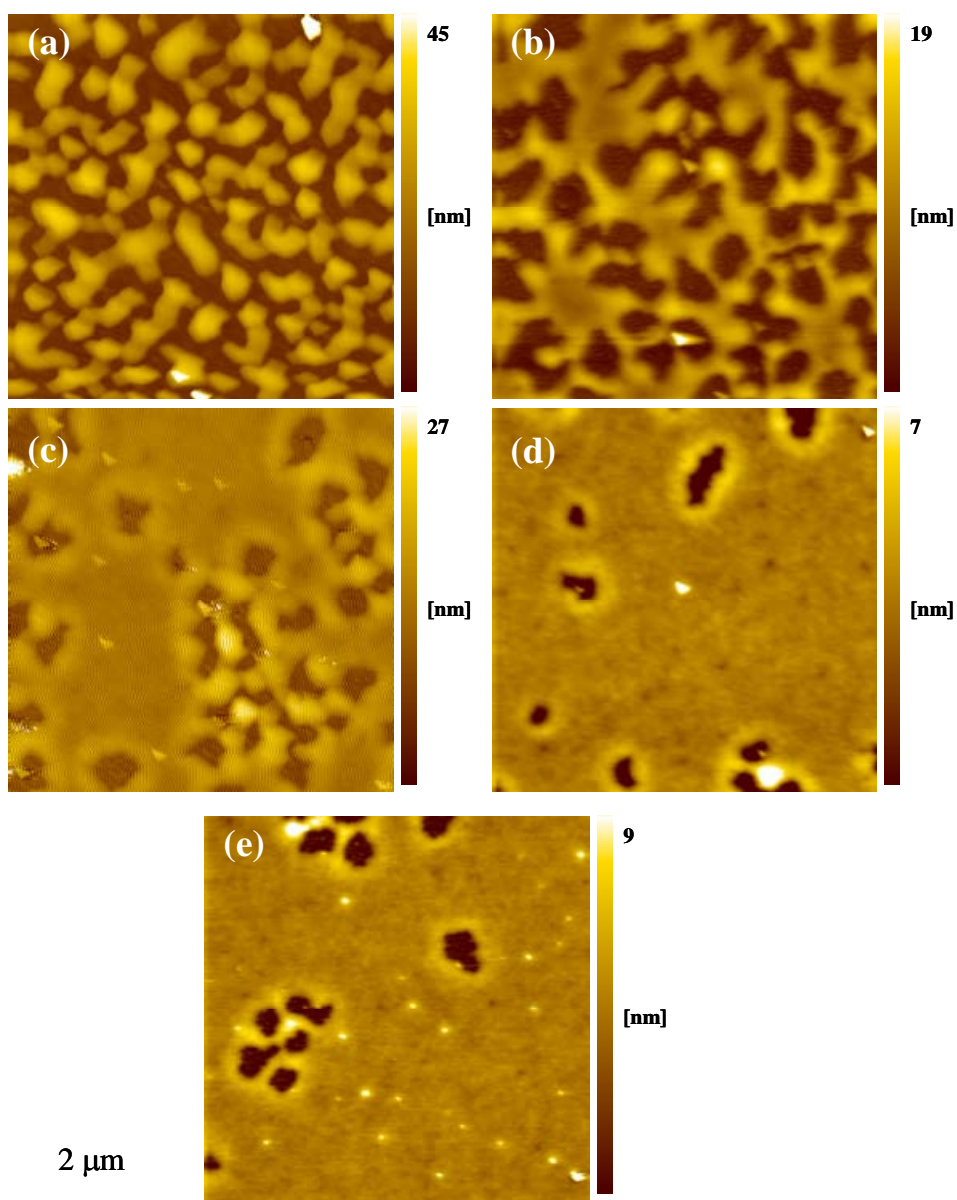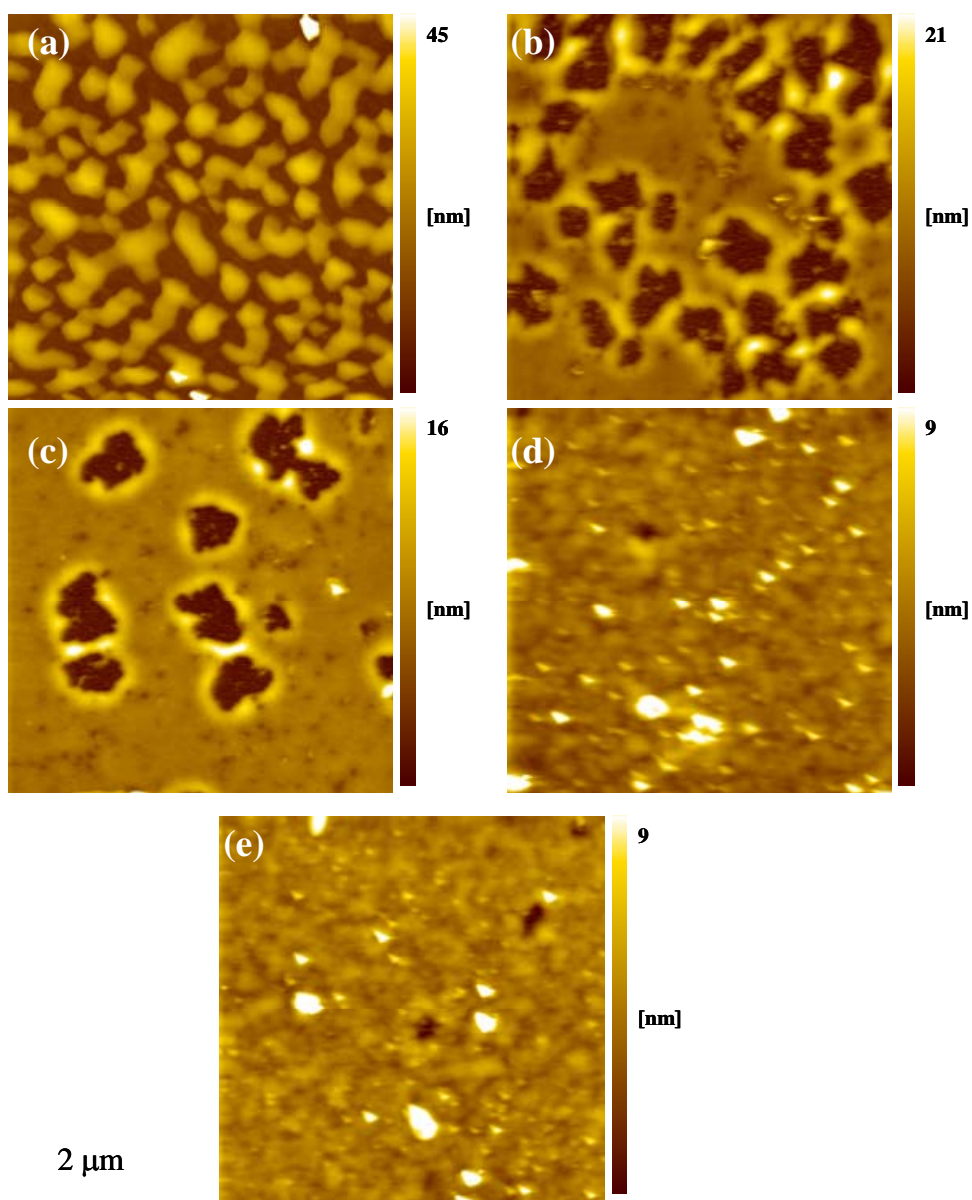
Figure 4.20 AFM topography image of~5 nm thick P(S-Cl45)/PS films annealed at 120 °C for 36 h. P(S-Cl45) copolymer concentrations are (a) 0 wt%, (b) 1 wt%, (c) 2 wt%, (d) 3 wt%, and (e) 4 wt%.
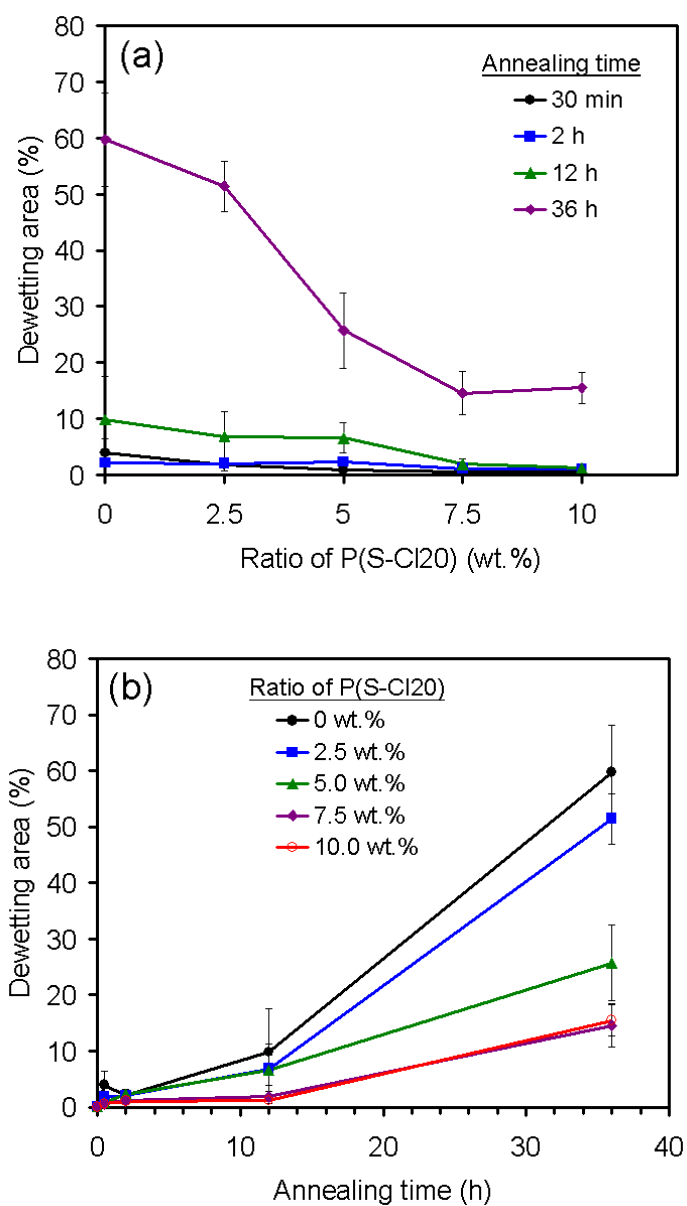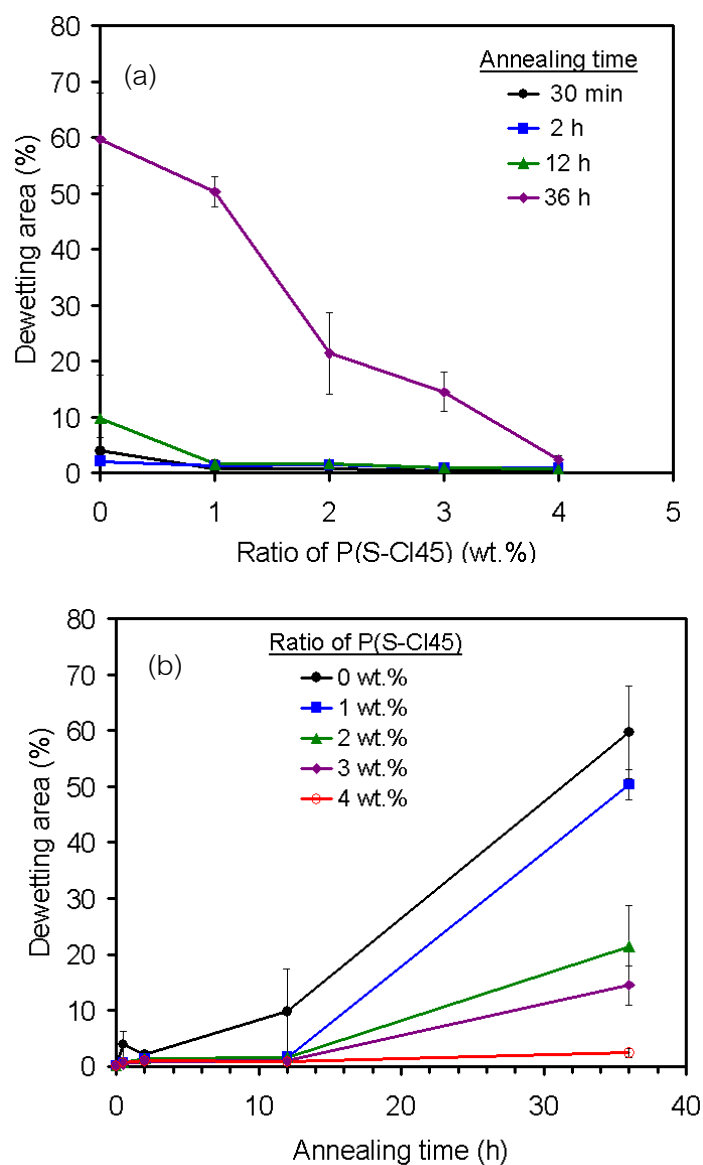
Figure 4.21 (a) dewetting area versus copolymer concentrations of ~5 nm thick PS and P(S-Cl45)/PS films. The films are annealed at 120 $^\circ$C for 30 min, 2 h, 12 h and 36 h. and (b) dewetting area versus annealing times of the films containing different concentrations of P(S-Cl45)

4.3. Effects of ClMS mole ratio in copolymers on film stability

In this study, we compare the efficiency of copolymers P(S-Cl5), (P(S-Cl20) and P(S-Cl45)) as dewetting inhibitors for PS thin film. For the copolymer with higher mole ratio of polar ClMS groups, one expects stronger interfacial interactions with polar SiOx/Si substrate, which should result in the increase of film stability. Figure 4.22 illustrates AFM topography images of ~5 nm thick P(S-Cl5)/PS, P(S-Cl20)/PS and P(S-Cl45)/PS films annealed at 120 $^\circ$C for 36 h. At this annealing condition, the dewetting of pure PS already reaches final stage where the continuous film disintegrates into large droplets (Figure. 4.22(a,f,k)). We observe that the addition of P(S-Cl5) copolymer containing 5 mol% of ClMS group into the 5 nm thick PS films lead to significant increase of their stability [41].

The addition of P(S-Cl20) into PS films also causes significant suppression of their dewetting dynamics. The PS films containing 0.5 and 1.0 mol% of P(S-Cl20) exhibit a structure of interconnected ridges and domains (Figure. 4.22(g,h)), corresponding to an intermediate stage of the dewetting. The increase of P(S-Cl20) concentration to 1.5 and 2.0 mol% further slows down the dewetting rate. Only some irregular holes are detected in these films, indicating an early stage of the dewetting. The depth of these holes is about 5.5$\pm$0.8 nm. The investigation of P(S-Cl45)/PS films provides similar results. The AFM topography images in Figure. 4.22(k-o) clearly show that the addition of small quantity of P(S-Cl45) into PS films leads to significant decrease of the dewetting rate. The AFM topography image of PS film containing 0.5 mol% of the P(S-Cl45) corresponds to an intermediate stage of the dewetting (Figure. 4.22(l)). The increase of P(S-Cl45) concentration to 1.0, 1.5 and 2.0 mol% results in systematically decrease of number and dimension of holes within the films. The PS film with 2.0 mol% of P(S-Cl45) contains only small number of holes.

Figure 4.23 illustrates AFM topography images of pure PS, P(S-Cl5)/PS, P(S-Cl20)/PS and P(S-Cl45)/PS films annealed at 120 $^\circ$C for 2, 12 and 36 h. The

concentration of P(S-Cl5), P(S-Cl20) and P(S-Cl45) in the films is 40, 10 and 4 wt.%, respectively, corresponding to the presence of ~2.0 mol% of ClMS group. At annealing time of 12 h, relatively large holes are formed in pure PS film while the P(S-Cl5)/PS film contains some small holes. The P(S-Cl20)/PS and P(S-Cl45)/PS films remain continuous. The discrepancy of film morphologies is clearly visible when the annealing time is further increased to 36 h. Total dewetting of pure PS film occurs at this annealing condition while the holes in (S-Cl5)/PS films significantly expands but remains connected. Only some small number of holes is observed in the P(S-Cl20)/PS and P(S-Cl45)/PS films. This result indicates that the efficiency of the copolymers as dewetting inhibitors varies with mole ratio of ClMS groups in the backbone. The copolymer with higher mole ratio of ClMS groups appears to be a better dewetting inhibitor.

To compare the efficiency of each copolymer in more details, dewetting area of the blended films annealed for 30 min, 2 h and 36 h is plotted versus the ClMS mole ratio in the copolymers as shown in Figure. 4.24. For the blended films containing 1.5 mol% of ClMS group, the dewetting area systematically decreases with increasing ClMS mole ratio in the copolymers (Figure. 4.24(a)). For the blended films containing 2.0 mol% of ClMS group, the discrepancy is only observed when the annealing time is increased to 36 h. The dewetting area of P(S-Cl5)/PS and P(S-Cl20)/PS films is ~14 % while that of the P(S-Cl45)/PS is only ~3 % (Figure. 4.24(b)). This observation indicates that the increase of polar ClMS group in the polymeric backbone leads to the increase of its efficiency as dewetting inhibitor. It requires much lesser amount of P(S-Cl45) to suppress the dewetting of PS film compared to the P(S-Cl20) and P(S-Cl5), respectively. This fundamental knowledge is important for designing the materials for using in the coating application.

The rationalization of this result is as follows. It has been known that slight difference of surface energy of segments within polymeric backbone can lead to significant segregation at interfaces [43] The ClMS segments with higher surface energy

are expected to segregate to SiOx/Si substrate while the styrene segments favorably interact with PS matrix. We suggest that the extent of interfacial segregation of the copolymers to SiOx/Si substrate increases with mole ratio of ClMS group within the backbone. Increasing mole ratio of ClMS group in copolymer reduces displacement between ClMS group and enhance strong dipolar force between polymeric thin films and substrate. Therefore, P(S-Cl45) chains are expected to mostly reside near the substrate while some of P(S-Cl5) chains may remain within PS matrix as illustrated in Figure. 4.25. In addition, the strength of dipolar interaction between the copolymers and SiOx/Si substrate is expected to be highest in the system of P(S-Cl45) due to the presence of the highest numbers of anchoring sites.
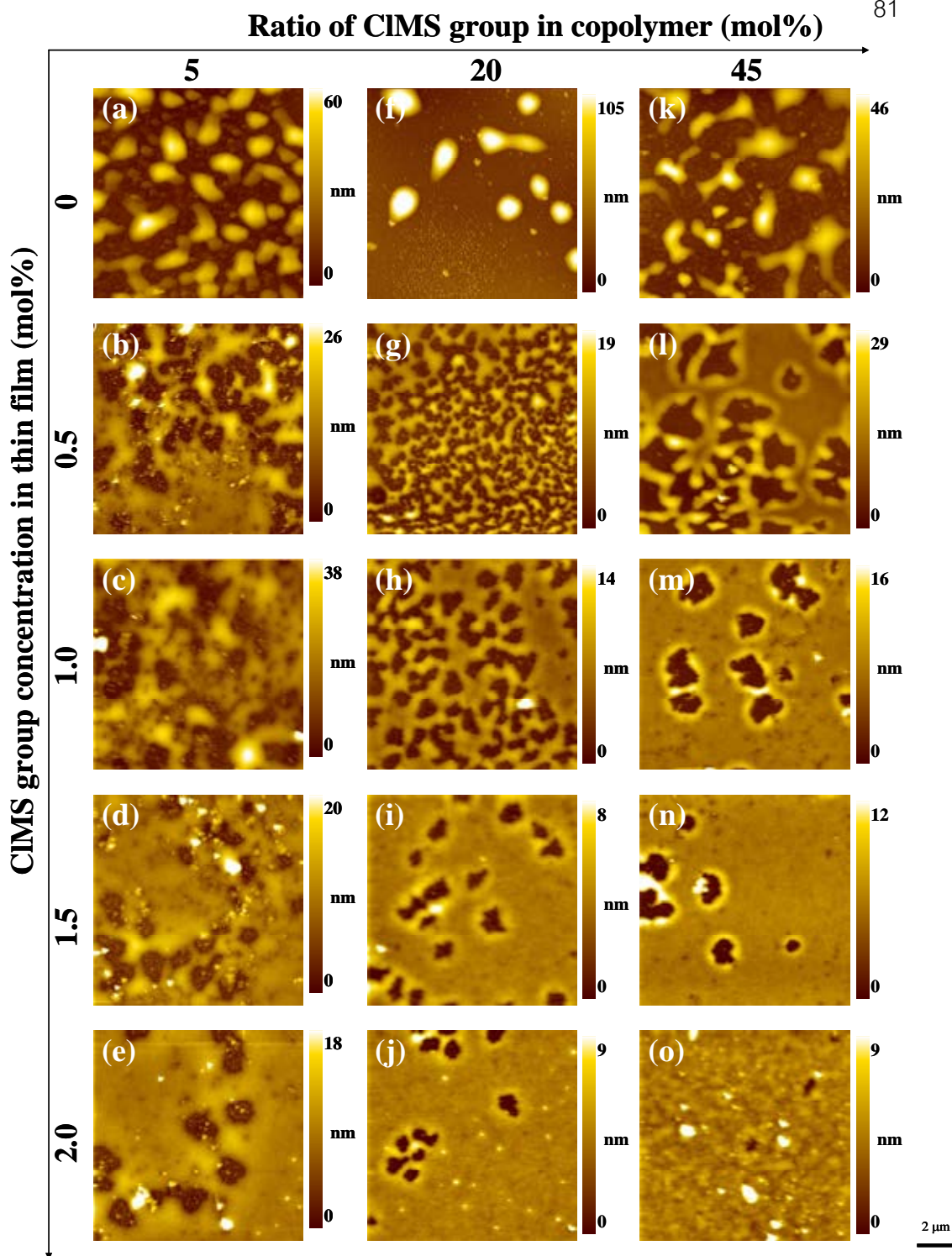
Figure 4.22 AFM topography images of P(S-Cl5)/PS (a-e), P(S-Cl20)/PS (f-j) and P(S-Cl45)/PS (k-o) ~5 nm thick films annealed at 120 °C for 36 h. Ratios of ClMS group within the films are 0, 0.5, 1.0, 1.5 and 2.0 mol%. Scan size is 8×8 μm^2.
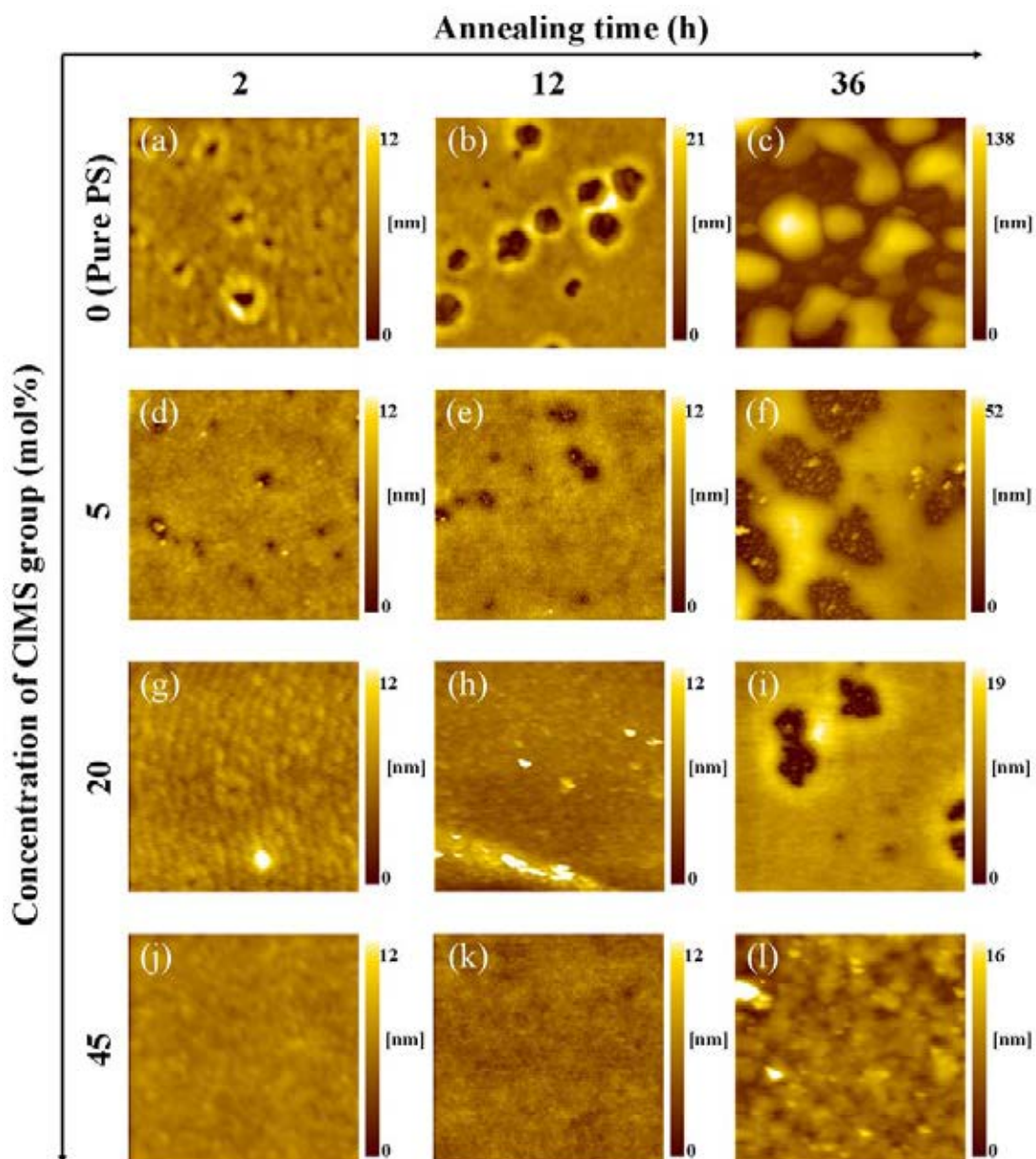
Figure. 4.23 AFM topography images of pure PS, P(S-Cl5)/PS, P(S-Cl20)/PS and P(S-Cl45)/PS ~5 nm thick films annealed at 120 $^{\circ}$C for 2 h, 12 h and 36 h. All P(S-Clx)/PS films contain 2.0 mol% of CIMS group. Scan size is 3×3 μm^2.
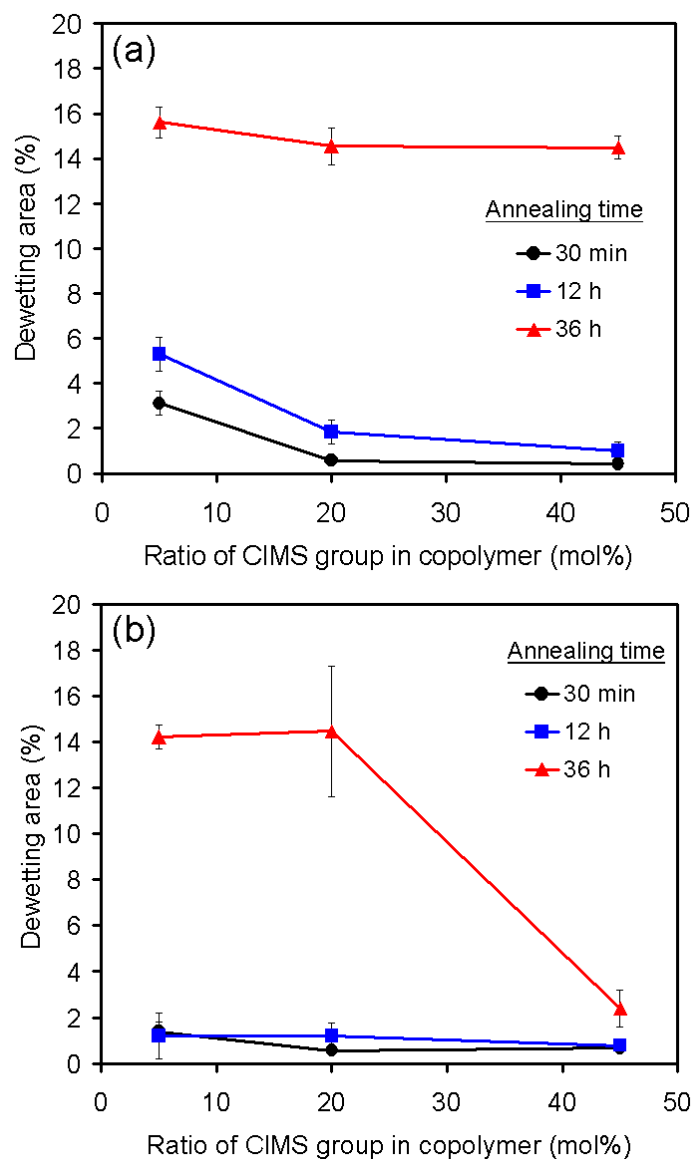
Figure. 4.24 Plots of dewetting area versus ratios of CIMS group in the copolymers. All P(S-Cl5)/PS, P(S-Cl20)/PS and P(S-Cl45)/PS films contain (a) 1.5 mol% and (b) 2.0 mol% of CIMS group. The films were annealed at 120 °C for 30 min, 12 h and 36 h.
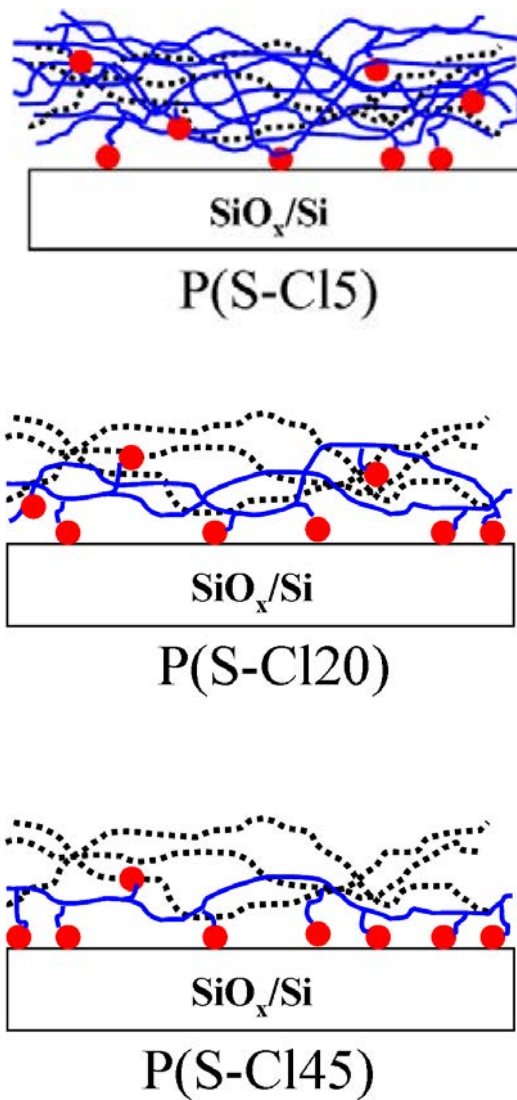
Figure 4.25 Illustration for interaction of the P(S-Cl5), P(S-Cl20) and P(S-Cl45) copolymers with SiOx/Si surface. The segregation of P(S-Cl45) chains to polar SiOx/Si is expected to be highest (see text).

4.4. Effects of P(S-Clx)/PS film thickness

Thin films of pure PS, P(S-Cl5)/PS, P(S-Cl20)/PS and P(S-Cl45)/PS with thicknesses of 5, 11 and 17 nm are fabricated. Film thickness is controlled by varying polymer concentrations while the spinning rate is kept constant. The annealing temperature for the 5 nm thick films is 120 $^{\circ}$C. Dewetting rate of the thicker films is rather slow at this condition. Therefore, the annealing temperature for the 11 and 17 nm thick films is increased to 165 $^{\circ}$C. The evolution of film morphology at different length scales is followed by utilizing AFM and optical microscopy (OM).

The AFM topography images of pure PS and P(S-Cl5)/PS films annealed for 36 h are illustrated in Figure. 4.26. The dewetting of pure PS films reaches final state at this annealing condition where hemispherical droplets of the polymer are observed. The dimension and number of the droplets vary with the film thickness. The addition of P(S-Cl5) copolymer into 5 nm thick PS films results in the increase of film stability. The dewetting area systematically decreases with increasing concentration of P(S-Cl5). The investigation of 11 nm thick P(S-Cl5)/PS films shows similar results (Figure. 4.26(f-j)). The film containing 40 wt.% of P(S-Cl5) is still smooth after annealing at 165 $^{\circ}$C for 36 h (Figure. 4.26(j)). The dewetting behaviors of 17 nm thick P(S-Cl5)/PS films are rather different. The increase of film stability is observed when the concentration of the added P(S-Cl5) is 10 and 20 wt.%. Further increasing amount of the copolymer to 30 and 40 wt.% leads to the opposite results. The AFM images in Figure. 4.26 (n,o) reveal large holes within the films. The large scale OM images provide consistent results. This observation indicates that the presence of relatively high amount of P(S-Cl5) within the 17 nm thick film causes the instability.

The effects of P(S-Cl5) on the stability of films with different thicknesses are summarized in Figure. 4.27. The plots of dewetting area versus annealing time show the increase of dewetting rate of the 17 nm thick films upon increasing P(S-Cl5)

concentration from 20 to 40 wt.% (Figure. 4.27(a)). The dewetting rates of films contain 40 wt.% of P(S-Cl5) at different thicknesses are compared in Figure. 4.27(b). It is obvious that the dewetting rate of the 5 and 11 nm thick films is much slower than that of the 17 nm thick film. Figure. 4.27(c) plots the dewetting area of the films annealed for 36 h as a function of P(S-Cl5) concentration. For the 5 nm and 11 nm thick films, the film stability systematically increases with concentration of the copolymer. For the 17 nm thick films, the improvement of film stability is observed when the P(S-Cl5) concentration is 10 and 20 wt.%. The dewetting of films containing higher amount of the copolymer is comparable to that of pure PS film. This result indicates that the effectiveness of P(S-Cl5) as a dewetting inhibitor depends on film thickness and copolymer concentration. We suggest that this behavior arises from the interfacial segregation of the copolymer. For the relatively thin films (5 and 11 nm), the polar ClMS groups of the P(S-Cl5) can effectively segregate to SiOx/Si surface (Figure. 4.28). The dipolar interaction of ClMS group with the substrate provides anchoring sites for the copolymer. For the thicker films (17 nm), some fraction of ClMS groups may remain within the PS matrix. This group is incompatible with PS matrix due to its higher polarity. Therefore, the free ClMS groups behave as nucleation sites for phase separation, which leads to the instability.

The investigation of P(S-Cl20)/PS and P(S-Cl45)/PS systems shows the opposite results. Figure 4.29 compares OM images of the 17 nm thick films of P(S-Cl5)/PS, P(S-Cl20)/PS and P(S-Cl45)/PS annealed at 165 °C for 36 h. It is clear that the stability of P(S-Cl20)/PS and P(S-Cl45)/PS films increases with concentration of the copolymers. The dewetting rates of the films containing 2 mol% of ClMS group are illustrated in Figure. 4.30(a). The dewetting rate of P(S-Cl20)/PS and P(S-Cl45)/PS systems is very low compared to that of P(S-Cl5)/PS. Figure. 4.30(b) also shows that the dewetting area systematically decrease with concentration of P(S-Cl20) and P(S-Cl45) copolymers. We believe that the extent of the copolymer segregation to polar SiOx/Si surface increases with concentration of polar ClMS group along the polymeric backbone. Therefore, the copolymers with high mole ratio of ClMS group are expected to mostly populate at

SiOx/Si surface, which in turn enhances the interfacial interactions between PS matrix and the solid substrate as shown in Figure 4.30(c-e). This observation is consistent with the result in section 4.2.
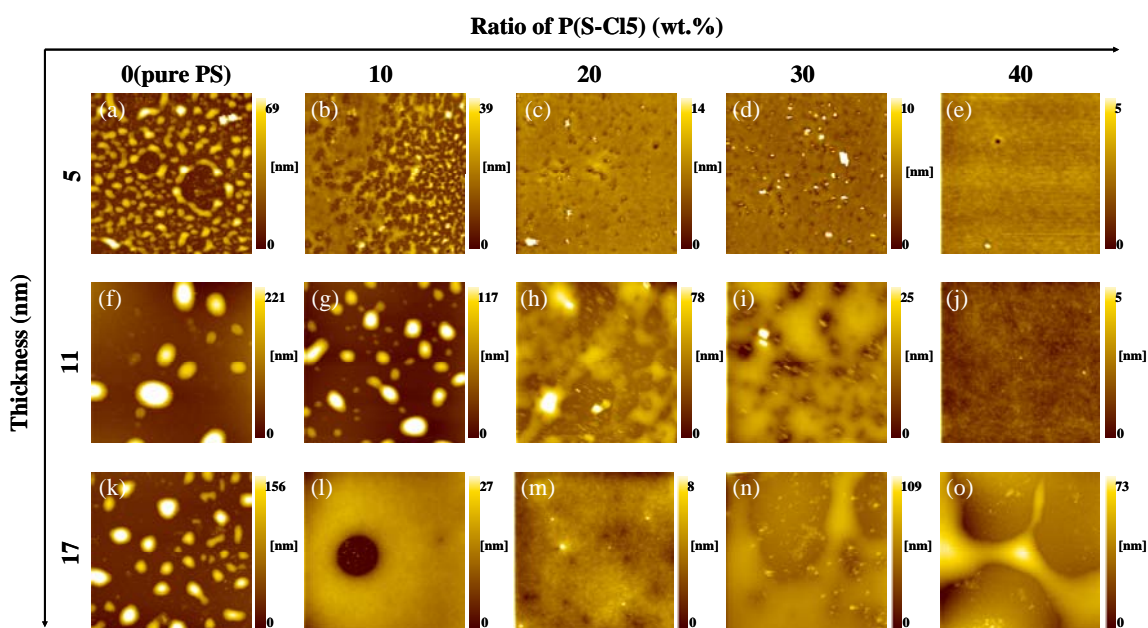
Figure. 4.26 AFM topography images of ~5, ~11 and ~17 nm thick P(S-Cl5)/PS films. Scan size is 8✕8 μm^2. Ratios of P(S-Cl5) are 0, 10, 20, 30 and 40 wt.%. The 5 nm thick films are annealed at 120 $^\circ$C while annealing temperature of the thicker films is 165 $^\circ$C. The annealing time is 36 h.
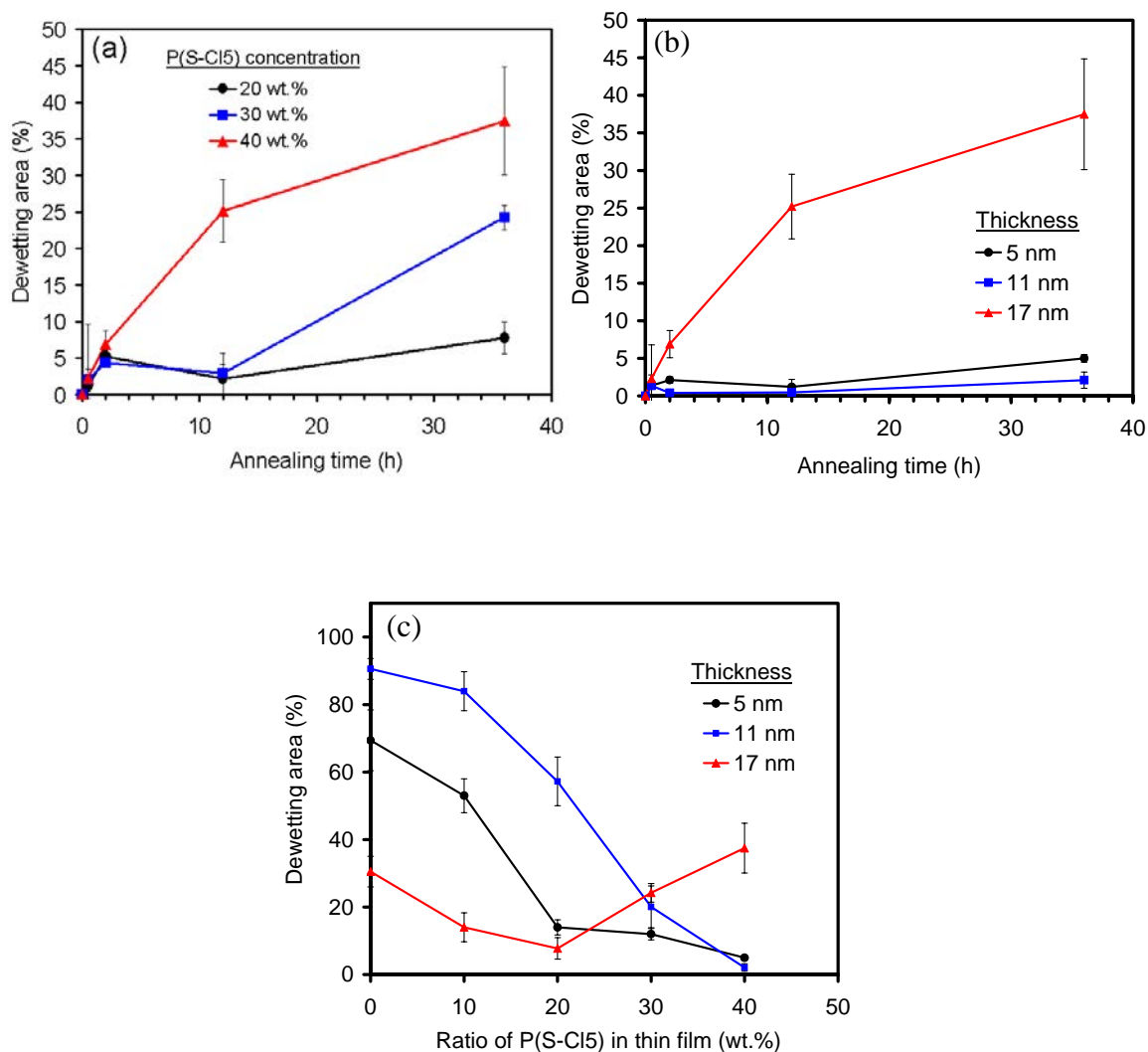
Figure. 4.27 (a) Plots of dewetting area versus annealing time of 17 nm thick P(S-Cl5)/PS films containing 20, 30 and 40 wt.% of the copolymer. (b) Plots of dewetting area versus annealing time of 5, 11 and 17 nm thick P(S-Cl5)/PS films containing 40 wt.% of the copolymer. (c) Plots of dewetting area versus concentration of P(S-Cl5) within the films. The films were annealed at 120 °C (5 nm) and 165 °C (11 nm and 17 nm) for 36 h.

5 nm   11 nm   17 nm
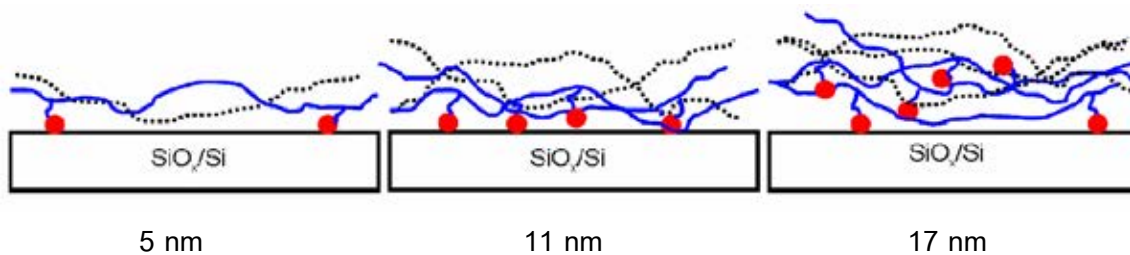
Figure. 4.28 Illustration for interaction of the P(S-Cl5) copolymer with SiO$_x$/Si surface in the films with different thicknesses.
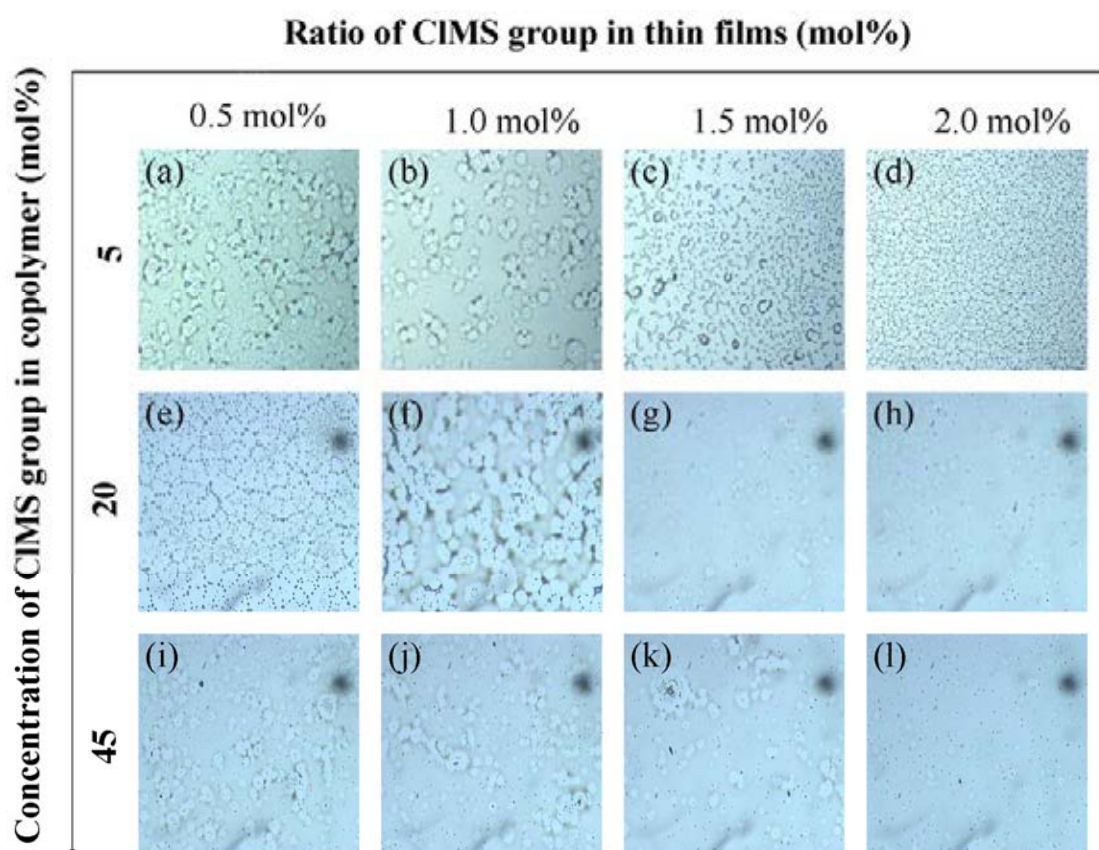
Figure. 4.29 Optical microscope images of 17 nm thick P(S-Cl5)/PS, P(S-Cl20)/PS and P(S-Cl45)/PS films annealed at 165 $^\circ$C for 36 h. Size of image is 80 × 80 μm^2.
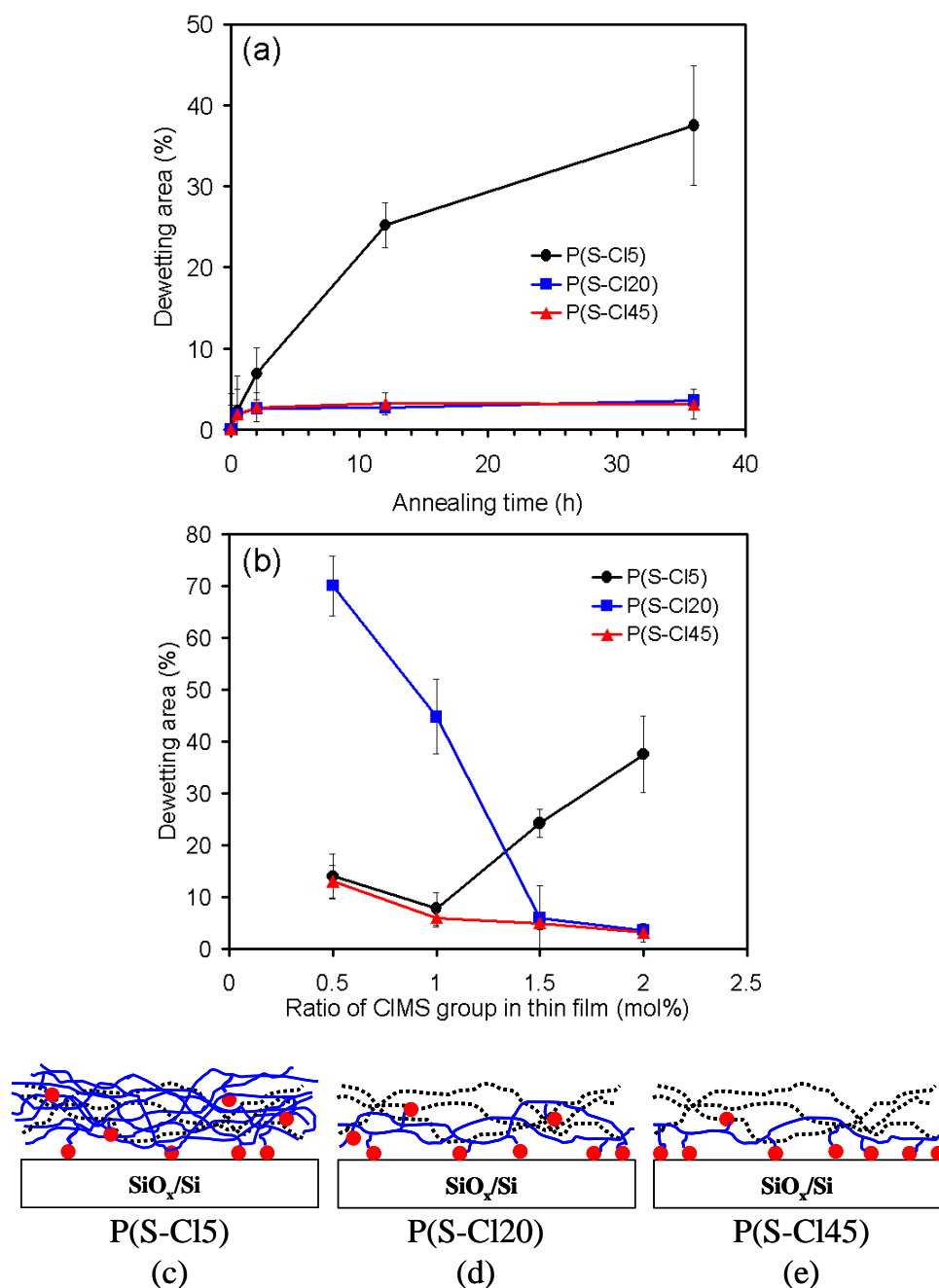
Figure 4.30 (a) Plots of dewetting area versus annealing time of 17 nm thick P(S-Cl5)/PS, P(S-Cl20)/PS and P(S-Cl45)/PS films containing 2.0 mol% of ClMS group. (b) Plots of dewetting area versus ratio of ClMS group within the 17 nm thick P(S-Cl5)/PS, P(S-Cl20)/PS and P(S-Cl45)/PS films. The films are annealed at 165 °C for 36 h. (c), (d) and (e) illustration for interaction of the P(S-Cl5), P(S-Cl20) and P(S-Cl45) copolymer with SiOx/SI surface in the 17 nm thick film.

4.5. Effects of Fe$_3$O$_4$ nanoparticle ratio on film stability

In this part, Fe$_3$O$_4$ nanoparticles are introduced as a dewetting inhibitor for PS films of thickness 5, 17 and 38 nm. Fe$_3$O$_4$ nanoparticles are used at concentrations of 0.005, 0.01, 0.02 and 0.03 wt%. All films are annealed at 165 $^\circ$C for 20, 30 and 60 min. Optical images of pure PS and Fe$_3$O$_4$/PS thin films (~17 nm thick) annealed at 165 $^\circ$C for 20, 40 and 60 min are shown in Figure 4.31(a-f). The result shows that total dewetting of PS film occurred at this annealing condition (Figure 4.31(a-c)). When small amount of Fe$_3$O$_4$ nanoparticle are added into PS film, dewetting dynamics are significantly reduced. As shown in Figure 4.31(d-f), the dewetting area of film (~17 nm) containing 0.01 wt% of Fe$_3$O$_4$ nanoparticles are much smaller compared to that of the pure PS film. The dewetting area of annealed pure PS film at 165 $^\circ$C for 20 min is around 92±1%. When Fe$_3$O$_4$ nanoparticles are added into system, the dewetting area of annealed PS film containing 0.01 wt.% Fe$_3$O$_4$ nanoparticles, annealed at 165 $^\circ$C for 20, 40 and 60 min, are around 17±2%, 17±1% and 42±5%, respectively.
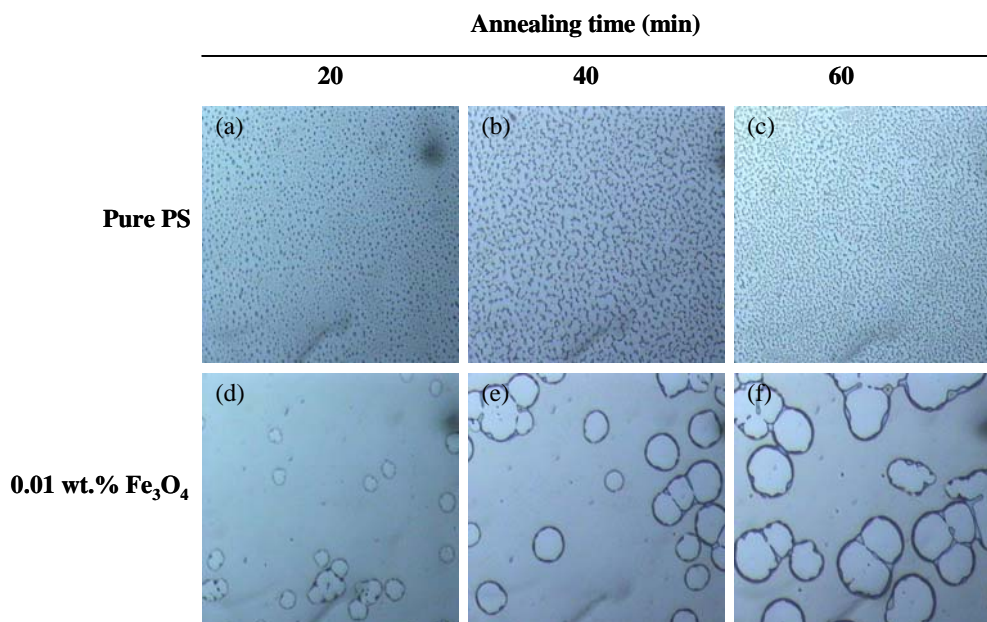
Figure 4.31 OM images of 17 nm thick (a-c) pure PS film (d-f) PS film containing 0.01 wt.% of Fe$_3$O$_4$ nanoparticles. The films are annealed at 165 $^\circ$C for 20, 40 and 60 min.

4.5.1 Effects of Fe_3O_4 nanoparticle ratios on stability of ~17 nm thick Fe_3O_4/PS films

Figures 4.32-4.34 show OM image of ~17 nm thick Fe_3O_4/PS films containing Fe_3O_4 nanoparticles range from 0-0.03 wt%. Films are annealed at 165 $^\circ$C for 20, 40 and 60 min, respectively. It is clear that the dewetting dynamics slow down significantly when the small amounts of Fe_3O_4 nanoparticles are added into the PS thin film. Figure 4.32 illustrates the surface morphology of thin films annealed for 20 min. In the pure PS film, film droplets are observed and dewetting area is around 92%. Addition of Fe_3O_4 nanoparticles results in dewetting suppression. At this annealing condition, the dewetting area detected in the film containing 0.005-0.03 wt% of the Fe_3O_4 are 32±5, 17±2, 11±2 and 7±2%, respectively. For short annealing time, it is clear that the stability of PS thin film systematically increases with ratios of the Fe_3O_4 nanoparticles. When the annealing times are increased to 40 min. Pure PS film already breaks up into droplets while the film containing 0.005 wt% of the Fe_3O_4 nanoparticle partially dewets the substrate as shown in Figure 4.33(a) and 4.33(b), respectively. Although the holes slightly expand in the films containing 0.01 wt.% of the Fe_3O_4 nanoparticle as shown in Figure 4.33(c), the films are stable at this annealing condition. For thin films containing 0.02 to 0.03 wt%, we have found that the dewetting areas enhance significantly on polymeric thin films, which are around 40%.

The dewetting behaviors of 17 nm thick Fe_3O_4/PS films are rather different for annealing time of 60 min. As shown in Figure 4.34, the increase of film stability is observed when the concentration of Fe_3O_4 is upto 0.01 wt.%. Further increasing the amount of the Fe_3O_4 nanoparticle to 0.02 and 0.03 wt.% leads to the opposite results. The OM images in Figure. 4.34 (d) reveal intermediate dewetting stage and Figure. 4.34 (e) shows total dewetting within the films. The dewetting area of thin film containing Fe_3O_4 nanoparticles range from 0-0.03 wt% are around 93, 86, 42, 84 and 82%, respectively. This observation indicates that the presence of relatively high amount of

Fe_3O_4 within the 17 nm thick film causes the instability. We suggest that increasing film stability by the addition of Fe_3O_4 nanoparticles at 0.05-0.01 wt% is the result of pining effect on polymeric thin films. On the other hand, increasing concentrations of Fe_3O_4 nanoparticles to 0.02 and 0.03 wt% causes nanoparticle aggregation and leads to dewetting dynamics.

Figure 4.35 shows the dewetting areas of 17 nm thick pure PS and Fe_3O_4/PS thin films as a function of annealing time. The dewetting rates of the thin films relate to the slopes of plots between the dewetting area and the annealing time. Thus, it is clear that the dewetting rate significantly decreases upon the addition of small amount of Fe_3O_4 nanoparticles into PS thin film. For short annealing time (20 min.), the dewetting area of Fe_3O_4/PS thin film is about 20 % while the dewetting area of pure PS film already reaches 90 %.

We also observed that the increase of Fe_3O_4 nanoparticles concentrations affected the stability of thin films. The dewetting behaviors of PS/Fe_3O_4 thin films with various Fe_3O_4 concentrations ranging from 0.005, 0.01, 0.02 and 0.03 wt%, were investigated. Figure 4.36 illustrates OM images of the thin films annealed at 165 $^\circ$C for 20, 40 and 60 min. For relatively short annealing time (20 min.), the dewetting areas systematically decrease with increasing ratio of Fe_3O_4 nanoparticles in thin films. The dewetting area of thin films containing 0.01, 0.02 and 0.03 wt% of Fe_3O_4 nanoparticles are about 18, 12 and 9%, respectively (Figure 4.37). When the annealing time is further increased to 40 and 60 min., the film containing 0.01 wt% of Fe_3O_4 nanoparticles exhibits the highest stability compared to other Fe_3O_4/PS thin films. Increasing the concentration of Fe_3O_4 nanoparticles to 0.02 and 0.03 wt.% does not result in a systematic increase of film stability (Figure 4.37). Therefore, the concentration is crucial in controlling the stability of polymeric thin films.
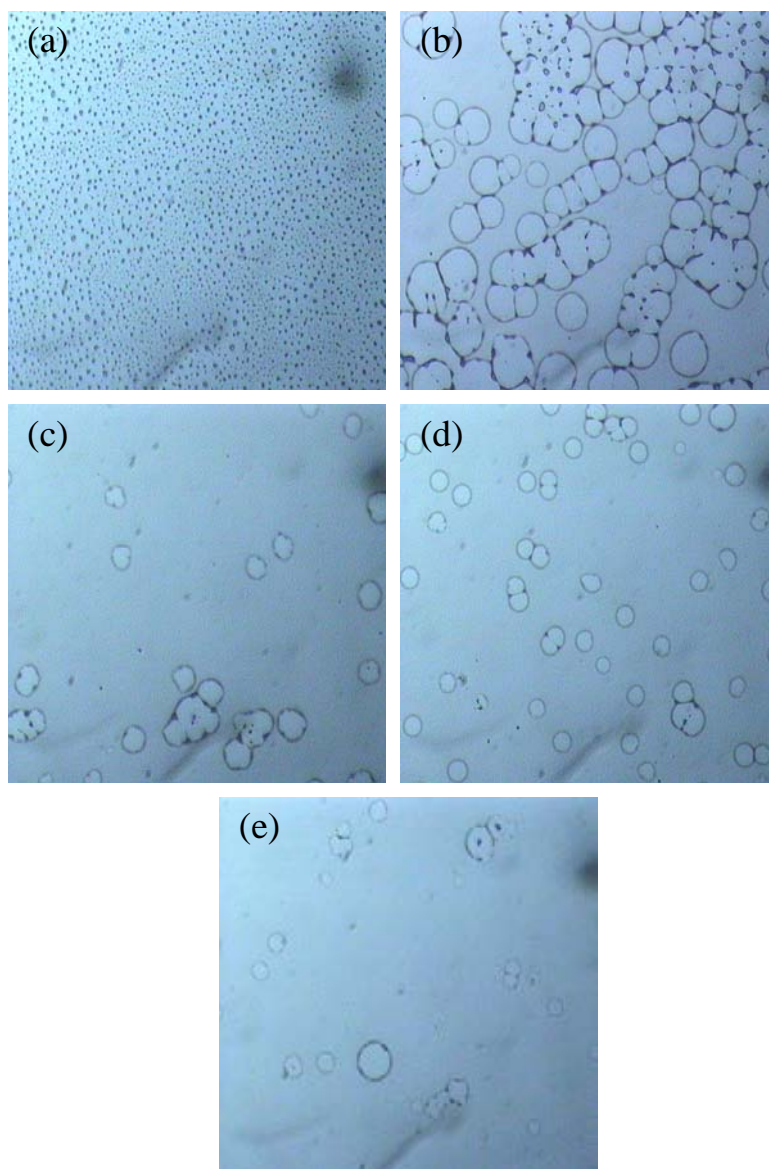
Figure 4.32 OM images of ~17 nm thick Fe_3O_4/PS films annealed at 165 $^\circ$C for 20 min. Ratios of Fe_3O_4 nanoparticles are (a) 0 wt%, (b) 0.005 wt%, (c) 0.01 wt%, (d) 0.02 wt%, and (e) 0.03 wt%.

Figure 4.33 OM images of ~17 nm thick Fe_3O_4/PS films annealed at 165 $^\circ$C for 40 min. Ratios of Fe_3O_4 nanoparticles are (a) 0 wt%, (b) 0.005 wt%, (c) 0.01 wt%, (d) 0.02 wt%, and (e) 0.03 wt%.

Figure 4.34 OM images of ~17 nm thick Fe_3O_4/PS films annealed at 165 $^\circ$C for 60 min. Ratios of Fe_3O_4 nanoparticles are (a) 0 wt%, (b) 0.005 wt%, (c) 0.01 wt%, (d) 0.02 wt%, and (e) 0.03 wt%.

Figure 4.35 Dewetting area versus annealing time of 17 nm thick pure PS and Fe_3O_4 /PS

(0.01/99.99 w/w) thin films annealed at 165 $^{\circ}$C

Figure 4.36 OM images of Fe_3O_4/PS thin films (~17 nm) containing different Fe_3O_4

nanoparticle concentration varying from 0 to 0.03 wt% in thin film annealed at 165 $^{\circ}$C for

20, 40 and 60 min.

Figure 4.37 Dewetting area of Fe_3O_4/PS thin films (~17 nm) versus Fe_3O_4 concentration. The films were annealed at 165 $^{\circ}$C for 20, 40 and 60 min.

4.5.2 Effects of Fe_3O_4 nanoparticle ratios on stability of ~38 nm thick Fe_3O_4/PS films

Figure 4.38-4.40 show OM images of ~38 nm thick Fe_3O_4/PS films containing Fe_3O_4 nanoparticles range from 0-0.03 wt.%, which are annealed at 180 $^{\circ}$C for 20, 40 and 60 min, respectively. The results of dewetting behavior in this condition are in agreement with ~17 nm thick Fe_3O_4/PS films. For short annealing time (20 min), the dewetting area of thin films containing Fe_3O_4 nanoparticles range from 0-0.03 wt% are aroud 36±4%, 27±4%, 11±2%, 19±5% and 23±5%, respectively, as shown in Figure 4.38. When increasing annealing time to 40 min, the dewetting area of thin films containing Fe_3O_4 nanoparticles range from 0-0.03 wt% are aroud 89±2%, 56±5%, 32±4%, 26±5% and 49±5%, respectively (Figure 4.39). Figure 4.40 shows OM images of thin films annealing for 60 min, the dewetting area of thin films containing Fe_3O_4 nanoparticle range from 0-0.03 wt% are aroud 91±1%, 71±2%, 45±5%, 29±4% and 52±5%, respectively. Figure 4.41 shows the dewetting area of 38 nm thick pure PS and

Fe_3O_4/PS thin film containing 0.02 wt.% of Fe_3O_4 nanoparticles as a function of annealing time. The dewetting rates of the thin films relate to the slopes of the plots. It is clear that the dewetting rate significantly decreases upon the addition of small amount of Fe_3O_4 nanoparticles into PS thin film. The dewetting area of Fe_3O_4/PS thin film is much smaller compared with that of pure PS thin film.

Effects of Fe_3O_4 nanoparticles on stability of ~38 nm films are concluded in Figure 4.42 and 4.43. For relatively short annealing time (20 min.), the dewetting areas decrease with increasing ratio of Fe_3O_4 nanoparticles in thin films. At this annealing condition, the dewetting area of thin films containing 0.005-0.03 wt% of Fe_3O_4 nanoparticle are less than 20%. When the annealing time is increased to 40 and 60 min., the film containing 0.02 wt% of Fe_3O_4 nanoparticle exhibits the highest stability compared to other Fe_3O_4/PS thin films. However, the increase of Fe_3O_4 nanoparticles concentration to 0.03 wt% decreases the film stability. The results suggest that high concentration of Fe_3O_4 causes nanoparticles aggregation, which leads to film instability. Therefore, the concentration is crucial for controlling the stability of polymeric thin film.
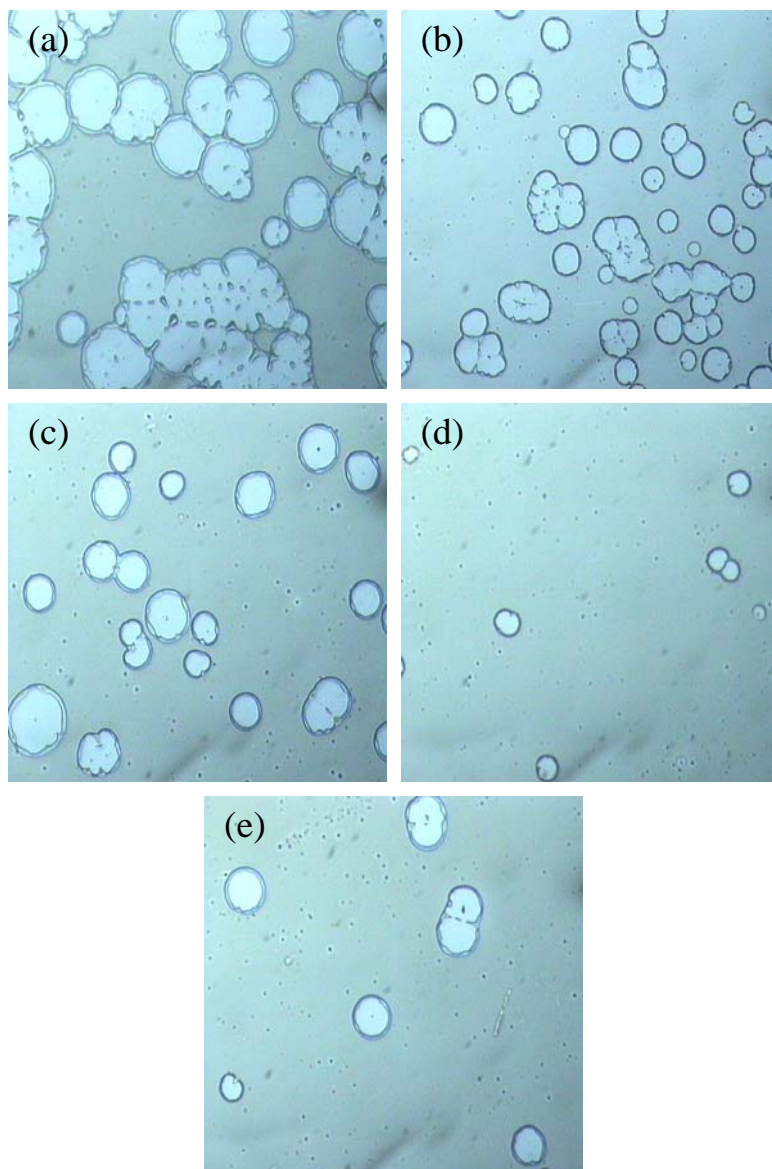
Figure 4.38 OM images of ~38 nm thick Fe$_3$O$_4$/PS films annealed at 180 $^\circ$C for 20 min. Ratios of Fe$_3$O$_4$ nanoparticles are (a) 0 wt%, (b) 0.005 wt%, (c) 0.01 wt%, (d) 0.02 wt%, and (e) 0.03 wt%.
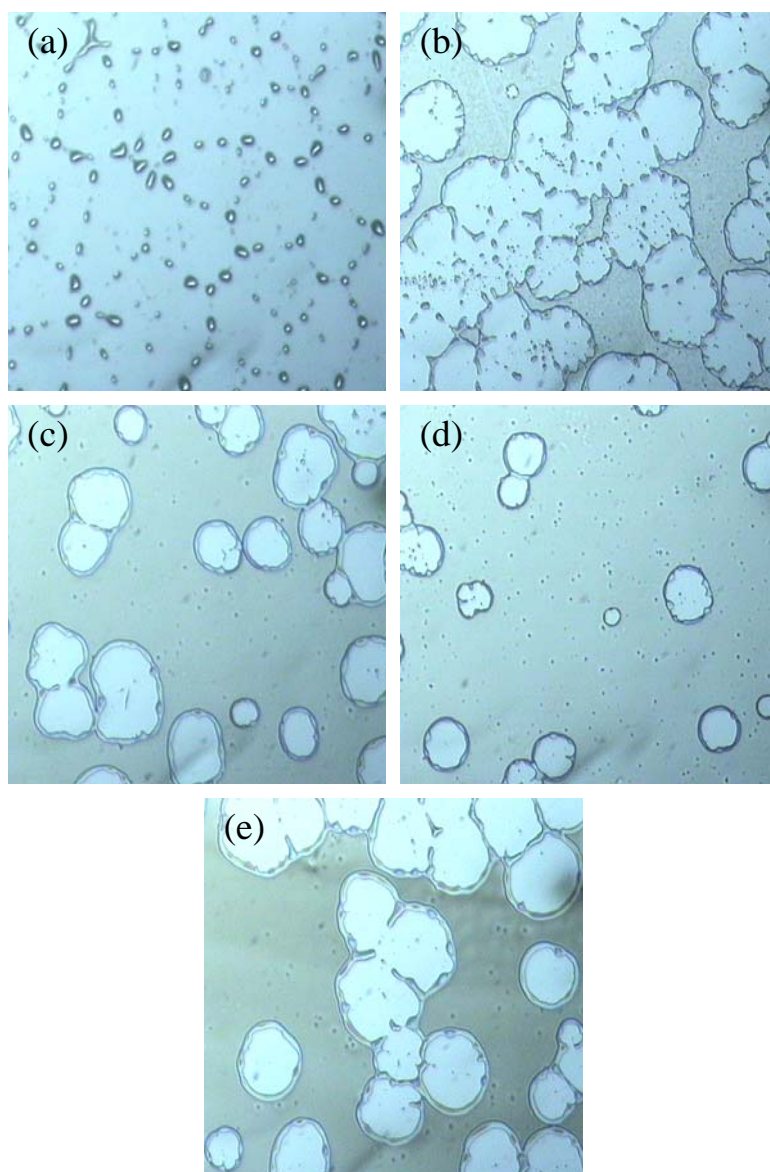
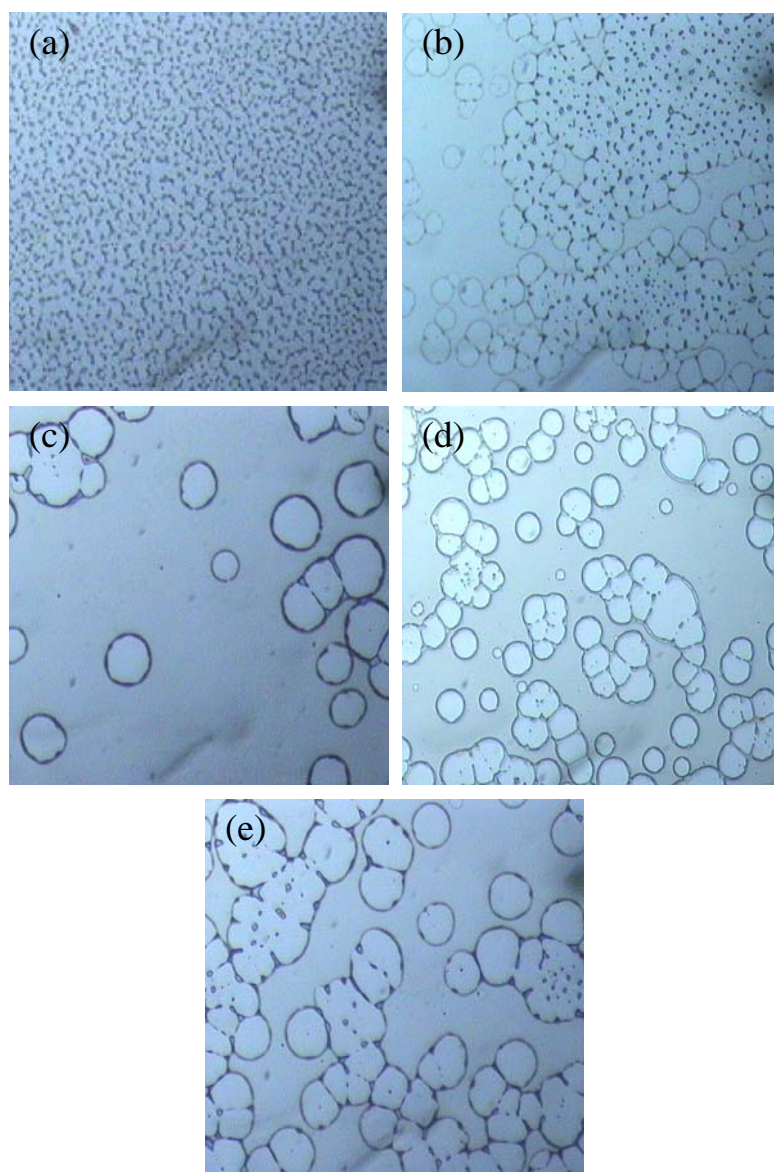Figure 4.39 OM images of ~38 nm thick Fe$_3$O$_4$/PS films annealed at 180 $^{\circ}$C for 40 min. Ratios of Fe$_3$O$_4$ nanoparticles are (a) 0 wt%, (b) 0.005 wt%, (c) 0.01 wt%, (d) 0.02 wt%, and (e) 0.03 wt%.
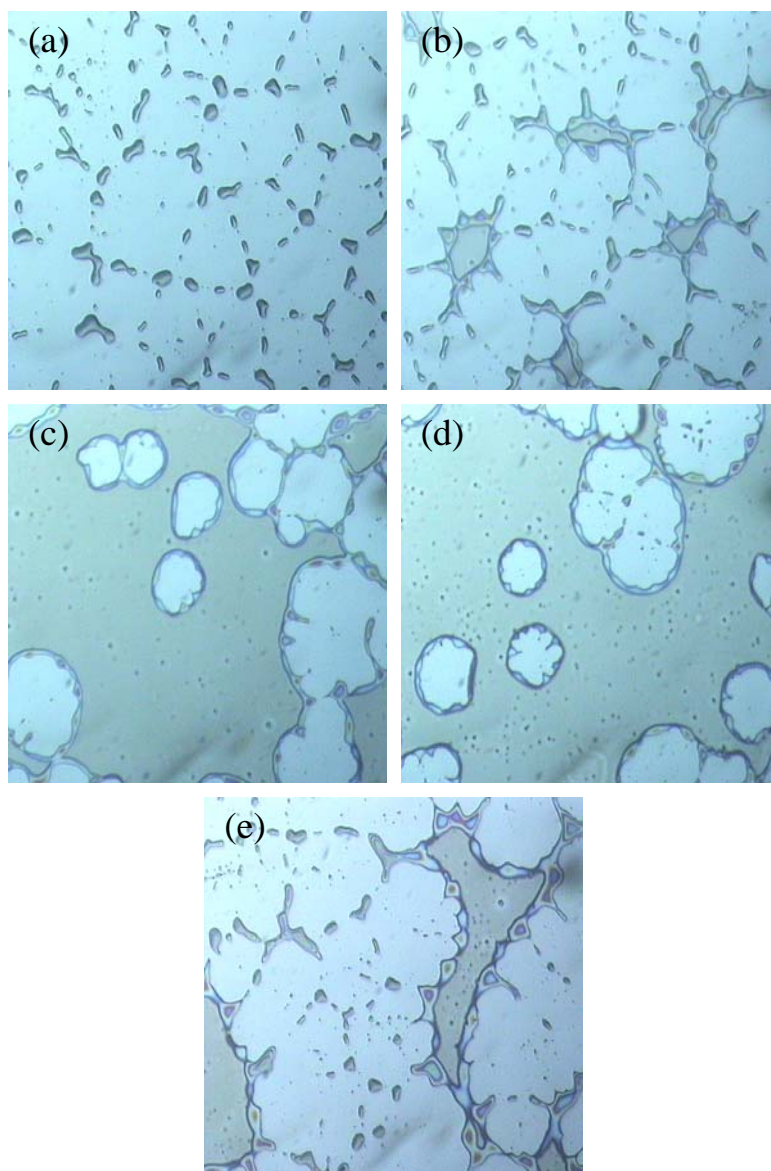
Figure 4.40 OM images of ~38 nm thick Fe$_3$O$_4$/PS films annealed at 180 $^\circ$C for 60 min. Ratios of Fe$_3$O$_4$ nanoparticles are (a) 0 wt%, (b) 0.005 wt%, (c) 0.01 wt%, (d) 0.02 wt%, and (e) 0.03 wt%.
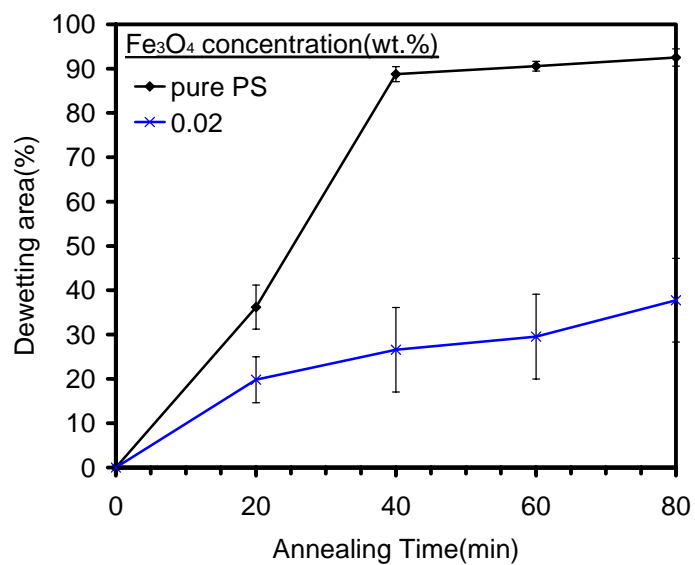
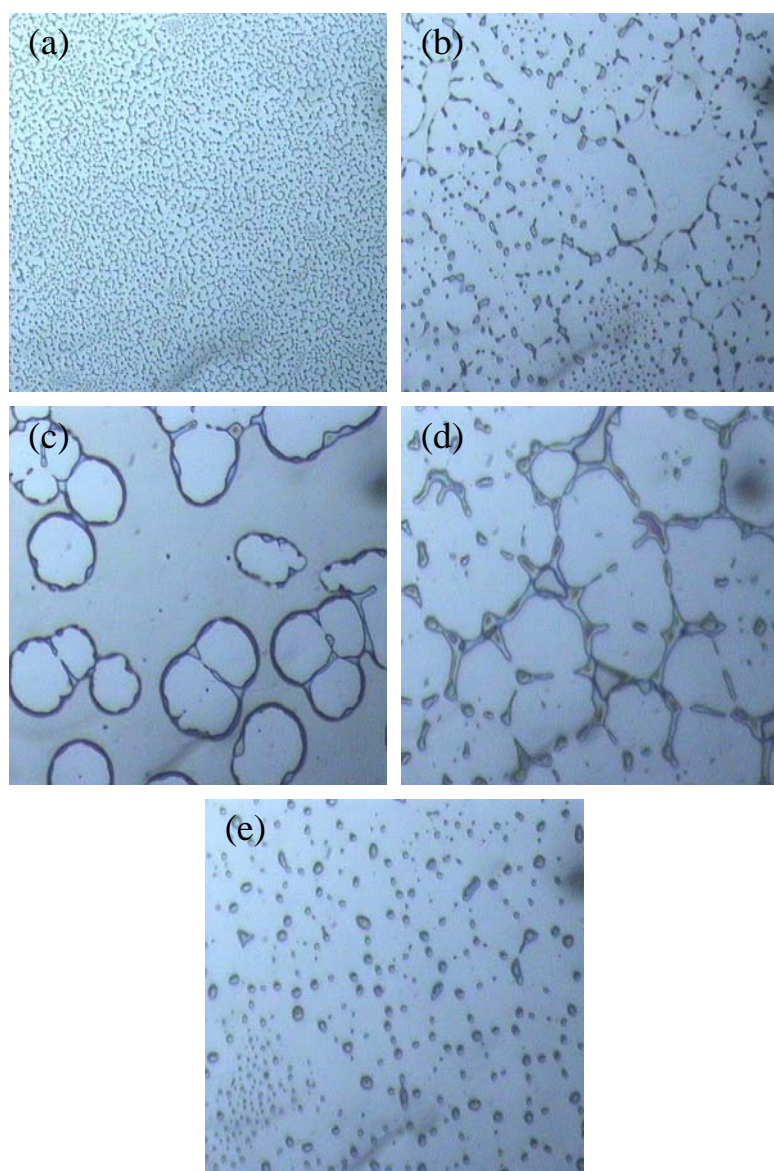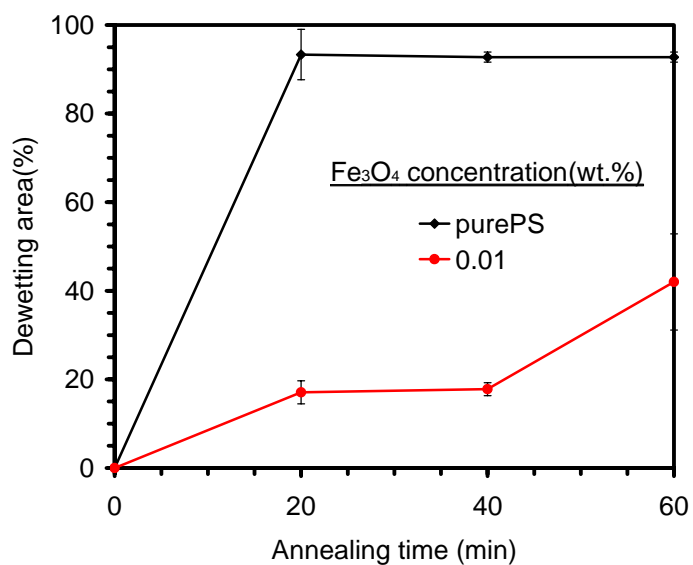Figure 4.41 Dewetting area versus annealing time of 38 nm thick pure PS and Fe_3O_4/PS (0.02 /99.98w/w) thin films annealed at 180 °C.
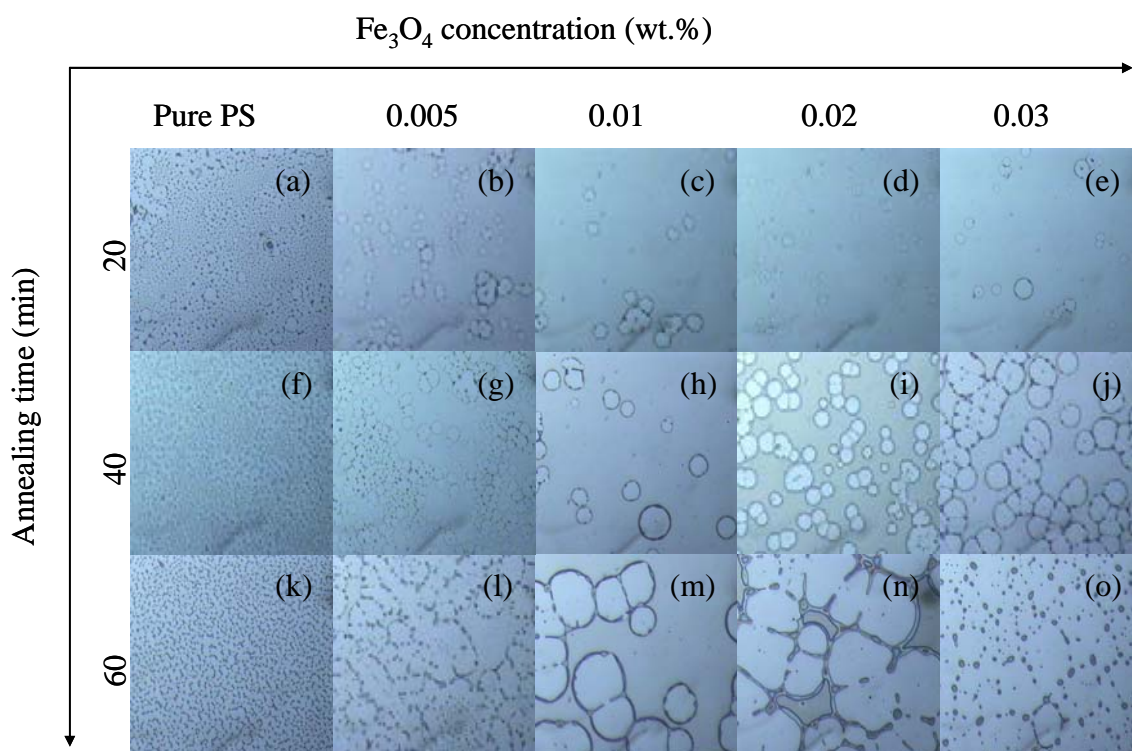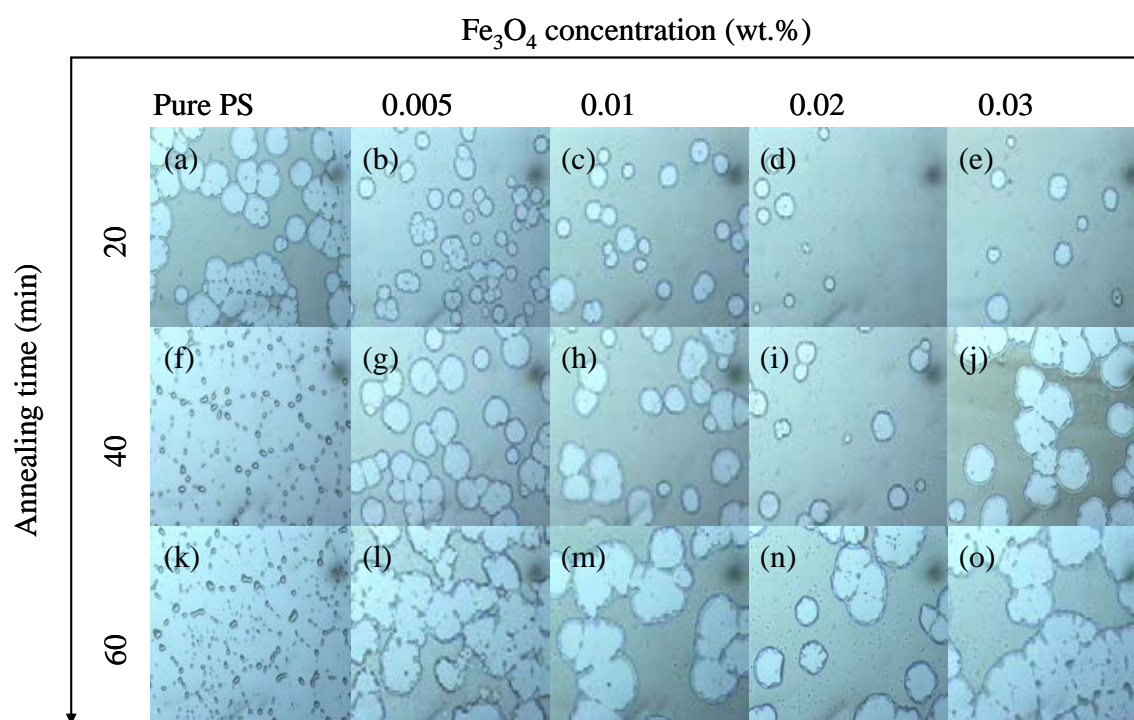

Figure 4.42 OM images of Fe_3O_4/PS thin films (~38 nm) containing different Fe_3O_4 nanoparticles concentrations varying from 0 to 0.03 wt% annealed at 180 °C for 20, 40 and 60 min.
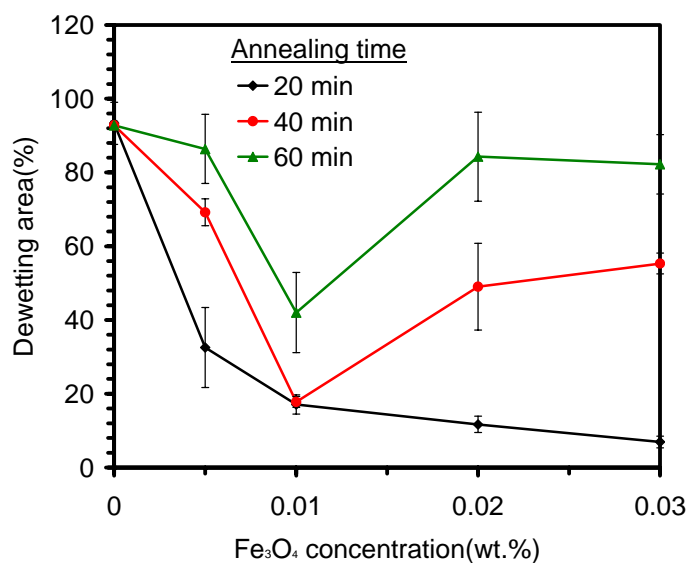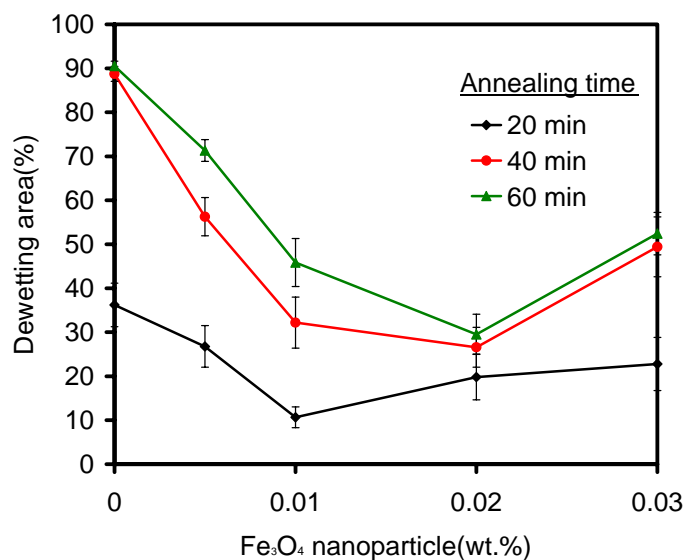
Figure 4.43 Dewetting area of Fe_3O_4/PS nanoparticle thin films (~38 nm) versus Fe_3O_4 nanoparticle concentration. The films were annealed at 165 °C for 20, 40 and 60 min.

4.6. Effects of Fe_3O_4/PS film thickness

Thin films of pure PS and Fe_3O_4/PS with thicknesses of 5, 17 and 38 nm are fabricated. The annealing temperature is 120 °C for the 5 nm thick films, 165°C for the 17 nm thick films and 180 °C for the 38 nm thick films. The evolution of film morphology at different length scales is followed by utilizing optical microscopy (OM). The OM images of 5 nm thick Fe_3O_4/PS films annealed for 20 min are illustrated in Figure. 4.44. This result shows that pure PS thin film is smooth and homogeneous. On the other hand, the dewetting of films containing Fe_3O_4 nanoparticles range from 0.005-0.03 wt% reaches final state, where hemispherical droplets of the polymer are observed at this condition. Therefore, the addition of Fe_3O_4 nanoparticles into 5 nm thick PS films results in the decrease of film stability and accelerates dewetting dynamics on thin film as shown in Figure 4.44. This is due to the size of Fe_3O_4 nanoparticles, ~9 nm, which is larger than the film thickness. Thus, Fe_3O_4 nanoparticles act as impurities which accelerates dewetting dynamics on thin film.

For 17 nm thick Fe_3O_4/PS films, annealing at 165 $^\circ$C for 20 min, films are smooth and continuous. The annealing time is increased to 60 min to study the dewetting process and the result is shown in Figure 4.44. With addition of Fe_3O_4 at 0.01 wt%, stability of Fe_3O_4/PS films increase via a result of pining as shown in Figure 4.46. However, further increasing amount of the Fe_3O_4 nanoparticles to 0.02 and 0.03 wt.% leads to the opposite results. The OM images in fFigure 4.44 reveal large holes within the films. This observation indicates that the presence of >0.01 wt% Fe_3O_4 nanoparticles within the 17 nm thick film causes the instability.

When increasing film thickness to 38 nm, results are similar to those of 17 nm thick Fe_3O_4/PS films. For short annealing time (20 min), the addition of Fe_3O_4 nanoparticles slightly reduce the dewetting dynamics. The dewetting area of pure PS is about 36% and thin film containing Fe_3O_4 nanoparticles ranging from 0.005-0.03 wt.% are around 27, 11, 20 and 23%, respectively. For annealing time of 60 min, increasing ratios of Fe_3O_4 nanoparticles to 0.02 wt% suppress the dewetting dynamics as shown in Figure 4.44. However, the film stability decreases with addition of 0.03 wt% Fe_3O_4 nanoparticles.

The dewetting dynamics of films with different thicknesses are compared in Figure 4.45. It is obvious that the dewetting rates of the 17 nm and 38 nm thick films are much slower than that of the 5 nm thick films. For film thickness of 5 nm, the addition of Fe_3O_4 nanoparticles leads to dewetting because the size of Fe_3O_4 particles is larger than the film thickness. Therefore, Fe_3O_4 nanoparticles are the origin of the dewetting process. For film thickness of 17 nm, the addition of Fe_3O_4 nanoparticles at 0.01 wt% increase film stability. However, increasing Fe_3O_4 nanoparticles concentration to 0.02 and 0.03 wt% leads to completely dewetting on thin film with dewetting areas of more than 80%. For 38 nm thick films, the results are similar with 17 nm thick films in which 0.03 wt% of Fe_3O_4 nanoparticles cause a decreasing in film stability.The dewetting area

of 38 nm films containing 0-0.03 wt% Fe_3O_4 nanoparticles are around 90, 70, 45, 30 and 5, respectively.

This result indicates that the effectiveness of Fe_3O_4 as a dewetting inhibitor depends on film thickness and Fe_3O_4 nanoparticles concentration. When the film thickness is less than the size of the nanoparticle additives (5 nm thick films), the nanoparticles act as impurities, which are the origin of dewetting. For 17 and 38 nm thick films, addition of Fe_3O_4 nanoparticles at optimum amounts improves film stability due to pinning effect of the Fe_3O_4 nanoparticles that can effectively segregate to SiO_x/Si surface. However, if the concentration of Fe_3O_4 nanoparticles is too high, particle agglomeration can occur, which leads to dewetting of the thin films as shown in Figure 4.47.
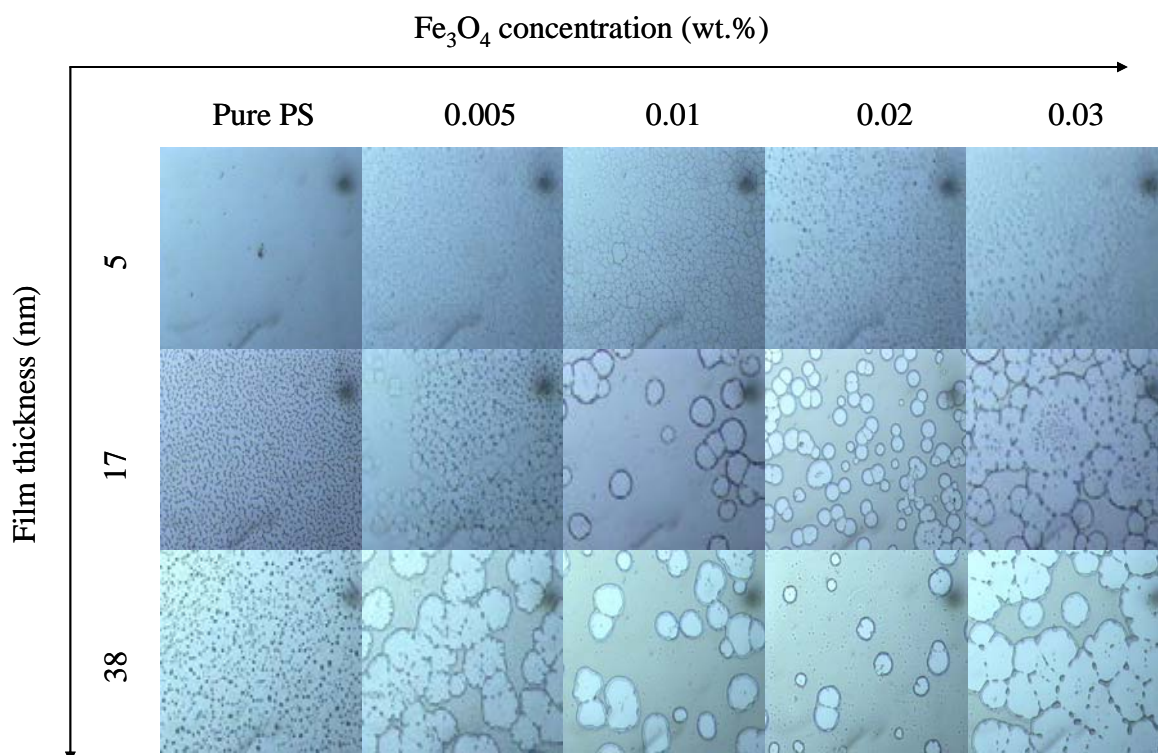
Figure 4.44 OM images of ~5, 17 and 38 nm thick Fe_3O_4/PS films with 0-0.03 wt% nanoparticles annealed at 120, 165 and 180°C, respectively.
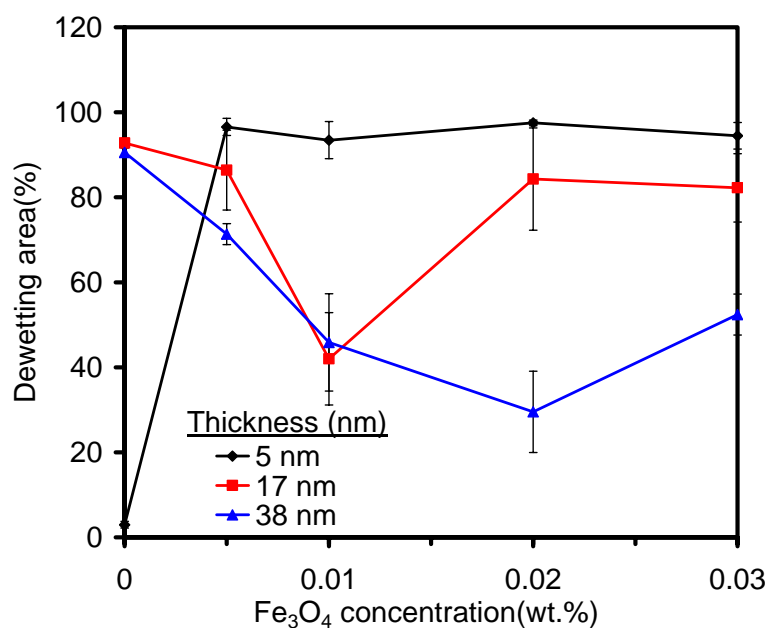
Figure 4.45 Dewetting area versus the Fe_3O_4 nanoparticle concentration of ~5, 17 and 38 nm thick Fe_3O_4/PS films annealed for 60 min.
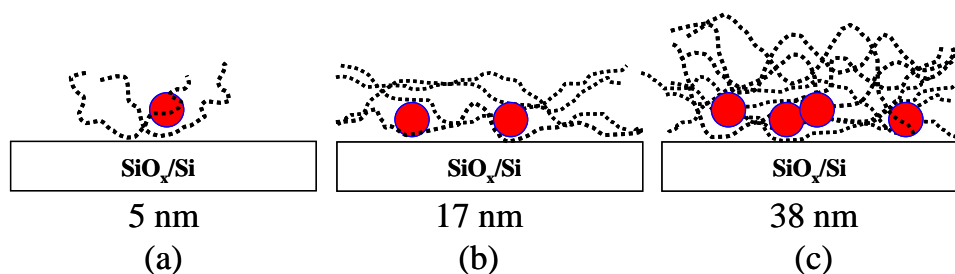
Figure 4.46 Illustration for result of pining of the Fe_3O_4 nanoparticle concentration at 0.005, 0.01 and 0.02 of ~5, 17 and 38 nm thick Fe_3O_4/PS films, respectively.
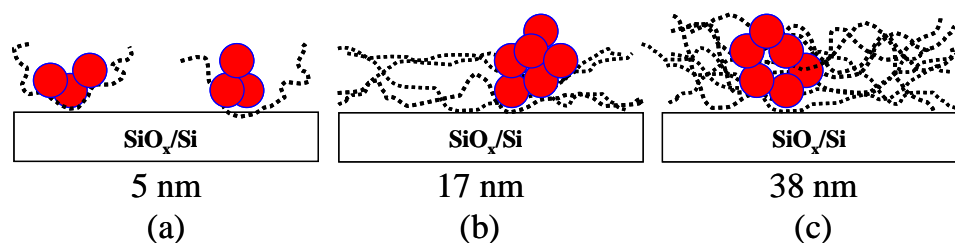
Figure 4.47 Illustration for result of pining of the Fe_3O_4 nanoparticle concentration at 0.03 of ~5, 17 and 38 nm thick Fe_3O_4/PS films.

CHAPTER V

CONCLUSIONS

This research demonstrates that poly(styrene-stat-chloromethylstyrene)(P(S-ClX)) copolymers and Fe_3O_4 nanoparticles can be utilized as a dewetting inhibitor for PS thin film of thickness less than 50 nm. We can conclude that :

1.   The existence of ClMS group in P(S-ClX) copolymer causes the increase of the polar component (γ_s^h) . Therefore, the addition of P(S-ClX) copolymers containing ClMS group into PS film enhances the interfacial dipolar interaction with SiO_x/Si substrate, which increases film stability.

2.   An addition of only 1 mol% of ClMS group in the polymeric thin film can drastically retard the dewetting dynamics while the alteration of physical properties of the film is at the minimum.

3.   The effectiveness of the P(S-ClX) copolymers as a dewetting inhibitor is found to vary with their chemical structures. The P(S-ClX) copolymers with higher ratio of polar ClMS group exhibit much higher efficiency. The increase of ClMS groups along the backbone of copolymer allows short distance between the ClMS groups, which in turn enhances the interfacial interactions between PS matrix and solid substrate via dipolar interaction.

4.   For the relatively thin films (5 and 11 nm), the polar ClMS groups of the P(S-Cl5) can effectively segregate to SiOx/Si surface, providing anchoring sites for the copolymer. For the thicker films (17 nm), fractions of ClMS groups may remain within the PS matrix. This group is incompatible with PS matrix due to its high polarity. Therefore,

the free ClMS groups behave as nucleation sites for phase separation, which leads to the instability of the film.

5.   The addition of small quantity of Fe_3O_4 nanoparticles causes retardation of dewetting dynamics in Fe_3O_4/PS thin film of thickness 17 and 38 nm due to pinning effect. For 5 nm thick PS films, the nanoparticles act as impurities which accelerate dewetting dynamics of the film.

6. The dewetting dynamics of Fe_3O_4/PS thin films depends on the concentration of the nanoparticles. Best stability for thin films of thickness 17 and 38 nm are to add Fe_3O_4 concentration at 0.01 and 0.02 wt%, repectively. When increasing Fe_3O_4 cocentration to 0.03 wt%, film stability decreases to less than 0.02 wt% of Fe_3O_4. These results suggest that high concentration of Fe_3O_4 nanoparticles cause agglomeration, which are similar with dust or impurity in thin film and lead film instability.

FUTURE WORK

Suggestions for future work :

1.   Study the use of polymers with different structures such as dendrimers and three-arm polymers as dewetting inhibitors

2.   Study effects of the size of nanoparticles on dewetting suppression efficiency

3.   Vary types of nanoparticles for extensive applications

REFERENCES

[1] L. Xue, Y. Han. Pattern formation by dewetting of polymer thin film. Prog. Polym. Sci 36 (2011) : 269-293.

[2] P. Volodin, A. Kondyurin, Dewetting of thin polymer film on rough substrate: I. Theory J. Phys. D: Appl. Phys. 41 (2008) : 065306-065327.

[3] E. Bertrand, T.D. Blake, J. De Coninck. Dynamics of dewetting at the nanoscale. Eur. Phys. J. 166 (2009) : 173-176.

[4] M. Geoghegan, G. Krausch, Wetting at polymer surfaces and interfaces. Prog. Polym. Sci. 28 (2003) : 261-302.

[5] D.G. Bucknall, Influence of interfaces on thin polymer film behaviour. Prog. Mater. Sci. 49 (2004) : 713-786.

[6] G. Reiter. Unstable thin polymer films: rupture and dewetting processes. Langmuir 9 (1993) : 1344-1351.

[7] R. Konnur, K. Kargupta, A. Sharma. Instability and morphology of thin liquid films on chemically heterogeneous substrates . Phys. Rev. Lett. 84 (2000) : 931-942.

[8] G. Reiter. Direct visualization of random crystallization and melting in arrays of nanometer-size polymer crystals . Phys. Rev. Lett. 87 (2001) : 186101-186111.

[9] R. Xie, A. Karim, J.F. Douglas, C.C. Han, R.A. Weiss. Spinodal dewetting of thin polymer films. Phys. Rev. Lett. 81 (1998) : 1251-1262.

[10] R. Mukherjee, S. Das, A. Das, S. K. Sharma, A. K. Raychaudhuri, A. Sharma. Stability and Dewetting of Metal Nanoparticle Filled Thin Polymer Films: Control of Instability Length Scale and Dynamics. ACS Nano 4 (2010) : 3709-3724.

[11] F. Ania, F.J. Baltá-Calleja, S. Henning, D. Khariwala, A. Hiltner, E. Baer. Study of the multilayered nanostructure and thermal stability of PMMA/PS amorphous films. Polymer 51 (2010) : 1805-1811.

[12] J. You, S. Hua, Y. Liao, K. Song, Y. Mena, T. Shi, L. An. Composition effect on dewetting of ultrathin films of miscible polymer blend. Polymer 50 (2009) : 4745-4752.

[13] H. Ogawa, T. Kanaya, K. Nishida, G. Matsuba, Phase separation and dewetting in polystyrene/poly(vinylmethyl ether) blend thin films in a wide thickness range. <u>Polymer</u> 49 (2008) : 254-262.

[14] R. Traiphol, Influences of chain heterogeneity on instability of polymeric thinfilm:Dewetting of polystyrene, polychloromethylstyrenes and its copolymers <u>J. Colloid Interface Sci</u>. 310 (2007) : 217-228.

[15] X. Zhai, R.A. Weiss, Wetting Behavior of Lightly Sulfonated Polystyrene Ionomers on Silica Surfaces. <u>Langmuir</u> 24 (2008) : 12928-12935.

[16] G.T. Carroll, M.E. Sojka, X. Lei, N.J. Turro, J.T. Koberstein, Photoactive Additives for Cross-Linking Polymer Film: Inhibition of Dewetting in Thin Polymer Films. <u>Langmuir</u> 22 (2006) : 7748-7754.

[17] H.J. Schulze, K.W. Stöckelhuber, A. Wenger, The influence of acting forces on the rupture mechanism of wetting-nucleation or capillary waves. <u>Colloid Surface A</u> 192 (2001) : 61-72.

[18] J. Zhao, S. Jiang, Q. Wang, X. Liu, X. Ji, B. Jiang, Effect of molecular weight, solvent and substrate on dewetting morphology of polystyrene films. <u>Appl. Surf. Sci</u>. 236 (2004) : 131-140.

[19] N. Hosaka, N. Torikai, H. Otsuka, A. Takahara, Structure and Dewetting Behavior of Polyhedral Oligomeric Silsesquioxane-Filled Polystyrene Thin Films. <u>Langmuir</u> 23 (2006) : 902-907.

[20] N. Hosaka, H. Otsuka, M. Hino, A. Takahara, Control of Dispersion State of Silsesquioxane Nanofillers for Stabilization of Polystyrene Thin Films. <u>Langmuir</u> 24 (2008) : 5766-5772.

[21] J.M. Kropka, P.F. Green, Control of Interfacial Instabilities in Thin Polymer Films with the Addition of a Miscible Component. <u>Macromolecules</u> 39 (2006) : 8758-8762.

[22] J.H. Xavier, S. Sharma, Y.S. Seo, R. Isseroff, T. Koga, H. White, A. Ulman, K. Shin, S.K. Satija, J. Sokolov, M.H. Rafailovich, Effect of Nanoscopic Fillers on Dewetting Dynamics. <u>Macromolecules</u> 39 (2006) : 2972-2980.

[23] H.J. Chung, K. Ohno, T. Fukuda, R.J. Composto, Internal Phase Separation Drives Dewetting in Polymer Blend and Nanocomposite Films. Macromolecules 40 (2007) : 384-388.

[24] H. Ogawa, T. Kanaya, K. Nishida, G. Matsuba, Composition fluctuations before dewetting in polystyrene/poly(vinyl methyl ether) blend thin films. Polymer 49 (2008) : 2553-2559.

[25] S.A. Akhrass, R.V. Ostaci, Y. Grohens, E. Drockenmuller, G. Reiter, Influence of progressive Cross-linking on Dewetting of Polystyene Thin Films. Langmuir 24 (2008) : 1884-1890.

[26] Y. Liao, J. You, T. Shi, L. An, P.K. Dutta, Phase Behavior and Dewetting for Polymer Blend Films Studied by In Situ AFM and XPS: From Thin to Ultrathin Films. Langmuir 23 (2007) : 11107-11111.

[27] S. Sharma, M.H. Rafailovich, D. Peiffer, J. Sokolov, Control of Dewetting Dynamics by Adding Nanoparticle Fillers. Nano Letters. 1 (2001) : 511-514.

[28] M.M. Abul Kashem, J. Perlich, L. Schulz, S.V. Roth, W. Petry, P. Müller-Buschbaum, Maghemite Nanoparticles on Supported Diblock Copolymer Nanostructure. Macromolecules 40 (2007) : 5075-5083.

[29] L. Xu, X. Yu, T. Shi, L. An, Dewetting of Linear Polymer/Star Polymer Blend Film. Macromolecules 41 (2008) : 21-24.

[30] M. Hamieh, S. A. Akrass, T. Hamieh, P. D. S. Gabriele, T. V. E. Raphaël, G. Reiter. Influence of Substrate Properties on the Dewetting Dynamics of Viscoelastic Polymer Films. J. Adhesion 83 (2007) : 367-381.

[31] X. Zhang, F. K. Lee, O. K. C. Tsui. Wettability of End-Grafted Polymer Brush by Chemically Identical Polymer Films. Macromolecules 41 (2008) : 8148-8151.

[32] M. A. Holmes, M. E. Mackay, R. K. Giunta, Nanoparticles for dewetting suppression of thin polymer films used in chemical sensors . J. Nanopart. Res. 9 (2007) : 753-762.

[33] S.-H. Choi, B. Z. Newby, Dynamic contact angle in rim instability of dewetting holes J. Chem. Phys 124 (2006) : 054702-054713.

[34] J. Koo, K. Shin, Y.-S. Seo, T. Koga, S. Park, S. Satija, X. Chen, K. Yoon, B. S. Hsiao, J. C. Sokolov, M. H. Rafailovich. J. Koo, K. Shin, Y.-S. Seo, T. Koga, S. Park, S. Satija, X. Chen, K. Yoon, B. S. Hsiao, J. C. Sokolov, M. H. Rafailovich, Macromolecules 40 (2007) 9510. Macromolecules 40 (2007) : 9510-9516.

[35] K.A. Barnes, J.F. Douglas, D.W. Liu, A. Karim, Influence of nanoparticles and polymer branching on the dewetting of polymer films. Adv. Colloid Interface Sci. 94 (2001) : 83-104.

[36] X. Li, Y. Han, L. An, Inhibition of thin polystyrene film dewetting via phase separation. Polymer 44 (2003) : 5833-5841.

[37] R. Oslanec, A.C. Costa, R.J. Composto. Effect of Block Copolymer Adsorption on Thin Film Dewetting Kinetics. Macromolecules 33 (2000) : 5505-5512.

[38] A.C. Costa, R.J. Composto, P. VlĆek. Dewetting of thin film blends containing block copolymer: effects of nonadsorbing block length and substrate Hydrophobicity. Macromolecules 36 (2003) : 3254-3260.

[39] M.E. Mackay, Y. Hong, M. Jeong, S. Hong, T.P. Russell, C.J. Hawker, R. Vestberg, J.F. Douglas. Influence of Dendrimer Additives on the Dewetting of Thin Polystyrene Films . Langmuir 18 (2002) : 1877-1882.

[40] J.A. Orlicki, J.S. Moore, I. Sendijarevic, A.J. McHugh. Role of End-Group Functionality on the Surface Segregation Properties of HBPs in Blends with Polystyrene: Application of HBPs as Dewetting Inhibitors. Langmuir 18 (2002) : 9985-9989.

[41] S. Sangjan, N. Traiphol, R. Traiphol. Improvement of ultrathin polystyrene film stability by addition of poly(styrene-stat-chloromethylstyrene) copolymer: An atomic force microscopy study . Thin Solid Films 518 (2010) : 4879-4884.

[42] D.Y. Kwok, A.W. Neumann, Contact angle measurement and contact angle interpretation. Adv. Colloid Interface Sci. 81 (1999) : 167-249.

[43] R. Traiphol, D.W. Smith Jr., D. Perahia, J. Polym. Sci. B 40 (2002) : 2817-2825.

[44] S. Chattopadhyay, A. Datta. Morphological changes of Au nanoparticles in Au-polystyrene nanocomposite: A combined spectroscopy, atomic force microscopy and X-ray scattering study. Synth. Met. 155 (2005) : 365-367.

[45] H.Yildirim Erbil. Solid and Liquid Interfaces. UK : Blackwell Publishing, 2006.

[46] T. Gregory, M.E. Sojka. Photoactive additives for cross-linking polymer films: Inhibition of dewetting in thin polymer films. Langmuir 22 (2006) : 7748-7754.

[47] B.Z. Newby, K. Wakabayashi, R.J. Composto. Confinement induced stabilization in polymer blend thin films. Polymer 42 (2001) : 9155-9162.

[48] Z. Hao, W. Ruibing, Z. Gang, Y.A. Bai. covalently attached film based on poly(methacrylic acid)-capped Fe_3O_4 nanoparticles. Thin solid films 429 (2003) : 167-173.

[49] K.A. Barnes, A. Karim, J.F. Douglas, A.I. Nakatani, H. Gruell, E.J. Amis. Suppression of dewetting in nanoparticle-filled polymer films. Macromolecules 33 (2000) : 4177-4182.

[50] S. Herminghaus, K. Jacobs, K. Mecke, J. Bischof, A. Fery, M. Ibn-Elhaj.Spinodal dewetting in liquid crystal and liquid metal films. Science 282 (1998) : 916-919.

[51] R. Verma, A. Sharma, I. Banerjee, K. Kargupta. Spinodal instability and pattern formation in thin liquid films confined between two plates. J Colloid Interf. Sci. 296 (2006) : 220-232.

[52] J. Zhao, S. Jiang, Q. Wang, X. Liu, X. Ji, B. Jiang. Effects of molecular weight, solvent and substrate on the dewetting morphology of polystyrene films. Appl. Surf. Sci. 236 (2004) : 131-140.

[53] J.C. Meredith, A.P. Smith, A. Karim, E.J. Amis. Combinatorial Materials Science for Polymer Thin-Film Dewetting. Macromolecules 33 (2000) : 9747-9756.

[54] Y. Feng, A. Karim, R.A. Weiss, J.F. Douglas, C.C. Han. Control of Polystyrene Film Dewetting through Sulfonation and Metal Complexation. Macromolecules 31 (1998) : 484-493.

[55] R.S. Krishnan, M.E. Mackey. Influence of Molecular Architecture on the Dewetting of Thin Polystyrene films. Langmuir 21 (2005) : 5770-5776.

[56] A.C. Costa, R.J. Composto, P. Vlcek. Dewetting and Adsorption in Homopolymer
Films Containing Tribloack Copolymer: Role of Chain Architecture and
Anchoring Block Molar Fraction. The Journal of Adhesion 81 (2005) : 683-698.

[57] C. Stuart, H. Andrew, N. Chiara. Interplay between Dewetting and Layer Inversion in
Poly(4-vinylpyridine) /Polystyrene Bilayer. Langmuir 26 (2010) : 15989–15999.

[58] B. Weidenfeller, M. Hofer, F. Schilling, Internal friction studies of particulate filled
polypropylene. Composites J. 33 (2002) : 1041-1053.

[59] S. Meerod, G. Tumcharern, U. Wichai, M. Rutnakornpituk, POLY(ETHYLENE
GLYCOL)METHYL ETHER-B-POLYESTER DISPERSANT FOR MAGNETIC CORE-
SHELL NANOPARTICLE. Polymer 49 (2008) : 3950-3956.

[60] K.R. Reddy, K.P. Lee, A.I. Gopalan. Self-assembly approach for the synthesis of
electro-magnetic functionalized Fe3O4/polyaniline nanocomposites: Effect of
dopant on the properties. Colloids and Surface 320 (2008) : 49-56.

[61] J. You, Y. Liao, Y. Men, T. Shi, L. An. Film Thickness Dependence of Phase
Separation and dewetting Behaviors in PMMA/SAN Blend Films. Langmuir 26
(2010) : 14530–14534.

[62] R. Oslanec, A.C. Costa, R.J. Composto. Effect of Block Copolymer Adsorption on
Thin Film Dewetting Kinetics. Macromolecules 33 (2000) : 5505-5512.

[63] J. You, Y. Liao, Y. Men, T. Shi, L. An, X. Li. Composition Effect on Interplay between
Phase Separation and Dewetting in PMMA/SAN Blend Ultrathin Films.
Macromolecules 44 (2011) : 5318–5325

[64] E. Bertrand, T.D. Blake, J. De Coninck. Dynamics of dewetting. Colloid and Surface
A 369 (2010) : 141-147.

[63] X. Xia, E. Metwalli, M. A. Ruderer, V. Korstgen, P. Busch. Nanostructured diblock
copolymer films with embedded magnetic nanoparticles. J. Phys. 23 (2011)
254203-254212.

[64] L. Xue, Y. Han. Autophobic Dewetting of a Poly(methyl methacrylate) Thin Film on a
Silicon Wafer Treated in Good Solvent Vapor. Langmuir 25 (2009) : 5135-5140

117

[65] E. Bertrand, T.D. Blake, V. Ledauphin, G. Ogonowski, J. D. Coninck. Dynamics of Dewetting at the Nanoscale Using Molecular Dynamics. Langmuir 23 (2007) : 3774-3785.

[66] C. Wang, G. Krauch, M. Geoghegan. Dewetting at a Polymer-Polymer Interface: Film Thickness Dependence. Langmuir 17 (2001) : 6269-6274.

[67] N. Rehse, C. Wang, M. Hund, M. Geohegan, R. Magerie, G. Krausch. Stability of thin films on corrugated substrate. Eur. Phys. J. 4 (2001) 69-75.

[68] C. Lorenz-Haas, P. Muller-Buschbaum. J. Kraus, D.G. Bucknall, M. stamm. Nucleated dewetting of thin polymer films. Appl. Phys. 74 (2002) : 383-385.

[69] G. Henn, D.G. Bucknall, M. Stamm, P. Vanhoorne, R. Jerome. Chain End Effects and Dewetting in Thin Polymer Films. Macromolecules 29 (1996) : 4305-4313.

[70] G. Reiter. Evolution of Rim Instabilities in the Dewetting of Slipping Thin Polymer Films. The Journal of Adhesion 81 (2005) : 381-395.

[71] G. Reiter, M. Sferrazza, P. Damman. Dewetting of thin film polymer films at temperatures close to the glass transition. Eur. Phys. J. 12 (2003) : 133-138.

[72] G. Reiter, R. Khanna. Kinetics of Autophobic Dewetting of polymer films. Langmuir 16 (2000) : 6351-6357.

[73] K. Kargupta, R. Konnur, A. Sharma. Spontaneous Dewetting and Patterns in Evaporating Thin Liquid Films on Homogeneous and Heterogeneous Substrates. Langmuir 17 (2001) : 1294-1305.

[74] K. Kargupta, R. Konnur, A. Sharma. Instability and Pattern Formation in Thin liquid Films on Chemically Heterogeneous Substrates. Langmuir 16 (2000) : 10243-10253.

[75] A. Verma, A. Shama. Submicrometer Pattern Fabrication by Intensification of Instability in Ultrathin Polymer Films under a Water-Solvent Mix. Macromolecules 44 (2011) :4928-4935.

[76] L. Xu, A. Sharma, S. W. Joo. Substrate Heterogeneity Induced and Slip in Polymer Thin Flims: Dewtting on Silanized Surfaces with Variable Grafting Density. Macromolecules 43 (2010) : 7759-7762.

[77] K.M. Ashley, D. Raghavan, J.F. Douglas, A. Karim. Wetting-Dewetting Transition
Line in Thin Polymer Films. Langmuir 21 (2005) : 9518-9523.

[78] A. Sehgal, V. Ferreiro, J.F. Douglas, E.J. Amis, A. Karim. Pattern-Directed Dewetting
of Ultrathin Polymer Films. Langmuir 18 (2002) : 7041-7048.

[79] Y.A. Akpalu, A. Karim, S.K. Satija, N.P. Balsara. Suppression of Lateral Phase
Separation in Thin Polyolefin Blend Films. Macromolecules 34 (2001) : 1720-
1729.

[80] X. Han, C. Luo, Y. Dai and H.Liu. Effect of Polymer-Substrate Interactions on the
Surface Morphology of Polymer Blend Thin Films. Journal of Macromolecular
 Science 47 (2008) : 1050-1061.

[81] G. Liang, J. Xu, Z. Fan. Effect of Substrate Surface on Dewetting Behavior and
Chain Orientation of Semicrystalline Block Copolymer Thin Films. J. Phys. Chem
110 (2006) : 24384-24389.

[82] C.C. Wu, H.C. Chang. Estimating the thickness of hydrated ultrathin poly(o-
phenylenediamine) film by atomic force microscopy. Analytica Chimica Acta 505
(2004) : 239-246.

[83] C. Ton-That, A.G. Shard, R.H.Bradley. Thickness of spin-cast polymer thin
films determined by angle-resolved XPS and AFM tip-scratch methods.
Langmuir 16 (2000) : 2281-2284.

[84] K. Tanaka, A. Takahara, T. Kajiyama. Film thickness dependence of the
surface structure of immiscible polystyrene/poly(methyl methacrylate) blends.
Macromolecules 29 (1996) : 3232-3239.

[85] V. Torrisi, F. Ruffino, A. Licciardello. Memory effects in annealed hybrid gold
nanoparticles/block copolymer bilayers. Nanoscale Research Letters 6 (2011) :
167-173.

APPENDICES

Appendix A

Properties of polymers and copolymers

Properties of PS

Sample Name : polystyrene

Sameple # : P2459-S

Structure :
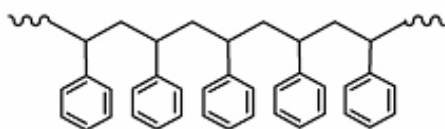
Composition :

Mn x 10^3	PDI
34.3	1.04

Synthesis procedure :

Polystyrene is obtained by polymerization

Characterization :

The molecular weight and polydispersity index (PDI) are obtained by size exclusion chromatography (SEC) in THF.

Solubility :

Polystyrene is soluble in DMF, THF, toluene and CHCl3. It precipitates from methanol, ethanol, water and hexanes.

Properties of P(S-Cl5)

Sample name : random copolymer poly(styrene-co-chloromethyl styrene)

Sample # : P2128 SSMeClran

Structure
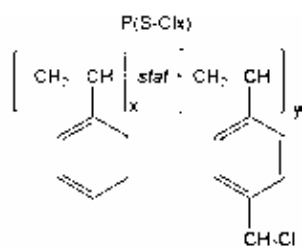
x = 0.95, y = 0.05

Composition :

PSMeCl (mol%) : 5.33

Mn x 10^3 PS-co-PSMeCl	PDI
29.2	1.12
T_g for random polymer	$103^{\circ}C$

Synthesis Procedure

Random copolymer poly(styrene-co-chloromethylstyrene) is prepared by redical polymerization of styrene and p-chloromethyl styrene in the presence of TEMPO

Characterization :

The polymer was analyzed by size exclusion chromatography (SEC) to obtain the molecular weight and polydispersity index (PDI). The copolymer composition was

calculated from H-NMR spectroscopy by comparing the peak area the aromatic protons of styrene at about 7.05 ppm with the protons of chloromethyl styrene at about 4.6 ppm

Thermal analysis :

Thermal analysis of the samples was carried out on the TAQ 100 differential scanning calorimeter at a heating rate of 10 $^{\circ}$C/min. The midpoint of the slope change of the heat flow plot of the second heating scan was considered as the glass transition temperature (Tg)

Solubility

Random copolymer poly(styrene-co-chloromethylstyrene) is soluble in $CHCl_3$, THF, DMF, toluene and precipitated out from methanal.

Properties of P(S-Cl20)

Sample name : random copolymer poly(styrene-co-chloromethyl styrene)

Sample # : P2132 SSMeClran

Structure
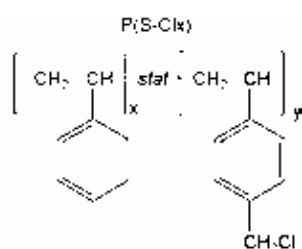
x = 0.80, y = 0.20

Composition :

PSMeCl (mol%) : 19.96

Mn x 10^3 PS-co-PSMeCl	PDI
27.9	1.18
T_g for random polymer	95°C

Synthesis Procedure

Random copolymer poly(styrene-co-chloromethylstyrene) is prepared by redical polymerization of styrene and p-chloromethyl styrene in the presence of TEMPO

Characterization :

The polymer was analyzed by size exclusion chromatography (SEC) to obtain the molecular weight and polydispersity index (PDI). The copolymer composition was

calculated from H-NMR spectroscopy by comparing the peak area the aromatic protons of styrene at about 7.05 ppm with the protons of chloromethyl styrene at about 4.6 ppm

Thermal analysis :

Thermal analysis of the samples was carried out on the TAQ 100 differential scanning calorimeter at a heating rate of 10 $^\circ$C/min. The midpoint of the slope change of the heat flow plot of the second heating scan was considered as the glass transition temperature (Tg)

Solubility

Random copolymer poly(styrene-co-chloromethylstyrene) is soluble in $CHCl_3$, THF, DMF, toluene and precipitated out from methanal.

Properties of P(S-Cl45)

Sample name : random copolymer poly(styrene-co-chloromethyl styrene)

Sample # : P2131 SSMeClran

Structure

P(S-Clx)
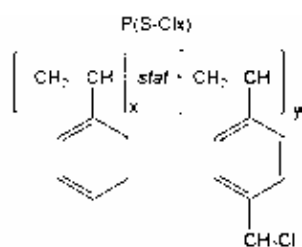
x = 0.55, y = 0.45

Composition :

PSMeCl (mol%) : 44.9

$Mn \times 10^3$ PS-co-PSMeCl	PDI
31.1	1.48
T_g for random polymer	$104^\circ C$

Synthesis Procedure

Random copolymer poly(styrene-co-chloromethylstyrene) is prepared by redical polymerization of styrene and p-chloromethyl styrene in the presence of TEMPO

Characterization :

The polymer was analyzed by size exclusion chromatography (SEC) to obtain the molecular weight and polydispersity index (PDI). The copolymer composition was

calculated from H-NMR spectroscopy by comparing the peak area the aromatic protons of styrene at about 7.05 ppm with the protons of chloromethyl styrene at about 4.6 ppm

Thermal analysis :

Thermal analysis of the samples was carried out on the TAQ 100 differential scanning calorimeter at a heating rate of 10 $^\circ$C/min. The midpoint of the slope change of the heat flow plot of the second heating scan was considered as the glass transition temperature (Tg)

Solubility

Random copolymer poly(styrene-co-chloromethylstyrene) is soluble in $CHCl_3$, THF, DMF, toluene and precipitated out from methanal.

Properties of PCIMS

Sample name : Poly(vinyl benzyl chloride)

Sample # : P520-VBC

Structure
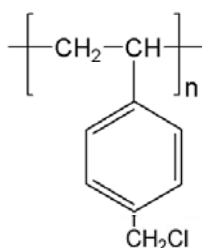
Composition :

$M_n \times 10^3$	PDI
15.3	2.16

Synthesis procedure

Poly(vinyl benzyl chloride) is obtained by free redical polymerization of 4-vinyl benzyl chloride or a mixture of 3- and 4-vinyl benzyl chloride. The reaction is shown below.
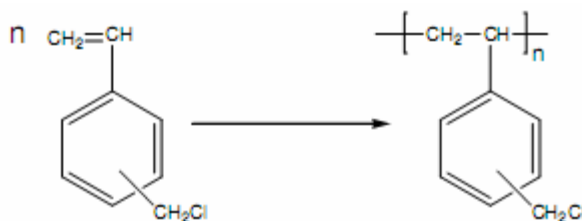
Solubility :

Polymer is soluble in DMF, THF, toluene and $CHCl_3$. It precipitates from methanol, ethanol, water and hexanes.

Appendix B

XRD analysis

Peaks Phase 1

Phase name   Peak Phase:0

Type	Position	I		
FP	30.22456	0.5645316	Cry Size Lor(nm)	11.4
			Cry Size Gauss(nm)	13.9
			k: 1, LVol-IB(nm)	5.555
			k: 0.89, LVol-FWHM(nm)	6.878
FP	35.59739	2.902368	Cry Size Lor(nm)	11.2
			Cry Size Gauss(nm)	8.6
			k: 1, LVol-IB(nm)	4.42
			k: 0.89, LVol-FWHM(nm)	5.170
FP	43.24246	0.7483688	Cry Size Gauss(nm)	5.0
			k: 1, LVol-IB(nm)	4.753
			k: 0.89, LVol-FWHM(nm)	4.503
FP	53.64191	1.133739	Cry Size Lor(nm)	6.9
			k: 1, LVol-IB(nm)	4.414
			k: 0.89, LVol-FWHM(nm)	6.171
FP	57.24489	3.414595	Cry Size Lor(nm)	7.4
			Cry Size Gauss(nm)	11.6
			k: 1, LVol-IB(nm)	3.912
			k: 0.89, LVol-FWHM(nm)	4.991
FP	62.81907	6.059873	Cry Size Lor(nm)	8.9
			Cry Size Gauss(nm)	14.1
			k: 1, LVol-IB(nm)	4.710
			k: 0.89, LVol-FWHM(nm)	6.020
FP	74.60763	1.590842	Cry Size Gauss(nm)	3.4

Total Cry Size Lor(nm)   9.18

      Cry Size Gauss(nm)   9.45

Appendix C

PROCEEDING

1.   Suntree Sangjan, Nisanart Traiphol* and Rakchart Traiphol, "Suppression the Dewetting Dynamics of Polymeric Thin Film by Addition of Fe_3O_4 Nanoparticles," Proceedings of The Pure and Applied Chemistry International Conference 2011 (PACCON 2011), 5-7 January 2011, Bangkok, Thailand.

2.   Nisanart Traiphol*, Suntree Sangjan and Rakchart Traiphol, "Suppression the Dewetting Polystyrene Thin Films by Blending with Poly(styrene-stat-chloromethyl styrene): The AFM Study," Proceedings of the 26th Annual Conference of the Microscopy Society of Thailand, January 28-30, 2009, Chiangmai, Thailand.

PRESENTATION

1.   Suntree Sangjan, Nisanart Traiphol* and Rakchart Traiphol, "Suppression the Dewetting Dynamics of Polymeric Thin Film by Addition of Fe_3O_4 Nanoparticles," Proceedings of The Pure and Applied Chemistry International Conference 2011 (PACCON 2011), 5-7 January 2011, Bangkok, Thailand.

2.   Suntree Sangjan, Nisanart Traiphol* and Rakchart Traiphol Suppression the Interfacial Instability of Ultrathin Polystyrene Films by Addition of Poly(styrene-stat-chloromethylstyrene) Additives The 6th Mathematics and Physical Science Graduate Congress 2010 (6th MPSGC), 13- 15 December 2010, University of Malaya, Malaysia

3.   Suntree Sangjan, Nisanart Traiphol*, Rakchart Traiphol, "Effects of Poly(styrene-stat-chloromethylstyrene) Additives on Dewetting Behaviors of Polystyrene Thin Films", 1st Polymer Conference of Thailand, 7-8 October 2010, Bangkok, Thailand.

4.   Suntree Sangjan, Nisanart Traiphol*, Rakchart Traiphol, "Versatile Method for Suppression the Interfacial Instability of Polystyrene Thin Films," A presentation, CHE-USDC CONGRESS II, August 27-29, 2009, Chonburi, Thailand.

5.   Suntree Sangjan, Nisanart Traiphol*, and Rakchart Traiphol*, "Effects of Random Copolymer Poly(styrene-co-chloromethylstyrene) on Wetting Behavior of Polystyrene

Thin Films," A presentation, The 4th Mathematics and Physical Science Graduate Conference, December 17-19, 2008, Singapore.

6.   Suntree Sangjan, Nisanart Traiphol*, Rakchart Traiphol*, "Effects of Interfacial Interactions on Stability of Polymeric Thin Films," A presentation, The 34th Congress on Science and Technology Thailand (STT 34), October 31-November 2, 2008, Bangkok, Thailand.

7.   Suntree Sangjan, Nisanart Traiphol*, Rakchart Traiphol, "Increasing Stability of Polystyrene Thin Films by Addition of Random Copolymer Poly(styrene-co-chloromethylstyrene)," A presentation, CHE-USDC CONGRESS I, September 5-7, 2008, Chonburi, Thailand.

VITAE

Name: Suntree Sangjan   Date of Birth: 02/05/2520

Nationality: Thai   Email address: <u>faasstp@ku.ac.th</u>

EDUCATION

2539 - 2542   Prince of songkla university - bachelor's degree in physics

2543 – 2545   Chulalongkorn university - master's degree in physics

EMPLOYMENT

2545 – 2546   academician - The institute for the promotion of teaching science and technology

2547- the present   an instructor – Kasetsart university (Kamphaeng Saen Campus)

JOURNAL PUBLICATIONS

1. Suntree Sangjan, Nisanart Traiphol*, Rakchart Traiphol*, "Influences of Poly[(styrene)x-stat-(chloromethylstyrene)y]s Additives on Dewetting Behaviors of Polystyrene Thin Films: Effects of Polar Group Ratio and Film Thickness," submitted to Thin Solid Films (impact factor 1.909)

2. Suntree Sangjan, Nisanart Traiphol*, Rakchart Traiphol* "Improvement of ultrathin polystyrene film stability by addition of poly(styrene-stat-chloromethylstyrene) copolymer: An Atomic Force Microscopy study," Thin Solid Films 518 (2010) 4879-4883. (impact factor 1.909)